Modelling of thermally driven groundwater flow in a facility for disposal of spent nuclear fuel in deep boreholes

Niko Marsic, Bertil Grundfelt

Kemakta Konsult AB

September 2013

SKB

Modelling of thermally driven groundwater flow in a facility for disposal of spent nuclear fuel in deep boreholes

Niko Marsic, Bertil Grundfelt

Kemakta Konsult AB

September 2013

Summary

In this report calculations are presented of buoyancy driven groundwater flow caused by the emission of residual heat from spent nuclear fuel deposited in deep boreholes from the ground surface in combination with the natural geothermal gradient. This work has been conducted within SKB's programme for evaluation of alternative methods for final disposal of spent nuclear fuel.

The basic safety feature of disposal of spent nuclear fuel in deep boreholes is that the groundwater at great depth has a higher salinity, and hence a higher density, than more superficial groundwater. The result of this is that the deep groundwater becomes virtually stagnant. The study comprises analyses of the effects of different inter-borehole distances as well as the effect of different permeabilities in the backfill and sealing materials in the borehole and of different shapes of the interface between fresh and saline groundwater. The study is an update of a previous study published in 2006.

In the present study, the facility design proposed by Sandia National Laboratories has been studied. In this design, steel canisters containing two BWR elements or one PWR element are stacked on top of each other between 3 and 5 kilometres depth. In order to host all spent fuel from the current Swedish nuclear programme, about 80 such holes are needed. The model used in this study comprises nine boreholes spaced 100 metres alternatively 50 metres apart in a 3×3 matrix.

In one set of calculations the salinity in the groundwater was assumed to increase from zero above 700 metres depth to 10% by weight at 1,500 metres depth and below. In another set, a sharper salinity gradient was applied in which the salinity increased from 0 to 10% between 1,400 and 1,500 metres depth. A geothermal gradient of 16°C/km was applied. The heat output from the spent fuel was assumed to decrease by time in manner consistent with the radioactive decay in the fuel.

When the inter-borehole distance decreased from 100 to 50 metres, the maximum temperature increase in the rock between the boreholes increased from 5 to 10°C and the duration of the this thermal pulse increased. Also, the thermally induced groundwater flow rate increased. However, the travel times for the groundwater from the disposal zone to the mobile fresh water zone above the halocline remained much longer than the duration of the thermal pulse. Hence, the conclusion from previous studies that the thermal output from the fuel is insufficient to jeopardise the stability of the groundwater stratification is confirmed. It should be noted, though, that some mixing occurs at the halocline if the permeability of the borehole filling material is assumed to increase. This mixing is less pronounced in the case with the sharper salinity interface.

Based on the calculations performed in this study, it can be concluded that boreholes for disposal of spent nuclear fuel should not be spaced closer than 100 metres for the type of canisters assumed in this study. The results also indicated that the properties of the material used for backfilling the boreholes has some importance for the stability of the halocline.

Sammanfattning

I denna rapport redovisas beräkningar av grundvattenströmning på grund av termisk konvektion orsakad av restvärmeutvecklingen i använt kärnbränsle som tänks deponerat i djupa borrhål från markytan i kombination med den naturliga geotermiska gradienten. Arbetet har utförts inom ramen för SKBs arbete med utvärdering av alternativa metoder för slutligt omhändertagande av använt kärnbränsle.

Den viktigaste säkerhetsfunktionen vid slutförvaring av använt kärnbränsle i djupa borrhål är att grundvattnet på deponeringsdjup i princip kan antas vara stagnant, främst på grund av att det djupa grundvattnet har en högre salthalt och därmed högre densitet än det grundare grundvattnet. I studien belyses effekten av avståndet mellan deponeringshålen liksom av permeabiliteten hos återfyllnads- och förseglingsmaterial i borrhålet och utbredningen av övergångszonen mellan sött ytligare grundvatten och det djupare liggande salta vattnet. Studien utgör en uppdatering av en tidigare studie som publicerades 2006.

Den studerade anläggningsutformningen har föreslagits av Sandia National laboratories. Utformningen bygger på att stålkapslar som innehåller två BWR-element alternativt ett PWR-element staplas ovanpå varandra mellan 3 och 5 km djup. Det behövs cirka 80 sådana deponeringshål för att rymma allt använt bränsle från det nuvarande svenska kärnkraftsprogrammet. Den modell som använts i denna studie omfattar nio borrhål med ett inbördes avstånd av 100 alternativt 50 m och som ordnats i en 3×3 matris.

I en uppsättning beräkningar har salthalten antagits öka från noll ovanför 700 m djup till 10 % vid 1 500 m djup och därunder. I en annan beräkningsserie antas motsvarande ökning av salthalten ske över intervallet 1 400 till 1 500 m djup. Den geotermiska gradienten ansattes till 16 °C per km. Restvärmeutvecklingen i bränslet antogs minska över tid på samma sätt som det radioaktiva sönderfallet i bränslet.

När avståndet mellan borrhålen minskade från 100 till 50 m ökade temperaturstegringen i berget mellan borrhålen från 5 till 10 °C och värmepulsens varaktighet ökade. Däremot förblev grundvattnets transporttid från deponeringszonen till det rörligare söta grundvattnet ovanför saltsprång-skiktet väsentligt längre än värmepulsens varaktighet. Således kvarstår slutsatsen från tidigare studier att restvärmeutvecklingen från bränslet är otillräcklig för att störa grundvattenskiktningens stabilitet. Noteras kan dock att när man ökade permeabiliteten hos fyllmaterialet i borrhålet kunde en vis omblandning av vattnet vid språngskiktet noteras. Denna omblandning var mindre uttalad med det skarpare språngskiktet.

På grundval av beräkningarna i denna studie kan man dra slutsatsen att borrhål för slutförvaring av använt kärnbränsle inte bör förläggas närmare varandra än 100 m för den typ av kapslar som antagits i denna studie. Resultaten antyder också att egenskaperna hos det material som används för att fylla borrhålet kan ha en viss betydelse för språngskiktets stabilitet.

Contents

1   Background

In Sweden, as well as in all other countries with a nuclear power programme, disposal in mined facilities some hundred metres below the ground surface is presently regarded to be the principal route for the final disposal. Disposal of spent nuclear fuel in deep (4–5 km) boreholes has been studied as an alternative method for disposal of spent nuclear fuel or high-level radioactive waste. Since the second half of the 1980s, SKB as well as other organisations dealing with disposal of radioactive waste, has performed several studies of deep borehole disposal. A bibliography of such studies is presented by Grundfelt (2010). In this report, a modelling study of thermal buoyancy driven groundwater flow around spent fuel deposited in deep boreholes is presented. The study is performed within SKB's programme for studying alternative methods and represents an update of a previous study by Marsic et al. (2006).

The basic safety feature of disposal of spent nuclear fuel in deep boreholes is that the groundwater at great depth has a higher salinity compared to more superficial groundwater. The deep groundwater therefore has a higher density compared to the more superficial groundwater. The result of this is that the deep groundwater becomes virtually stagnant. This stagnancy in the groundwater system could potentially be compromised by the residual heat output from the deposited spent fuel and by the natural geothermal gradient creating a diving force for buoyancy driven upward flow.

Marsic et al. (2006) modelled thermally driven groundwater flow around a facility for disposal of spent nuclear fuel in deep boreholes in a facility design developed in the so-called Pass study, Project on Alternative Systems Study (SKB 1992). It has become apparent during the last decade that the design from the Pass study should be updated, e.g. in order to accommodate for developments in drilling technology. A consensus has developed that vertical and straight holes probably can be drilled to a depth of 5 km with a hole diameter of 0.445 m (17½") (e.g. Beswick 2008, Odén 2013). After the closure of the Yucca Mountain programme, Sandia National Laboratories, SNL, have developed a concept for disposal of spent nuclear fuel (Brady et al. 2009, Arnold et al. 2011).

 In the present study, thermally driven groundwater flow in a facility for disposal of spent nuclear fuel that is similar to that described by SNL has been modelled. In this modelling, the sensitivities of the results to variations in the distance between boreholes and to the description of the halocline have been analysed. In order to reduce the computational work, only a section of the facility comprising nine boreholes was modelled.

2 Model description

This chapter describes the main concepts used in the calculations and the assumed properties in the bedrock and the repository.

2.1 The modelled facility

SNL has developed a reference design of a repository for deep borehole disposal of spent nuclear fuel (Arnold et al. 2011). This design is based on the drilling of 5 km deep holes into crystalline rock. In the reference design the diameter of the borehole is 43.2 cm in the disposal zone. In order to assure free passage of the canisters during the disposal operation, lining of the borehole with a casing is paramount. The reference borehole dimension will limit the dimensions of the casing and the canister so that only one fuel element (BWR or PWR) can be hosted in each canister. In SNL's reference design, the fuel elements are assumed to be disassembled so that the fuel rods can be densely packed in the canister. In the Swedish programme, this would involve the remote handling disassembling of about 55,000 fuel elements and packaging of about 5 million fuel rods. SKB has concluded that this type of fuel consolidation is not realistic in the Swedish programme due to the potential risks for incidents and personnel exposure.

Because of the reasoning described above, a slightly modified facility design concurring with a design described by Brady et al. (2009) has been assumed in this study. The only difference from the SNL reference design is that the boreholes are assumed to be slightly wider, i.e. 44.5 cm, allowing canisters that can host one PWR or two BWR elements without disassembling the elements. Figure 2-1 shows the conceptual design of a disposal borehole used in the current study. The casing in the disposal zone has an inner diameter of 381 mm allowing a canister with outer diameter of 340 mm and an inner diameter of 318 mm containing one PWR element (302 mm inner diameter required) or two BWR elements (311 mm inner diameter required).

The canisters to be disposed are connected by couplings at the top of the borehole to form strings of 40 canister each (about 200 m long). The outer diameter of the coupling is 360 mm. A bridge plug is placed on top of each deployed canister string and a 10 m long concrete plug is cast on top of the bridge plug, in order to carry the weight of the canister strings to be disposed above the plug. Each borehole can potentially host 10 such canister strings, i.e. in total 400 canisters. Table 2-1 shows an estimation of the total number of canisters required for the disposal of the spent nuclear fuel from the Swedish programme. From this it can be estimated that slightly less than 80 boreholes are required for the current size of the programme.

Table 2-1. Dimensioning of a facility for disposal of spent nuclear fuel from the Swedish nuclear programme in deep boreholes.

	BWR	PWR
Length of fuel element, m	4.47	4.059
Fuel element cross section mm × mm	139×139	214×214
Diagonal, mm	196	302
Uranium mass per element, kg	183.3	461.4
Total element weight, kg	319.9	523.4
Total fuel amount in theprogramme (SKB 2010), tones U	8,802	2,969
Approximate number of fuel elements	48,020	6,435
Number of fuel elements per canister	2	1
Number of canisters	24,010	6,435
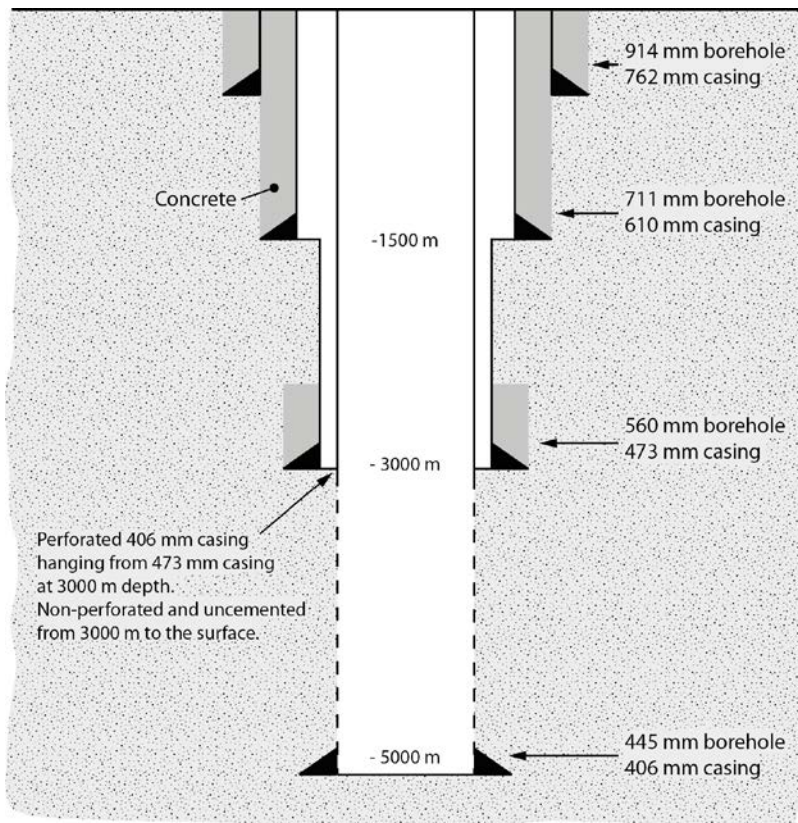
Figure 2-1. *Conceptual borehole design used for the modelling in the current study (modified from Brady et al. 2009).*

2.2 Geological and hydrogeological prerequisites

Juhlin et al. (1998) reviewed the available geo-scientific information about the conditions at great depth in Swedish bedrock. Smellie (2004) updated this review with more recent data. In a recent study by Marsic and Grundfelt (2013) data that were not available at the time of the study by Smellie have been reviewed. These reviews indicate that groundwater at greater depths have a high salinity and, in addition, have been isolated from more superficial groundwater systems for very long times. Moreover, although there are occurrences of conductive zones also in deep rock, it appears that the fracture frequency decreases with depth.

Juhlin et al.'s review (1998) results in an integrated geoscientific model of the bedrock and groundwater system in Sweden with a decreasing fracture frequency and increasing groundwater salinity with depth. In topographically flat areas of Fennoscandia the salinity below about 1–1.5 km is found to be high (several 10s of grams of dissolved solids per litre). The transition from essentially fresh water to the saline water appears to take place over a rage of some hundreds of metres. The high salinity in combination with a low hydraulic conductivity (10^{-10} m/s or lower) creates a virtually stagnant groundwater. Evidence for the stagnancy is found in the gas content and the stable isotope chemistry of the groundwater at these depths.

It should be noted that the knowledge base for this integrated geoscientific model consists of data from relatively few boreholes most of which have been drilled in geologies that are not necessarily compatible with the flat portions of southern Fennoscandia. Moreover, even though the trend appears to be a decreasing fracture frequency and hydraulic conductivity at depth, some of the boreholes reviewed are intersected by conductive fractures or fracture zones also at great depths. Also, in areas with a more expressed topographical relief, the penetration of meteoric water seems to be significantly deeper with a consequent shift downwards of the halocline.

2.3 Model description and methodology

2.3.1 General

The thermally driven groundwater flow was simulated using the finite element software CONNECTFLOW (version 9.1) developed by AMEC (AMEC 2012). The results were visualised using the 3D visualisation tool, also developed by AMEC. In addition, the resulting flow-field has been analysed using particle tracking from starting positions in the buffer material inside the boreholes.

In the calculations the distance between the boreholes was varied between 100 m and 52 m. Two sets of simulations were performed assuming a low and a higher permeability of the buffer material in the borehole. In addition, calculations were made for two variants of the initial distribution of salinity in the model, i.e. one variant with the salinity increasing linearly between 700 m and 1,500 m depth and one variant in which the salinity increases over a 100 m zone between 1,400 m and 1,500 m depth.

2.3.2 Finite element grid

A finite element grid based on the Base Case from Marsic et al. (2006) was created including nine disposal holes. The model is quadratic in the horizontal plane and the dimensions are 19,050 × 19,050 m. In the vertical dimension, the model extends down to 8,000 m depth. A regular grid was built from 84 element layers vertically (Z) and 99 elements in each horizontal direction (X and Y). This makes a total of 823,284 cuboid, eight-node finite elements prior to including the boreholes. Adding the borehole patches to the grid results in a finite element grid containing 854,289 elements with 1,735,645 nodes.

A model grid is usually a compromise between the need for refinement in the model and the resulting computational effort. The need to represent structures and features in the model properly puts certain requirements on the minimum grid refinement. Also, an increased grid refinement increases the numerical accuracy of the results. However, the cost in solution time caused by an increased grid refinement is normally greater than what comes only from the increase in number of finite element nodes because a decrease in element size normally requires also a reduction of the time step. Compared to the original Base Case in Marsic et al. (2006) the model grid used in the present study has more than three times as many elements. The reason for increasing the number of elements was to reduce the risk of numerical problems in the solution.

In Figure 2-2 and 2-3, the discretisation of the entire model grid is illustrated with vertical and horizontal sections through the centre of the model, respectively.
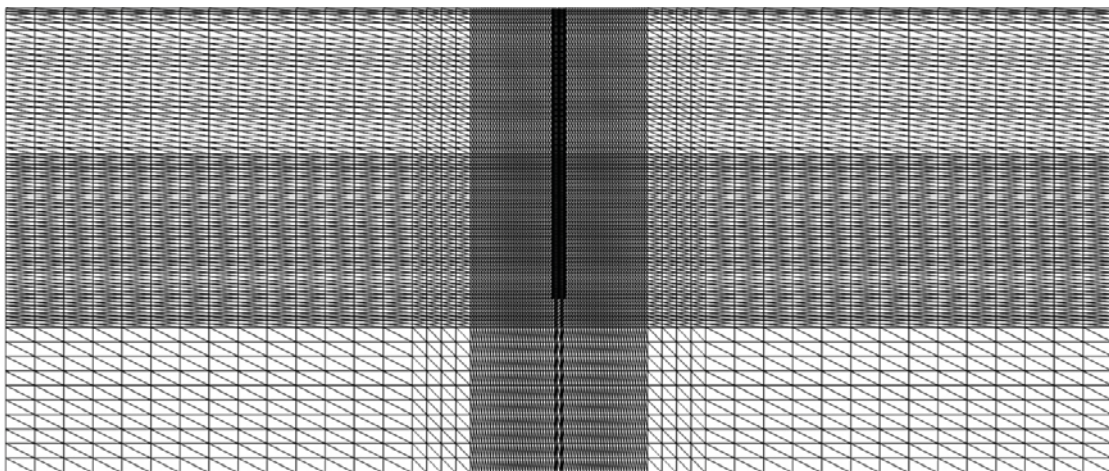
Figure 2-2. Vertical section showing the discretisation of the entire model grid. The borehole patches can be seen in the centre of the model (the triangles are an artefact of the visualisation program).
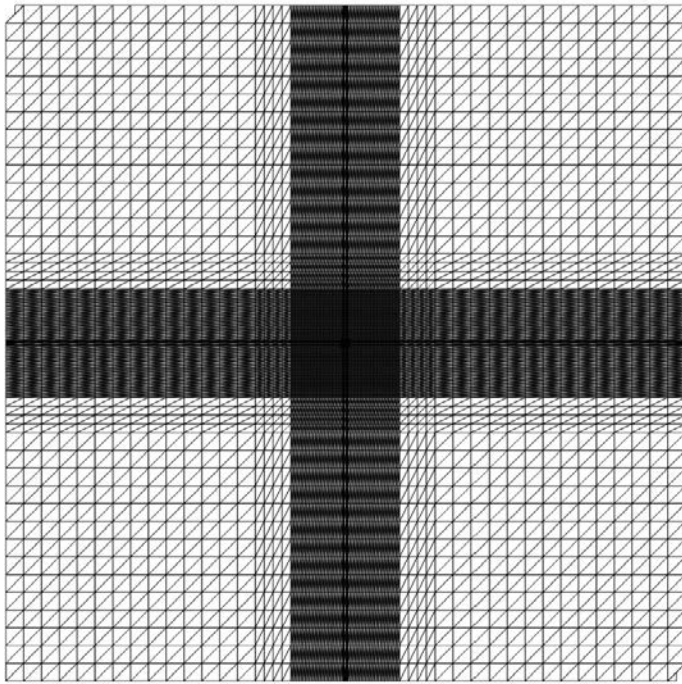
Figure 2-3. *Horizontal section showing the discretisation of the entire model grid. The denser discretisation around the boreholes can be seen in the centre of the model (the triangles are an artefact of the visualisation program).*
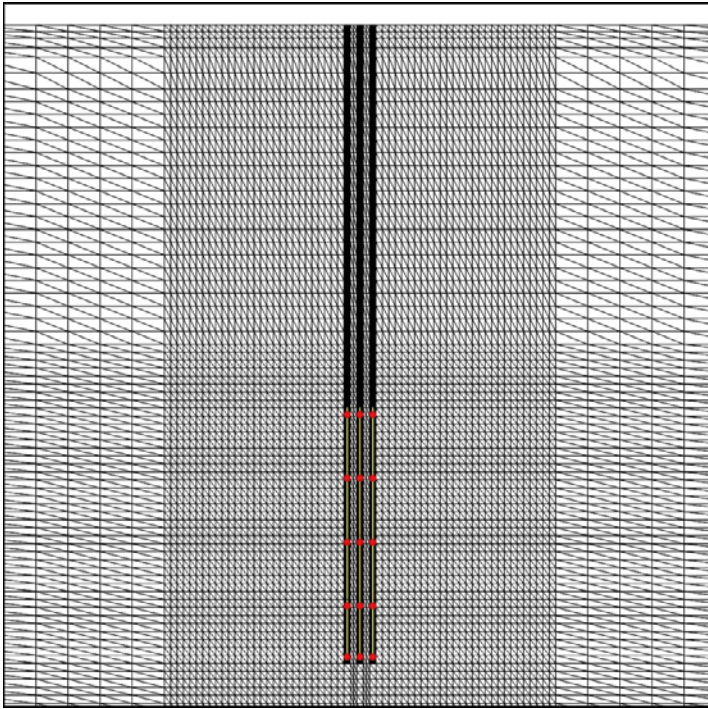
Figure 2-4 shows a close-up view of a vertical section through the centre of the model. The three centre boreholes are seen in the middle together with the particle release locations, shown as red markers. The vertical discretisation of the grid is 50 m in the top 100 m of the model. The vertical element size increases gradually down to 500 m depth where the element thickness is 125 m. Between –500 and –2,500 m the element thickness is 100 m. In the section containing the canisters plus an extra zone of 500 m above and below, i.e. at –2,500 to –5,500 m, the element thickness is 62.5 m. From –5,500 m the element thickness increases to 250 m all the way down to the bottom of the model at –8,000 m.

Figure 2-5 shows a close-up of a horizontal section through the centre of the model containing the nine modelled boreholes. The boreholes are placed in a regular 3×3 grid. Each borehole is placed in the centre of a 50×50 m patch. The borehole patches are separated in the horizontal plane by two 25 m elements. This gives a distance between the borehole centres of 100 m and forms a square repository area of 250×250 m. Outside of the repository area, the element sizes gradually increase from 50 m to 500 m.

As a sensitivity to the 100 m borehole distance an additional model was set up with a borehole distance of 52 m. The reason for choosing 52 m instead of 50 m is that it was easier to re-use the old grid without having to make too many time consuming structural changes.

In Figure 2-6, a 2 by 2 grid of vertical cross-sections through the bottom of the boreholes are presented. The top row shows the bottom of three boreholes and the bottom row shows a close-up view of the bottom of a single borehole. In the left column, the radial discretisation of the borehole patch is shown and in the right column the materials used in the model are shown; yellow-canister, orange-buffer, red-excavation damaged zone and blue-rock.

The borehole patch measures 50 m horizontally. The canisters (yellow) have a diameter of 340 mm and are surrounded by 52.5 mm of buffer material (orange). The canister and the buffer are represented by one element each in the radial direction. The DZ (Damaged Zone around the boreholes) (red) is assumed to have a radius of 445 mm surrounding the buffer and is represented by two elements in the radial direction. The remaining space in the borehole patch consists of rock (blue), i.e. from 0.89 m to 25.0 m radius. The rock section of the patch is radially discretised into 10 elements. The grid refinement was designed to represent the temperature and groundwater flow in the immediate vicinity of the boreholes with reasonable accuracy. This was checked using initial scoping calculations in Marsic et al. (2006).

Figure 2-4. *Vertical section (close-up view) showing the discretisation of the central part of the model grid containing three of the boreholes in the repository. Starting positions for the released particles are shown as red markers (the triangles are an artefact of the visualisation program).*
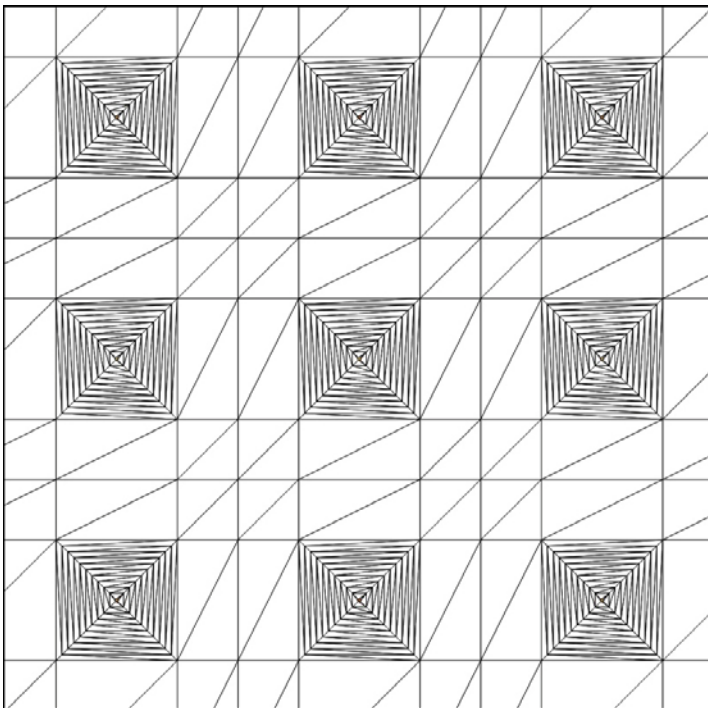
Figure 2-5. *Horizontal section (close-up view) showing the discretisation of the central part of the model grid containing the nine borehole patches (the triangles are an artefact of the visualisation program).*
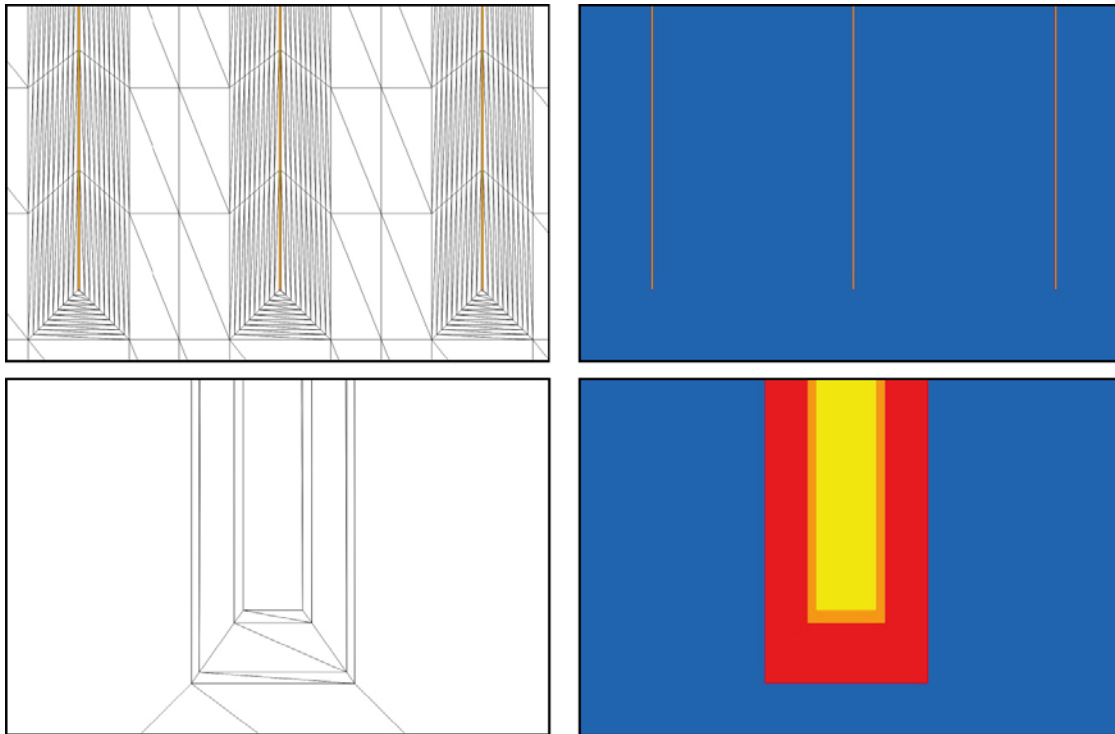
Figure 2-6. *Vertical section (close-up view) through three boreholes (top) and one single borehole (bottom) respectively, showing the radial discretisation (to the left) and materials (to the right): yellow-canister, orange-buffer, red-excavation damaged zone and blue-rock (the triangles are an artefact of the visualisation program).*

Figure 2-7 illustrates one single borehole on a horizontal section through the borehole. The top row shows the full width of the borehole patch while the bottom row shows a close-up view of the centre of the borehole patch containing the actual borehole. The left hand pictures show the discretisation of the borehole patch and the right hand side shows the different materials modelled. The azimuthal discretisation (perpendicular to the radius) around the canisters is four elements. This is applied for all materials, except the canisters, inside the borehole patch. Thus, in total the boreholes are discretised into 53 elements horizontally for each vertical element layer.

2.3.3 Material properties

The model properties used in the present study are based on the Base Case in Marsic et al. (2006). In order to be able to make a direct comparison to the previous results, a corresponding Base Case was set up in the present study, changing only the geometries of the grid and the heat source to represent the new borehole design and the decreased amount of spent fuel within each canister.

In order to further investigate the sensitivity of the groundwater flow pattern to changes in the material properties within the boreholes, a series of sensitivities were modelled gradually changing the hydraulic properties of the sealing and the buffer material.

The material properties of the Base Case are presented below. The rock has been divided into three depth intervals and one disturbed zone, DZ, around the boreholes with different hydraulic conductivities and porosities:

1. The upper 100 m of the ambient rock was assigned a hydraulic conductivity of 10^{-7} m/s.

2. In the depth interval –100 to –500 m the hydraulic conductivity was given the value 10^{-9} m/s.

3. The hydraulic conductivity below –500 m was set to 5×10^{-11} m/s.

4. The hydraulic conductivity of the DZ was given the value 5×10^{-9} m/s.

The porosity of the ambient rock was set to 10^{-4} and that of the DZ to 10^{-3}.
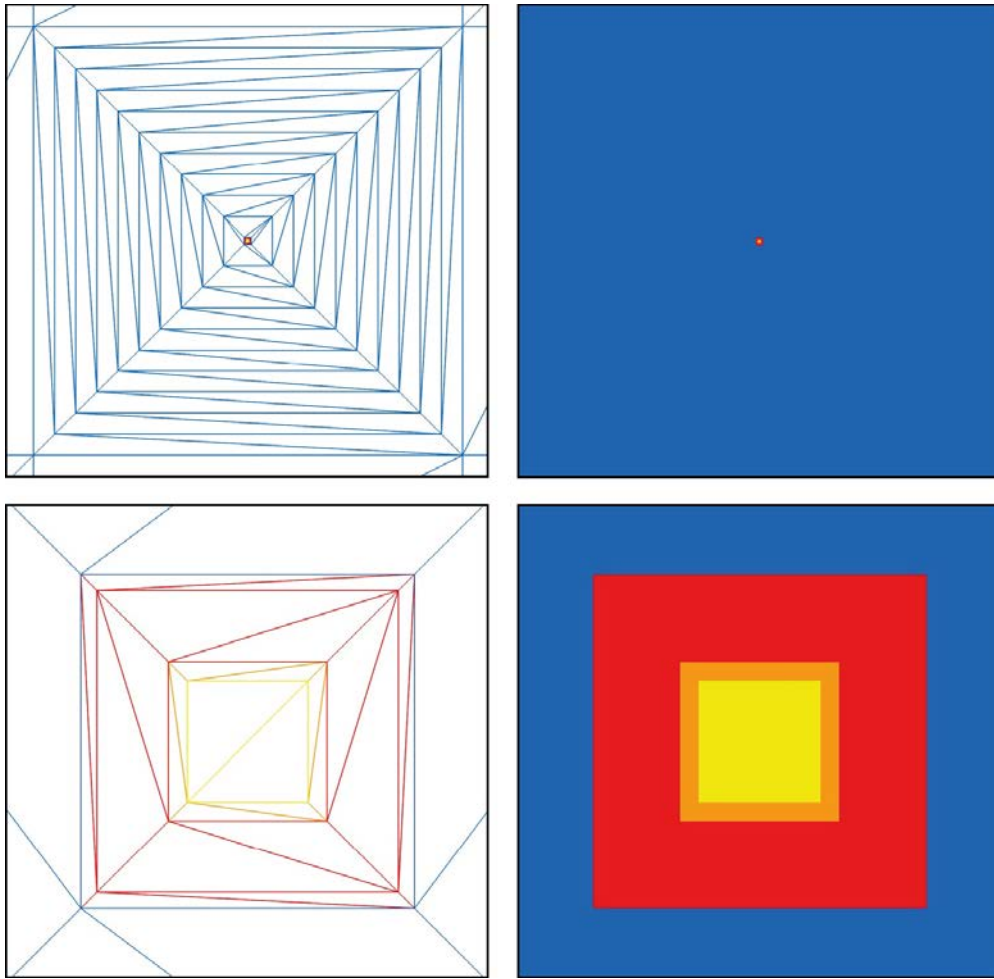
Figure 2-7. Horizontal section (close-up view) through one single borehole showing the azimuthal discreti-sation, borehole material: yellow-canister, orange-buffer, red-excavation damaged zone and blue-rock (the triangles are an artefact of the visualisation program).

The buffer around the canisters in the lower 2 km of the borehole was given a hydraulic conductivity of 10^{-9} m/s and a porosity of 0.3 based on the estimates made in the Pass-study (Birgersson et al. 1992). The underlying assumptions are that the deposition mud has an initial density of 1,600 kg/m^3 and the bentonite cushions between the canisters a density of 2,200 kg/m^3. The average density of the "buffer" in the deposition zone then becomes 1,900 kg/m^3.

The bentonite in the lower part of the sealing section of the borehole was assigned a hydraulic conductivity value of 5×10^{-11} m/s and a porosity of 0.3. The concrete plug in the upper part of the sealing section was given the same hydraulic conductivity value as the ambient rock in this depth interval, i.e. 10^{-7}–10^{-9} m/s, but the porosity of the concrete was set to 0.1. In addition, the asphalt seal was given the conductivity 10^{-9} m/s but with a porosity of 10^{-6}.

In the new design there are no bentonite cushions between the canisters. Hence, the hydraulic conductivity of the buffer in the deposition holes is likely to be significantly higher than in the Pass-design. Therefore, in addition to the Base Case simulations, a sensitivity study was conducted in which the hydraulic properties of the buffer and sealing were varied. In total, 22 sensitivity variants were simulated excluding the Base Case for the two different borehole distances. Only the variants with the highest permeability values of buffer and sealing will be reported and compared to the Base Case in this report.

The main mechanism for dispersion of the heat from the spent fuel into the rock is by heat conduction. The heat conductivity of the rock was given the value of 2.6 W/m,K and that of the buffer 1.0 W/m,K. For the specific heat of the rock a value of 780 J/kg,K was used and for the buffer 1,300 J/kg,K.

2.3.4 Boundary and initial conditions

On the vertical sides of the model, the hydraulic boundary condition was set no flux. This boundary condition applies to flow, solutes (salt) and heat transport through the lateral boundaries.

On the bottom boundary, a no flux boundary condition for water was used. For the salt (or Brine), a specified constant concentration corresponding to 10% by mass salinity was used. Salt is allowed to pass the bottom boundary into the model by diffusion only. Figure 2-8 shows the initial salinity profile in the model. The values presented are the fraction of the water that is brine (10% salt content). Hence, we see that the concentration of brine at the bottom of the model equals one whereas at the top, where the water is fresh, the brine concentration equals zero.

At the top boundary, a specified head boundary condition was used. For specified head, the model is assumed to be fully saturated and the datum is set at 0 m. Hence, the head is equal to the elevation of the topographic surface, i.e in this case a constant head equal to zero. The salt concentration was assigned a constant value of zero at the top surface.

The initial condition for salt was set to pure freshwater from the surface down to Z=−700 m. Below that the salinity increases linearly to full brine (10% salt content) at a depth of 1,500 m. Below Z=−1,500 m the groundwater is assumed to consist only of brine. This initial condition is illustrated in Figure 2-8. The black points in the figure indicate release locations for particles in the post processing. They are located in the disposal section of the boreholes well below the brine interface.

In order to investigate the sensitivity of the groundwater flow pattern to the position and shape of the saline interface, two additional variants were modelled. In these variants the transition from freshwater to full brine occurs between −1,400 and −1,500 m depth, thus corresponding to a much sharper interface compared to the base case.

For heat transport through the bottom boundary, a specified flux boundary condition was used with the value set to −41.8 mW/m^2. This value is consistent with a geothermal gradient of 16°C/km that appears to representative for Swedish bedrock, see e.g. Juhlin and Sandstedt (1989). At the top boundary, a specified value of T=6°C for the temperature was assigned. Together with the thermal gradient this gives an initial temperature of T=134°C at the bottom boundary at Z=−8,000 m. The initial condition for temperature in the rock and groundwater is shown in Figure 2-9. The black points in the figure indicate the particle release locations. The initial temperature within the disposal zone of the boreholes ranges from 54°C at Z=−3,000 m to 86°C at the bottom of the boreholes at Z=−5,000 m.
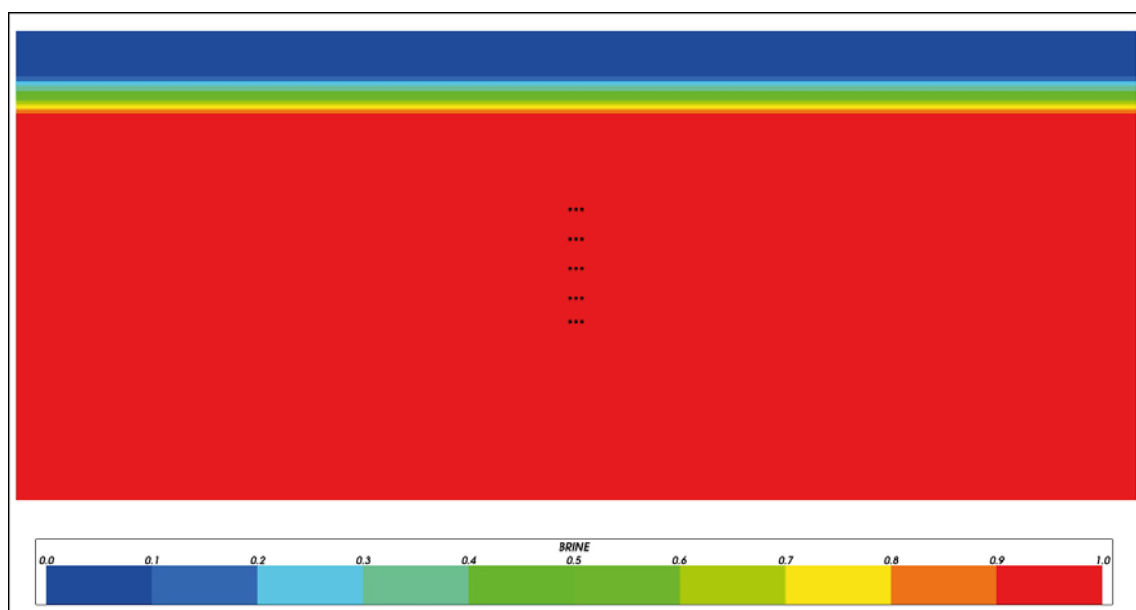
Figure 2-8. Vertical section though the centre of the model showing the initial distribution of Brine (10% salt content). Black points indicate the particle release locations.
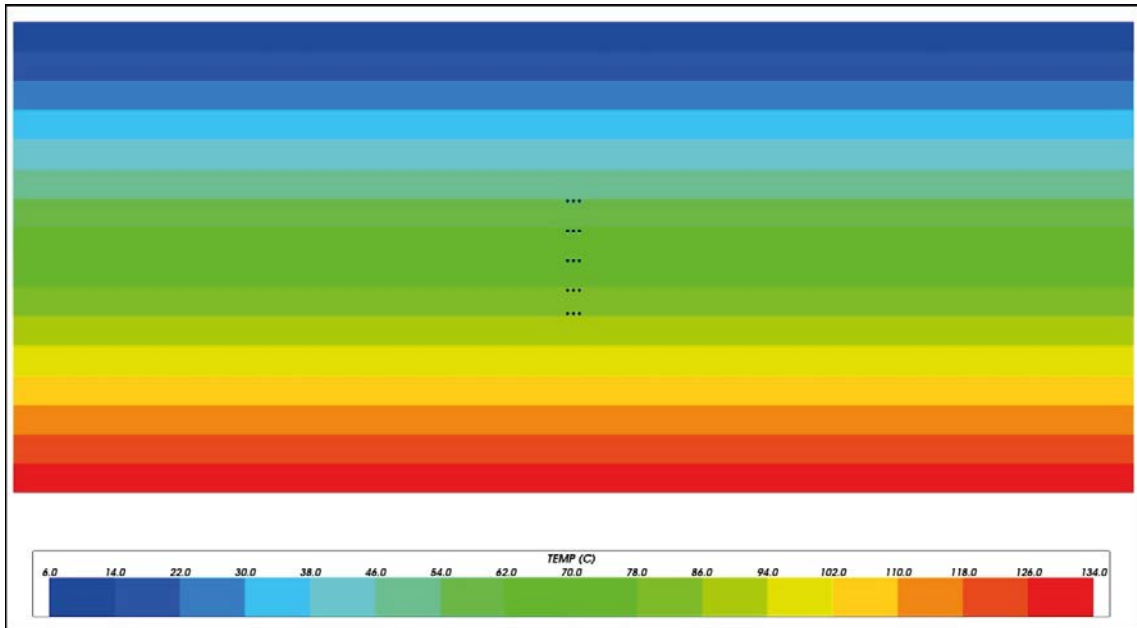
Figure 2-9. *Vertical section though the centre of the model showing the initial temperature distribution due to the geothermal gradient. Blue colour indicates lower temperature (T=6°C on the top surface) and red colour indicates higher temperature (T=134°C at the bottom of the model, Z=–8,000 m). Black points indicate the particle release locations.*

2.3.5   Heat source and temperature field

The heat output from the spent fuel in the canisters was modelled as a uniform heat source within each of the boreholes at a depth of Z=–3,000 m to Z=–5,000 m. Figure 2-10 shows a graph of the thermal output per metre borehole as a function of time used as input to the models used in Marsic et al. (2006) (blue line) and in the present study (red line) when calculating the heat flux from the source.

This data for Marsic et al. (2006) was obtained by taking the total heat output from the spent fuel, as estimated for an operation time of 40 years for the nuclear power plants (Agrenius 2006) as a basis for calculating the average heat output per canister. The average output per m borehole was then calculated by dividing the heat output from 300 canisters by 2,000 m of borehole length. For the present study, in which a smaller canister diameter is used (340 mm compared to 500 mm), the heat output was simply reduced by a factor of two, which approximately represents what can be fitted in terms of spent fuel within the smaller canisters.

Figure 2-11 and 2-12 show the temperature evolution and distribution due to the heat generated by the spent fuel in the canisters over a horizontal cross section at Z=–4,000 m through the nine modelled boreholes using a borehole distance of 100 m. The time range is from 1 year to 1,000 years. The heat generated by the canisters is dissipated into the surrounding rock by conduction whereby the temperature of the rock rises gradually. The borehole temperature at 4,000 m depth reaches a maximum of 80°C within a few years after disposal. However, already after 30 years, the temperature of the boreholes starts falling and after a couple of hundred years, the temperatures of the boreholes are similar to the rock temperature. After 50 years, the temperature increase of the rock in between the boreholes is approximately 3°C. After 500 years, the temperature increase is approximately 5°C. The effect of heating remains in the rock for at least 1,000 years, even if the temperature increase relative to the background geothermal temperature is not very pronounced at that time.

Figure 2-13 and 2-14 show the corresponding temperature evolution and distribution over a horizontal cross section at Z=–4,000 m for the nine modelled boreholes using a borehole distance of 52 m. Decreasing the distance between the boreholes clearly has a great effect on the temperature in the rock. The generated heat increases the temperature of the rock between the boreholes by 10°C in the first 100 years. The effect remains for at least 500 years and even after 1,000 years the temperature increase in the rock is approximately 6–7°C.

Thermal output per metre borehole
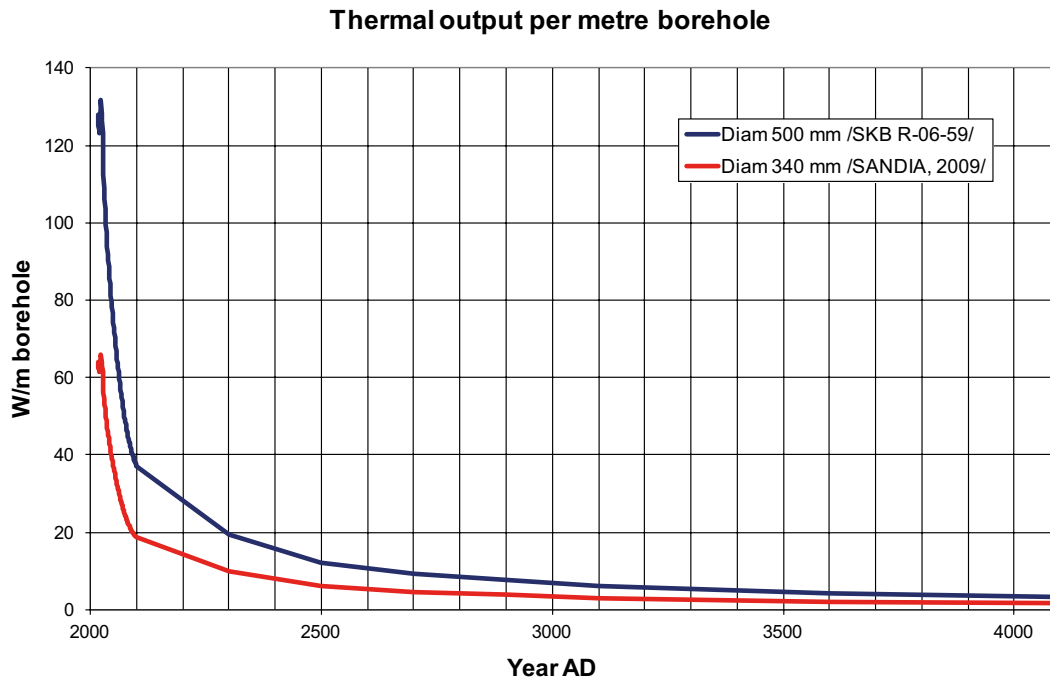
Figure 2-10. Thermal output calculated per metre borehole as a function of time, for two different canister diameters for a total of 40 years of operation of the Swedish nuclear power plants.

2.4 Transport performance measures

One objective of the presented sensitivity study is to investigate groundwater pathways from repository area to the surface. The approach taken is to track particles moving with the advective flow velocity from a range of release points until they reach the top surface. Although it would be possible in CONNECTFLOW to track particles as they move through a velocity field that evolves in time, it is preferred here to use only the velocity field from chosen snapshots in time. The reason for this is that the groundwater flow is solved for the first 1,000 years only, while the particles typically need to be tracked for times periods $> 10^6$ years. This would be practically impossible to accomplish. Hence, results are presented for particles release times equal to 10 years and 100 years of simulation.

Particles are released at five different levels distributed along the canister section of the boreholes at elevations $-3,050$, $-3,550$, $-4,050$, $-4,550$ and $-4,950$ m. In Figure 2-4 the starting positions for the released particles are shown as red markers. The particles are released in the buffer material surrounding the canisters, 20 cm out from the centre of the boreholes

To describe the groundwater flow and the transport of substances dissolved in the groundwater from the repository to the surface, the following concepts are used:

Travel time, $t_r = \sum_l \dfrac{n_e\, \delta_l}{q}$

Where:

δ_l is the length of a step in distance along the path,

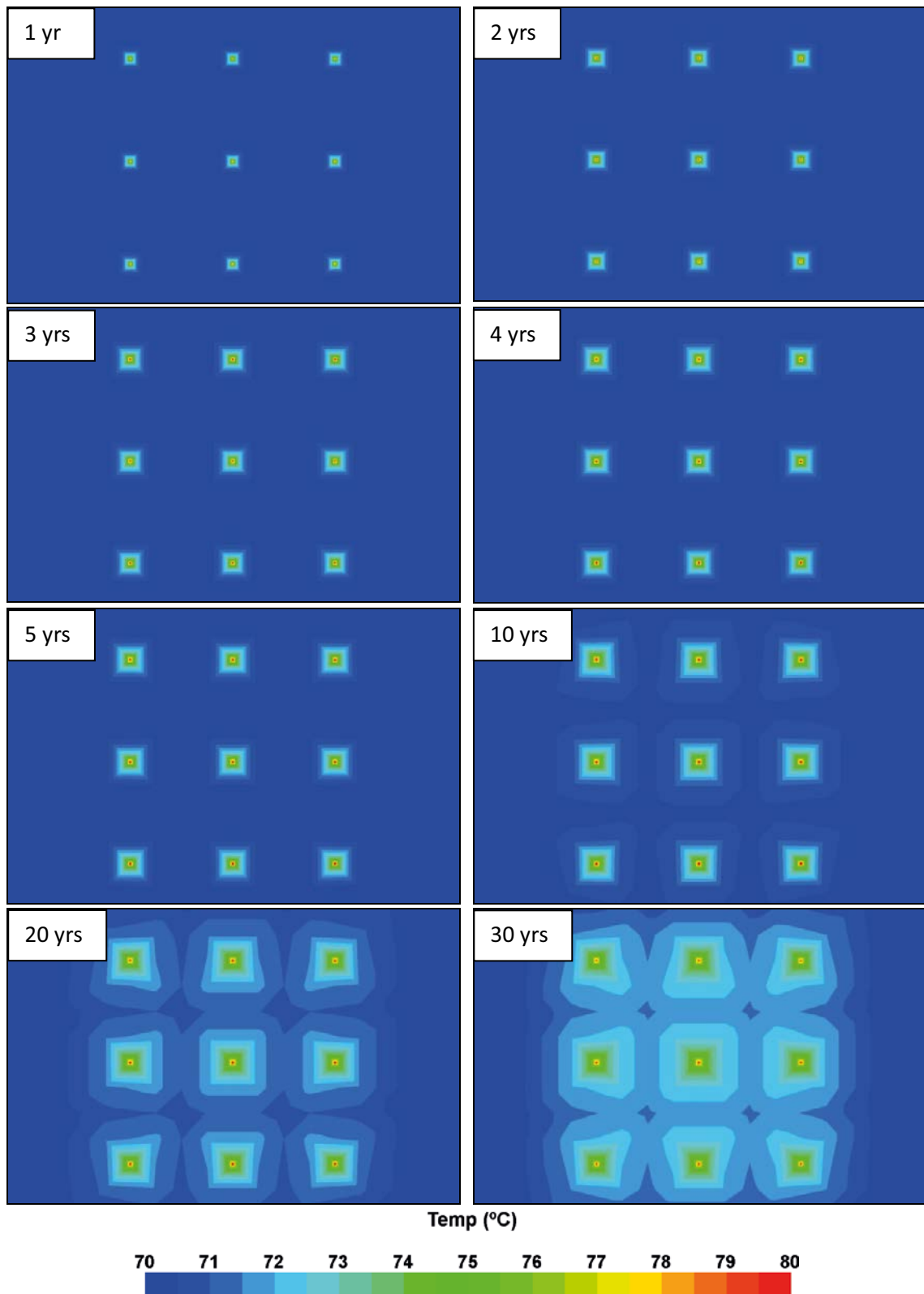l denotes steps along a path, for example through one finite-element,

n_e is the kinematic porosity,

q is the Darcy velocity,
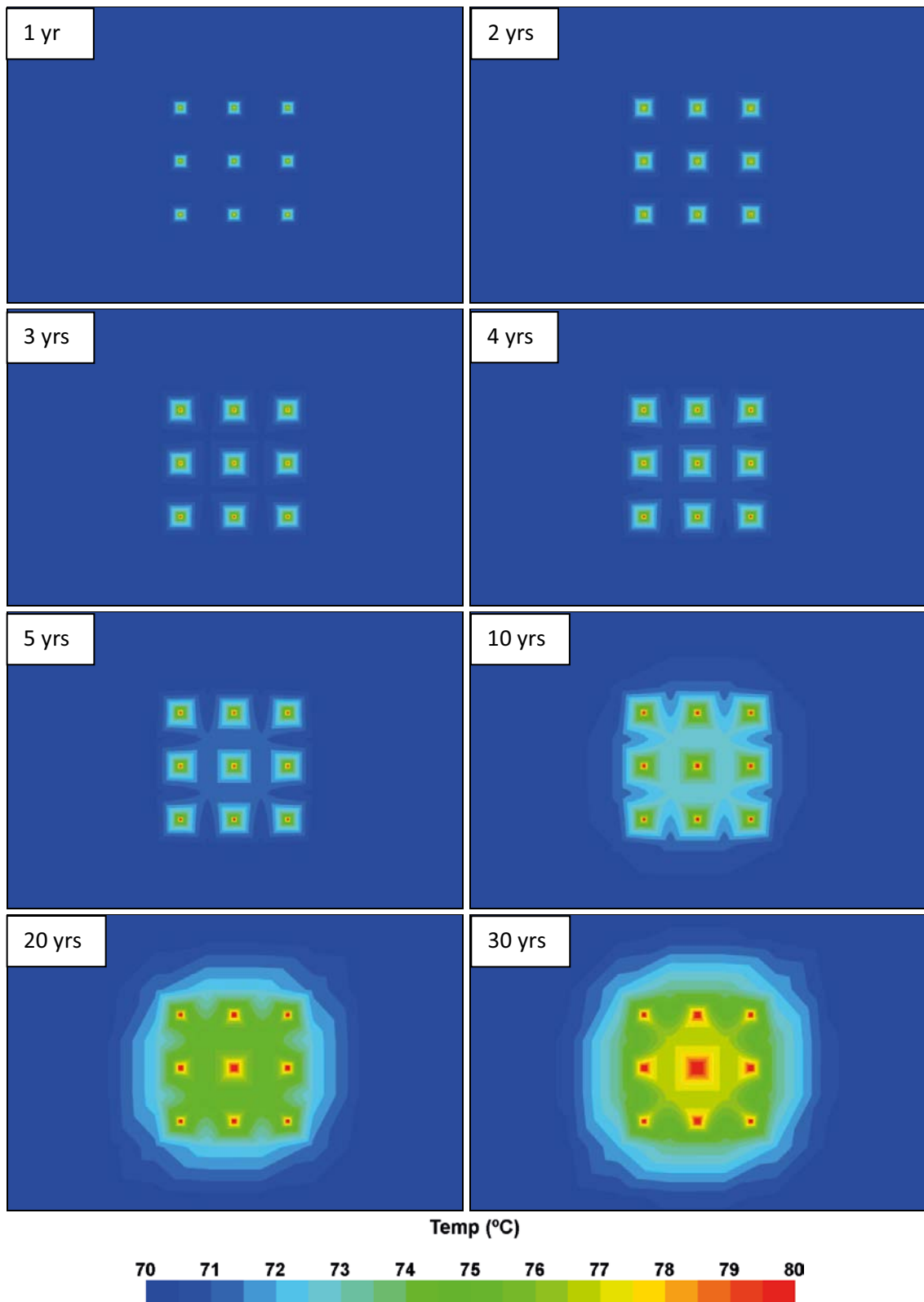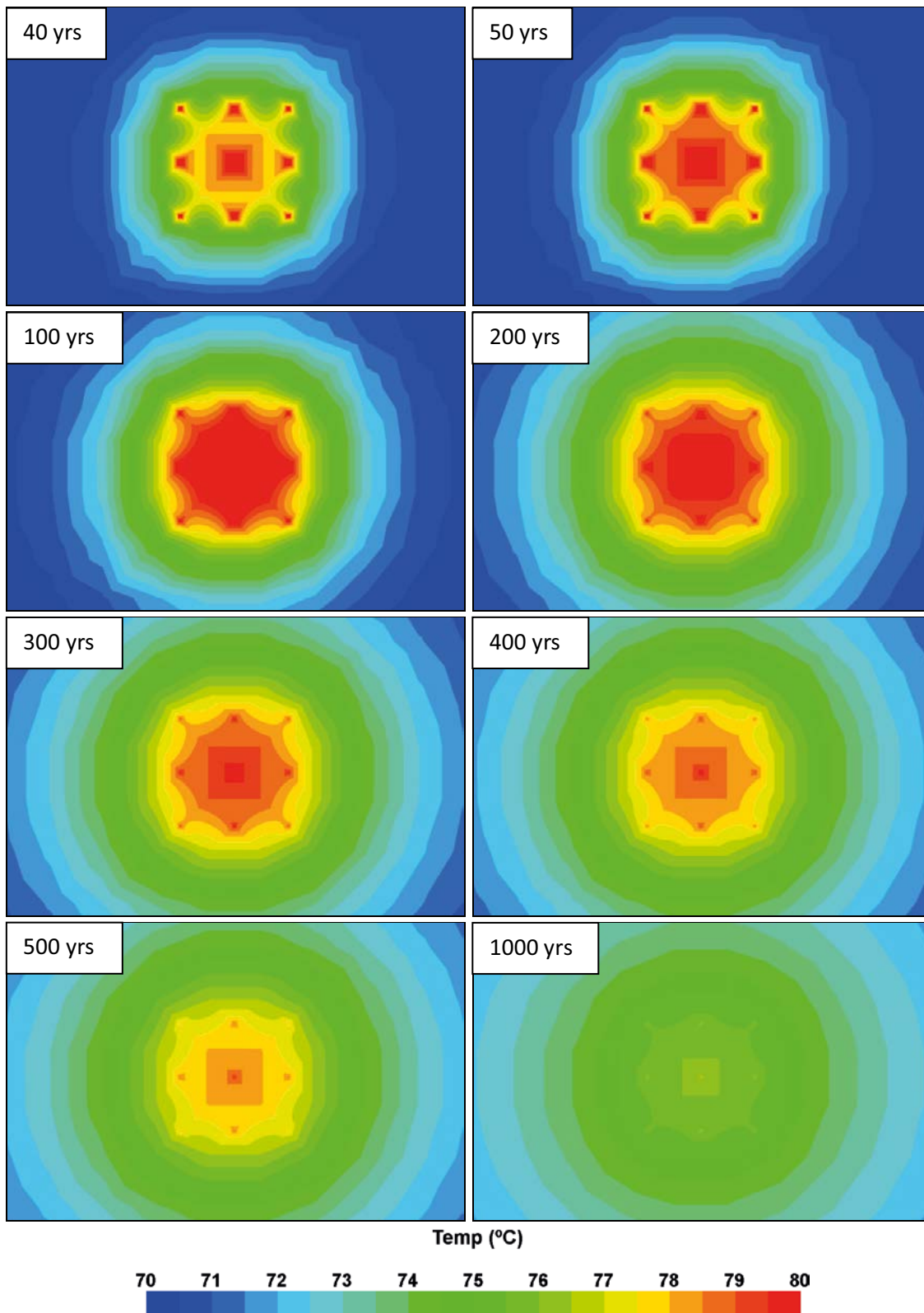
and

Path length, $L_r = \sum_l \delta_l$.

Figure 2-11. *Temperature evolution and distribution due to heat generated by the canisters over a horizontal cross section at Z=–4,000 m through all modelled boreholes using a borehole distance of 100 m. Blue colour indicates lower temperature and red colour indicates higher temperature. Time range: 1 to 30 years.*
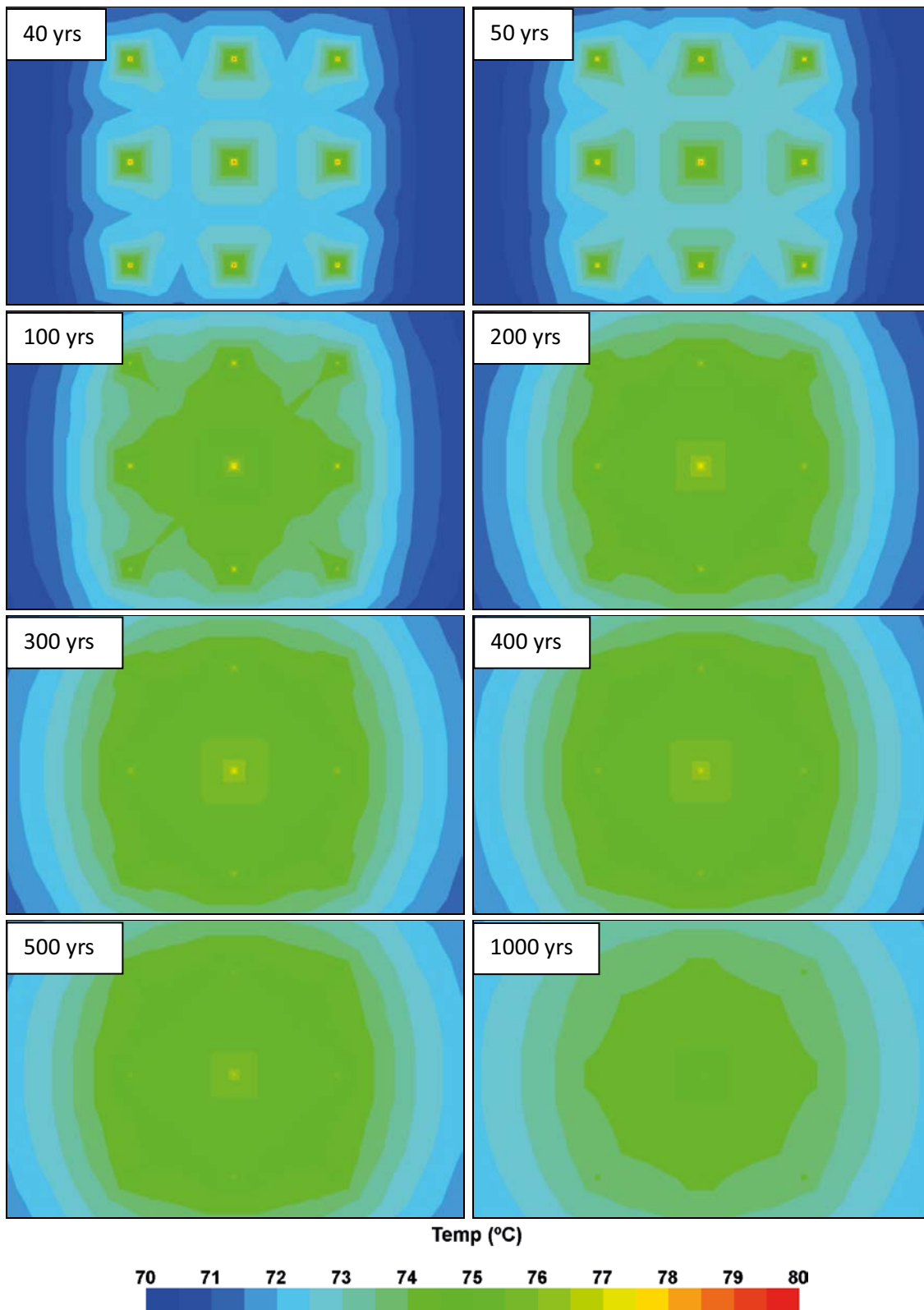
Figure 2-12. Temperature evolution and distribution due to heat generated by the canisters over a horizontal cross section at Z=–4,000 m through all modelled boreholes using a borehole distance of 100 m. Blue colour indicates lower temperature and red colour indicates higher temperature. Time range: 40 to 1,000 years.

Figure 2-13. Temperature evolution and distribution due to heat generated by the canisters over a horizontal cross section at Z=–4,000 m through all modelled boreholes using a borehole distance of 52 m. Blue colour indicates lower temperature and red colour indicates higher temperature. Time range: 1 to 30 years.

Figure 2-14. *Temperature evolution and distribution due to heat generated by the canisters over a horizontal cross section at Z=–4,000 m through all modelled boreholes using a borehole distance of 52 m. Blue colour indicates lower temperature and red colour indicates higher temperature. Time range: 40 to 1,000 years.*

3 Results

3.1 Summary of calculated variants

The understanding of the conditions at a depth of several km in crystalline rock is based on very few observations. A modelling exercise like the present should therefore be regarded as a generic study rather than an attempt to describe actual conditions. In Marsic et al. (2006), an extensive sensitivity analysis was carried out where the uncertainties of the following topics were studied:

- Buoyancy driven flow in the boreholes together with its sensitivity to the ambient hydraulic gradient and the quality of the borehole sealing.

- The occurrence of fracture zones intersecting the repository.

- The quality of the buffer in the disposal zone (2–4 km depth).

- The salinity distribution and the interaction between the heat source and the salinity.

- The depth of the disposal zone.

- Combinations of the above listed topics created to investigate under what conditions the ground-water flow conditions remain stable and virtually stagnant.

In the present study, also carried out as a sensitivity analysis, the focus has been on the effects on groundwater flow from reducing the borehole distance from 500 m, which was used in Marsic et al. (2006), to 100 m and 52 m respectively. In addition to this sensitivity analysis, the effects of changing the properties of the buffer and sealing in the borehole and the position and shape of the saline interface were analysed.

The buffer and the bentonite in the borehole sealing were changed gradually in a sensitivity study. However, only the variants with the greatest change in parameter values compared to the Base Case are reported here. These two parameter settings will still capture the full range of results from the performed sensitivity study and therefore the other variants would be of less interest.

A summary of the variants included in the sensitivity analysis and the properties applied is presented in Table 3-1 below. Some of the abbreviations and symbols used in the table may require further explanation:

- In the column "Model" a reference to the corresponding computer file name is given for traceability.

- BC denotes boundary condition.

- IC denotes initial condition.

- DZ denoted damaged zone.

The set-up of each case is further explained in the respective subsection of sections 3.2 to 3.4 below. The results are presented for particles release times equal to 10 years and 100 years of simulation. In the figures, Darcy velocity vectors and flow paths are shown on vertical cross-sections through the middle of the model. The size of the vectors is scaled according to the magnitude of the Darcy velocity which in some of the figures, where the Darcy velocities are high, give some vectors that are very large compared to others. To improve readability, the vectors are also coloured according to the magnitude of the Darcy velocity.

The flow paths are shown as 3D trajectories projected on 2D sections. In some of the figures, flow paths appear to be exiting the model; this however is only an artefact of presenting 3D trajectories on a 2D section. In addition, separate figures show flow paths coloured according to travel time along the flow paths.

Table 3-1. Summary of analysed variants in the sensitivity analysis and the properties used.

Case	Model	Description	Borehole c/c	Heat source	Top BC	Salt IC	Rock domain	Borehole properties
1	DBH_heat_2_3	Base Case Based on the Base Case, VDH_heat_2_1, in Marsic et al. (2006) Sensitivity to borehole distance	100 m	Included in all boreholes. Background thermal gradient in rock.	Constant uniform head	Brine fraction linearly increasing from 0 to 1 between Z=–700 and –1,500 m	Increased permeability above Z=–500 m, homogeneous below Z=0 to –100 m k=1E–7 m/s Z=–100 m to –500 m k=1E–9 m/s Z=–500 m to –8,000 m k=5E–11 m/s Z=0 to –8,000 m ne=1E–4	CONCRETE 1 k=1E–7 m/s CONCRETE 2 k=1E–9 m/s ne = 1E–1 ASPHALT k=1E–9 m/s ne = 1E–6 SEALING k=5E–11 m/s ne = 3E–1 BUFFER k=1E–9 m/s ne = 3E–1 DAMAGED ZONE k=5E–9 m/s ne = 1E–3
2	DBH_heat_3_3	Sensitivity to borehole distance	52 m	Same as Base Case	Same as Base Case	Same as Base Case	Same as Base Case	Same as Base Case
3	DBH_heat_2_17	Sensitivity to borehole properties	100 m	Same as Base Case	Same as Base Case	Same as Base Case	Same as Base Case	Same as Base Case but SEALING k=5E–7 m/s BUFFER k=1E–7 m/s
4	DBH_heat_3_17	Sensitivity to borehole properties	52 m	Same as Base Case	Same as Base Case	Same as Base Case	Same as Base Case	Same as Base Case but SEALING k=5E–7 m/s BUFFER k=1E–7 m/s
5	DBH_heat_6_3	Sensitivity to position of the saline interface	100 m	Same as Base Case	Same as Base Case	Brine fraction linearly increasing from 0 to 1 between Z=–1,400 and –1,500 m	Same as Base Case	Same as Base Case
6	DBH_heat_6_17	Sensitivity to position of the saline interface	100 m	Same as Base Case	Same as Base Case	Brine fraction linearly increasing from 0 to 1 between Z=–1,400 and –1,500 m	Same as Base Case	Same as Base Case but SEALING k=5E–7 m/s BUFFER k=1E–7 m/s

3.2 Sensitivity to borehole distance
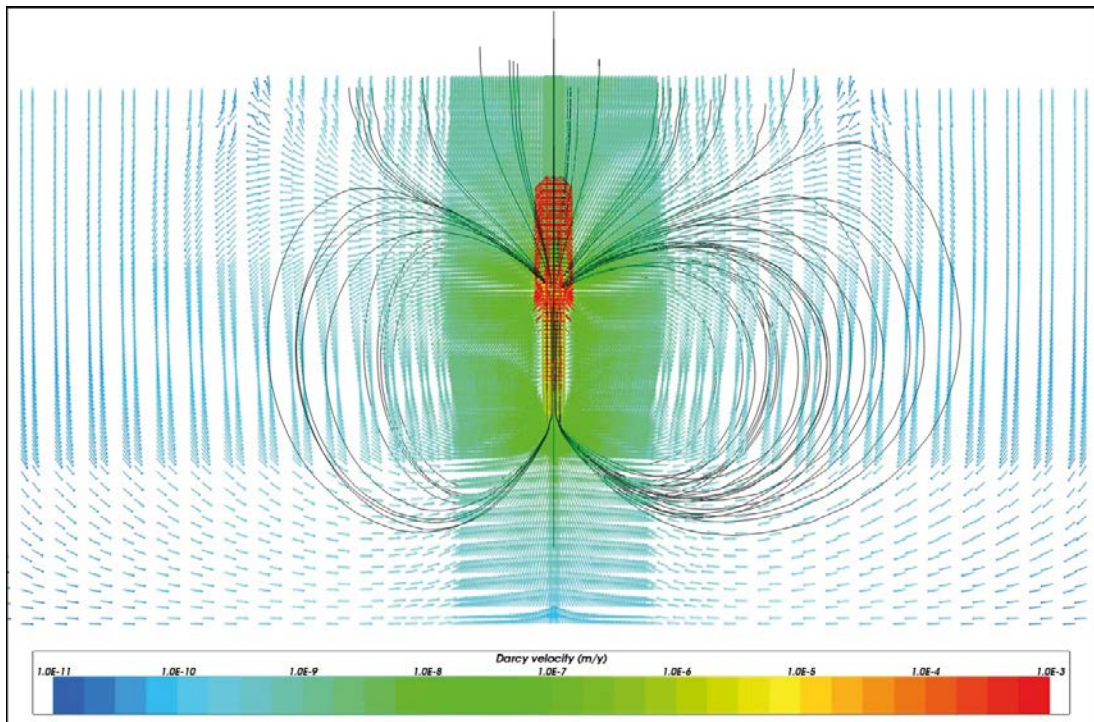
3.2.1 Case 1: 100 m borehole distance

Case 1 is the Base Case in the present study and is based on the original Base Case (VDH_heat_2_1) reported in Marsic et al. (2006). Compared to that model changes were made to the borehole geometries, borehole distances, grid discretisation and thermal output from the spent fuel in the canisters. In this case a borehole distance of 100 m was modelled compared to 500 m which was used in Marsic et al. (2006).

At the top surface of the model, a uniform constant head (Dirichlet) boundary condition is applied. The upper 700 m of the model is initially filled with freshwater. Between 700 and 1,500 m depth, the brine content increases from 0 to 100% (corresponding to 10% salinity). Below 1,500 m the model is initially filled with pure brine.

The permeability of the rock decreases with depth in the upper 500 m of the model. Below this level, the permeability is kept constant. Apart from the depth dependency in the top 500 m, the permeability is homogeneous throughout the model, i.e. no fracture zones or other structures are represented in this variant.

The properties of the upper 3,000 m of the boreholes were assigned the same values as the rock at the same level. Between 3,000 and 5,000 m depth the properties of the boreholes (buffer and the DZ) were assigned values that have been judged reasonable with respect to the assumed density of the buffer material and the rock stress situation around the borehole, see Section 2.3.3. A more detailed description of used properties is presented in previous sections.

Figure 3-1 and 3-2 show Darcy velocity vectors on a vertical section through the middle of the model for Case 1 with a borehole distance of 100 m after 10 years of simulation. Flow paths for particles released at five different depths in the buffer material of the boreholes are shown in black.

Figure 3-1. *Case 1 with a borehole distance of 100 m. Vertical section through the middle of the model showing Darcy velocity vectors. Flow paths are illustrating flow field at simulation time 10 years.*
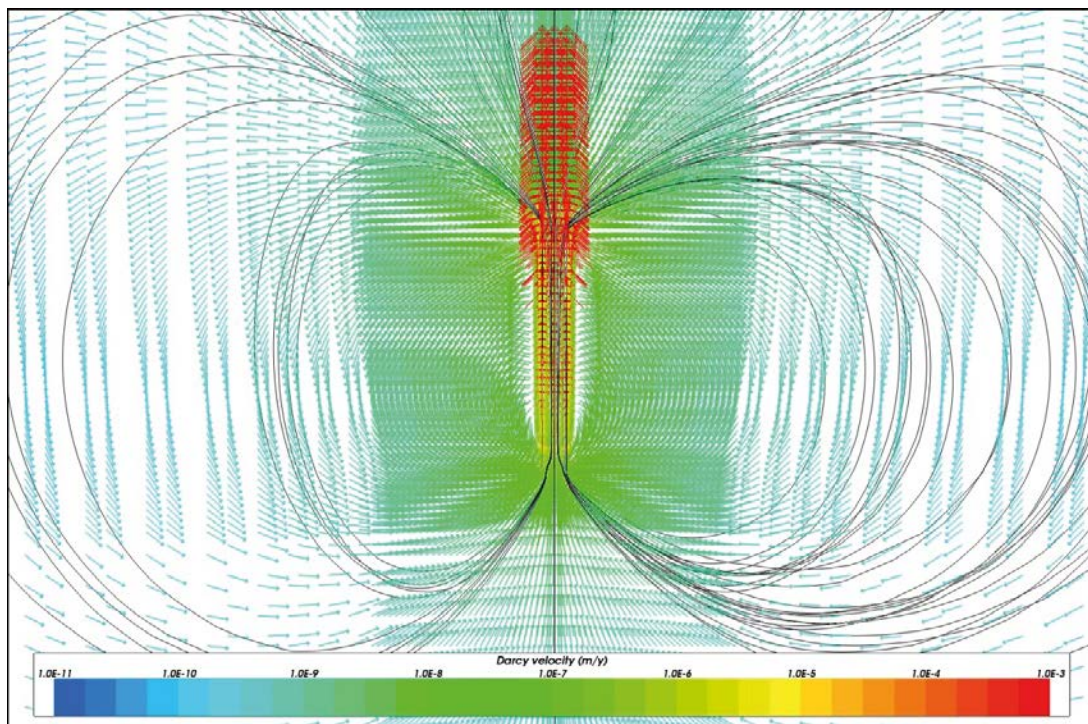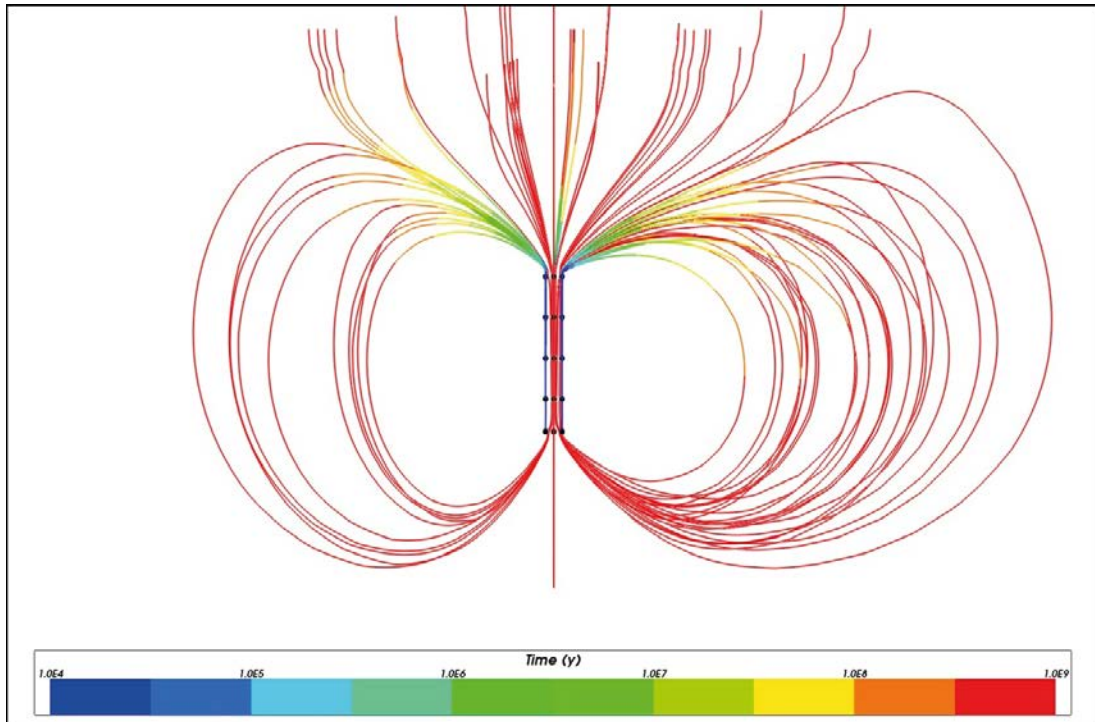
Figure 3-2. Case 1 with a borehole distance of 100 m. Vertical section (close-up view) showing Darcy velocity vectors. Flow paths are illustrating flow field at simulation time 10 years.

The velocity field around the boreholes is symmetric. This is expected however, since the whole model set-up is symmetric, including boundary conditions and geometries. There is slight skewness in the pathway pattern pushing some particles further out to the right in the picture. The reason for this is that the particles are not released symmetrically inside the boreholes. The particle release locations were calculated by adding 20 cm to the borehole centre coordinate (this corresponds to the buffer around the canisters), which consequently places the particles to the right (east) of the borehole centres. It would of course have been possible to make the particle tracking fully symmetric by releasing the corresponding particles on the left hand side of the boreholes as well but this was not considered necessary.

When the groundwater is heated by the hot canisters inside the boreholes, buoyancy causes groundwater to rise along the more permeable sections of the boreholes. In the buffer material and the DZ the Darcy velocity reaches up to 10^{-3} m/year. This is still a very low value and it would take about 10^6 years for a particle to travel from the mid-section of the borehole (Z=–4,000 m) to exit the top of the buffer zone at Z=–3,000 m. This travel time is significantly longer than the duration of the heat input from the spent fuel, hence the calculated flow time is only hypothetical. Above the repository area, the flow is vertical and directed out through the top surface of the model. When the groundwater flow along the vertical sides of the repository reaches above the canisters it bends off in an outward direction from the repository forming a large convection cell around the repository area. However, it should be noted that the flow velocities are very low, typically in the range of 10^{-8}–10^{-10} m/year outside the repository, meaning that the mixing of freshwater and brine and flushing of the system is extremely slow. This is also reflected in the advective travel times for the released particles, see Figure 3-3, where the pathways of the released particles are coloured by travel time along the paths. The calculated range for particles released at 10 years is about 10^8 years. Obviously, such extreme time scales are only hypothetical and not very meaningful since the flow field, due to *inter alia* the decay of the heat source, would have changed completely during the time period. Thus, the conclusion should be that postulating the given boundary conditions, bedrock and repository characteristics, the groundwater situation in and around the repository is stable and the resulting flow velocities very small.
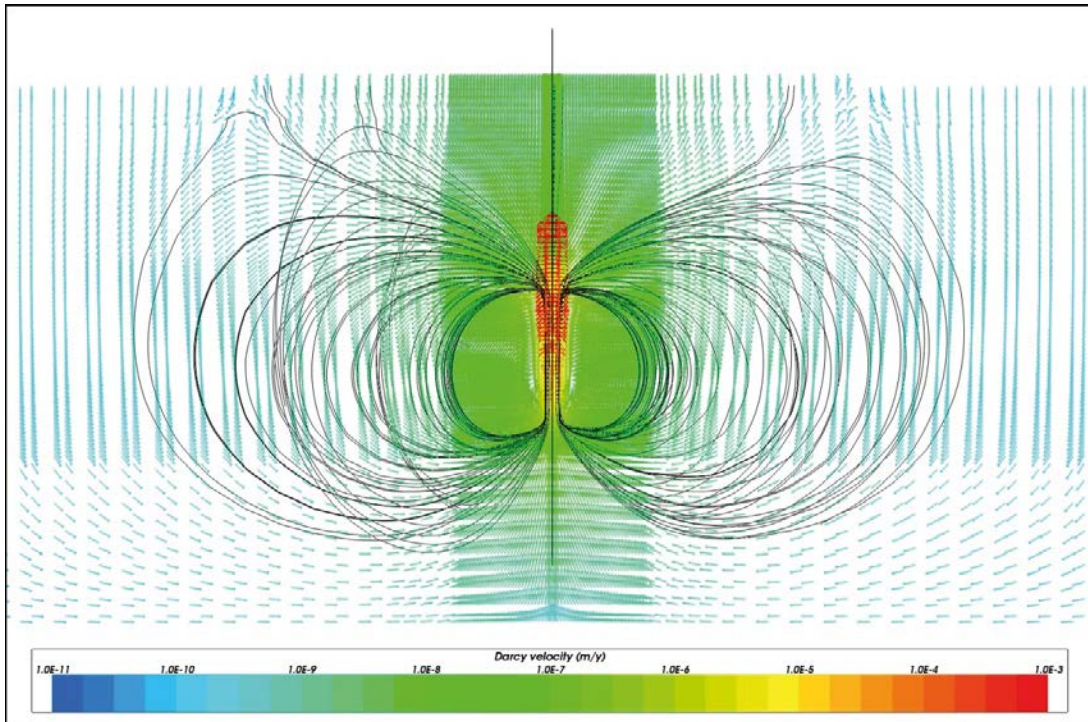
Figure 3-3. *Case 1 with a borehole distance of 100 m. Vertical section showing flow paths coloured by advective travel time along the paths. Flow paths are illustrating flow field at simulation time 10 years.*

It should be noted that the pathways generated in a fully symmetric model will not behave as would be expected in a model with a realistic rock structure representation and a top boundary reflecting the topography. In such a case, there would be more particles going straight to the top boundary. However, there are particles started from the centre boreholes, which do not fall into this numerically induced loop, and therefore provide reasonable results regarding travel time. As a further consequence of this particle behaviour, it would not be meaningful to perform a full statistical analysis of the ensemble of released particles. Rather one has to select a subset of particles that actually reach the top surface directly from the release locations without making an artificial loop through the model. This will give an indication of what time range to expect from the particle travel times.

In Table 3-3, a statistical summary of the modelled cases is shown. The table shows the minimum and maximum values of the calculated transport performance measures. The maximum initial Darcy velocity is $2.8 \cdot 10^{-3}$ m/year and the minimum travel time is $1.8 \cdot 10^8$ years. It is also clear that the shortest pathways come from particles released at the top of the canister sections of the boreholes.

Figure 3-4 to 3-6 show results for a snapshot at 100 years of simulation time. The results are somewhat different to the situation at 10 years even if the orientation of the flow field is similar to before. The magnitude of the Darcy velocity has increased about an order of magnitude outside and above the repository volume due to the conduction of heat radially out from the canisters to the rock. Between the boreholes, however, the velocities have decreased somewhat due to the decrease in canister temperature and hence loss of thermal driving force. The combined effect of this is shorter travel time for some paths. The statistics in Table 3-3 confirm this picture and show that the initial Darcy velocity has decreased slightly at 100 years. On the other hand, the travel time has decreased by one order of magnitude, which would seem to be in contradiction to the change in initial Darcy velocity. The explanation is however that even if the velocities in the boreholes have decreased, the velocities outside the canister section have increased even more so the combined effect is still faster particles measured up to the top surface.

Figure 3-4. Case 1 with a borehole distance of 100 m. Vertical section through the middle of the model showing Darcy velocity vectors. Flow paths are illustrating flow field at simulation time 100 years.
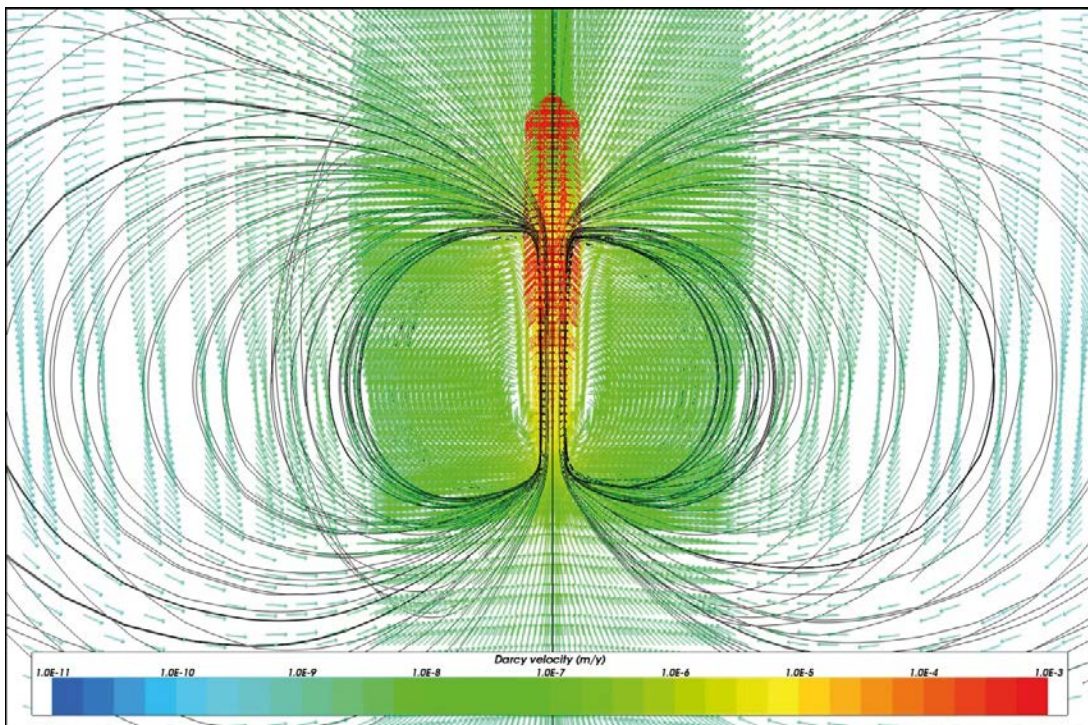
Figure 3-5. Case 1 with a borehole distance of 100 m. Vertical section (close-up view) showing Darcy velocity vectors. Flow paths are illustrating flow field at simulation time 100 years.

SKB P-13-10
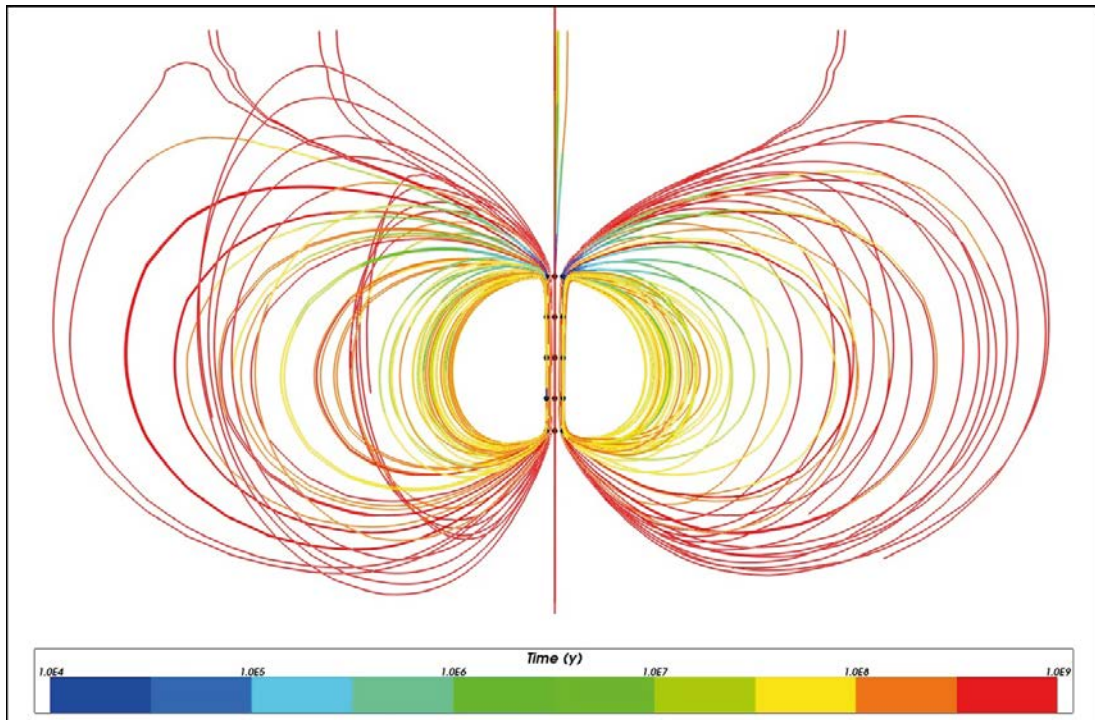
Figure 3-6. *Case 1 with a borehole distance of 100 m. Vertical section showing flow paths coloured by advective travel time along the paths. Flow paths are illustrating flow field at simulation time 100 years.*

3.2.2 Case 2: 52 m borehole distance

Case 2 is based on the Case 1 model and makes use of the same properties in all aspects with the exception for the distance between boreholes. The same number of boreholes (nine) were used with the same properties as in Case 1 but the distance between them was reduced to 52 m instead of 100 m. The distance between the boreholes affects the temperature of the rock between the boreholes because the conduction of heat away from the repository area is limited by the rock volume within the repository. This means that there will be a critical distance between the boreholes under which the temperature in the rock will increase enough to create significant upward flow jeopardising the stability of the brine at depth. In Marsic et al. (2006), the distance between the boreholes was 500 m and there was no significant heat effect on the rock between the boreholes. The purpose of this sensitivity is to analyse what the effects are on groundwater flow when the boreholes are placed closer together.

Figure 3-7 and 3-8 show Darcy velocity vectors on a vertical section through the middle of the model for Case 2 with a borehole distance of 52 m after 10 years of simulation. Flow paths for particles released at five different depths in the buffer material of the boreholes are shown in black. The groundwater flow pattern and water velocities around the boreholes are broadly the same as for Case 1.

In Figure 3-9, the pathways of the released particles are coloured by travel time along the paths. The figure shows that the travel times are of the same magnitude, about 10^8 years, as for the previous case after 10 years of simulation.

The transport performance measures shown in Table 3-3 confirm what it seen in Figure 3-7 to 3-9. The maximum initial Darcy velocity is $3 \cdot 10^{-3}$ m/year which is slightly higher than for Case 1 and the minimum travel time is $1.2 \cdot 10^8$ years which is somewhat shorter than for Case 1. It is also clear that the shortest pathways come from particles released at the top of the canister sections of the boreholes.
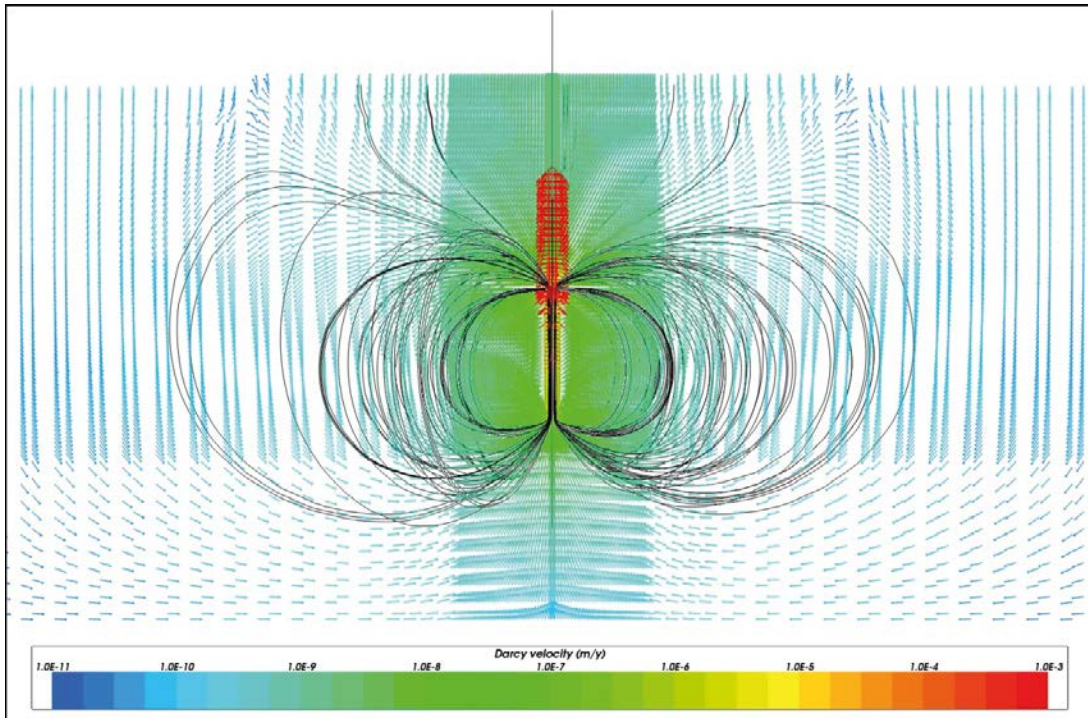
Figure 3-7. *Case 2 with a borehole distance of 52 m. Vertical section through the middle of the model showing Darcy velocity vectors. Flow paths are illustrating flow field at simulation time 10 years.*
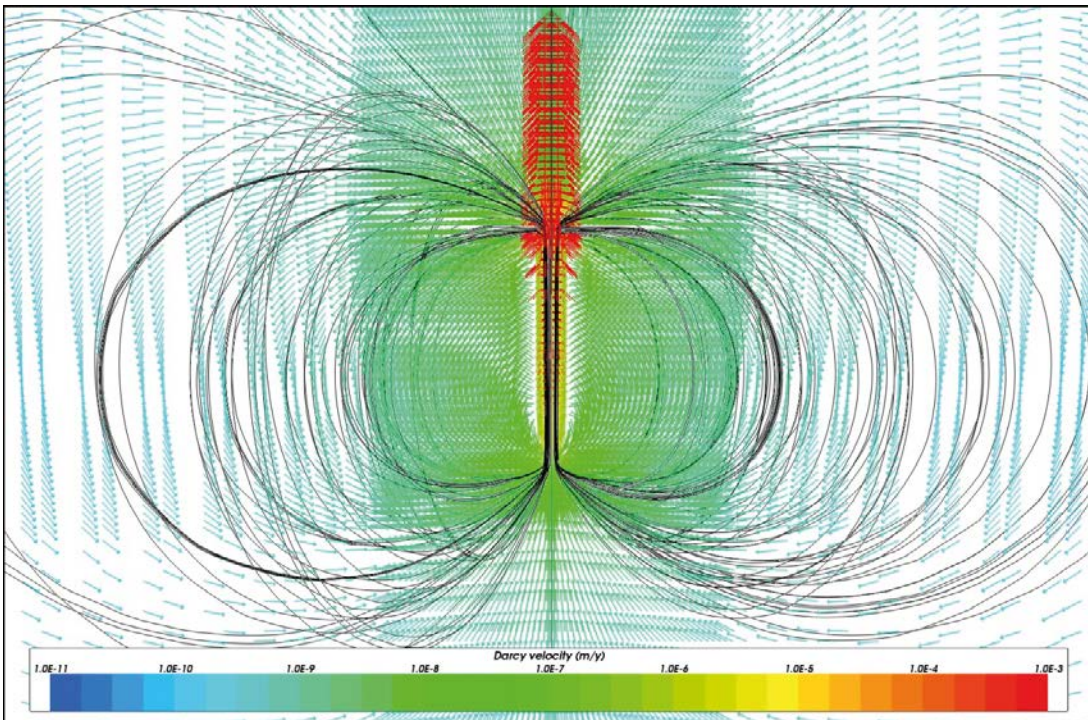
Figure 3-8. *Case 2 with a borehole distance of 52 m. Vertical section (close-up view) showing Darcy velocity vectors. Flow paths are illustrating flow field at simulation time 10 years.*
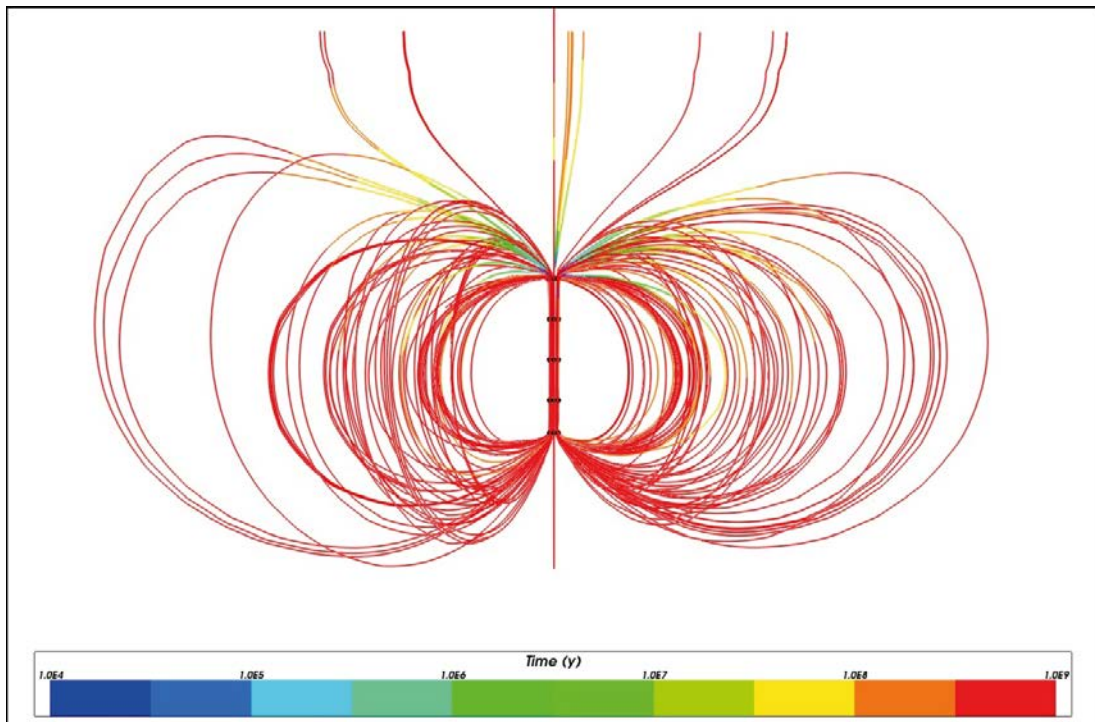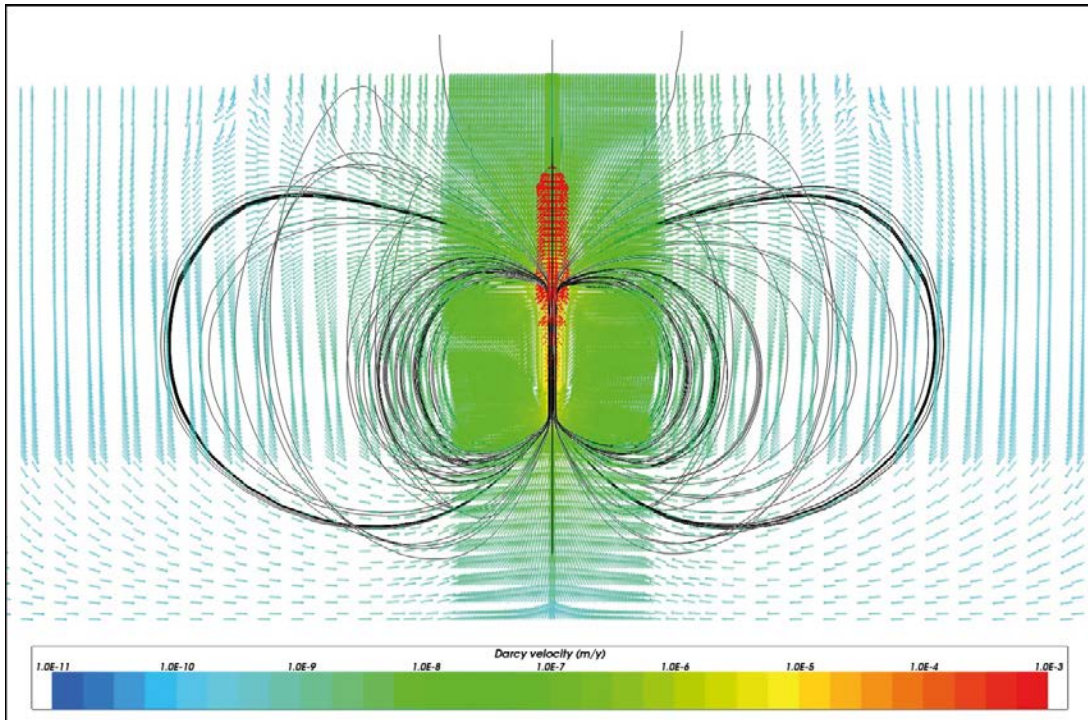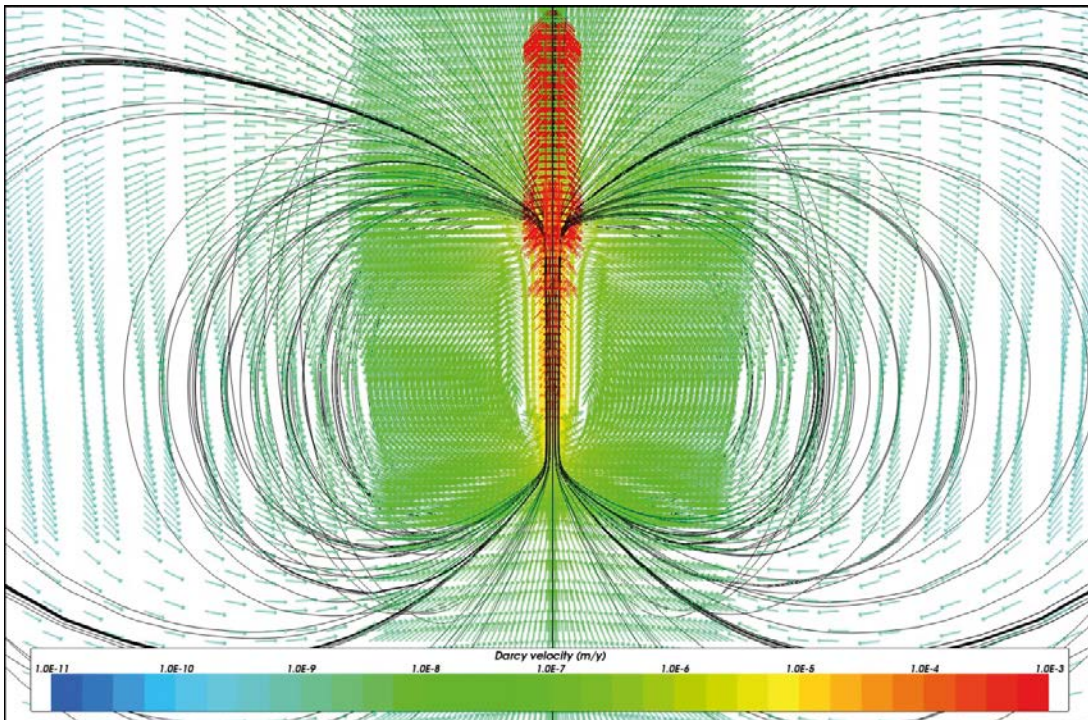
Figure 3-9. Case 2 with a borehole distance of 52 m. Vertical section showing flow paths coloured by advective travel time along the paths. Flow paths are illustrating flow field at simulation time 10 years.

Figure 3-10 to 3-12 show results for a snapshot at 100 years of simulation time for Case 2. The results are somewhat different to the situation at 10 years even if the orientation of the flow field is similar to before. The magnitude of the Darcy velocity has increased about an order of magnitude outside and above the repository volume due to the conduction of heat radially out from the canisters to the rock.

In Case 1, using a 100 m borehole distance, the temperature decreased with time close to the boreholes while the temperature between the boreholes remained raised by approximately 5°C, compared to the geothermal gradient, for a couple of hundred years. With the reduced borehole distance in Case 2, the heating effect on the surrounding rock is much more pronounced. The raise in temperature remains at about 10°C for a few hundred years and subsequently causes an increase in groundwater flow velocities

The statistics in Table 3-3 confirm this and show that the initial Darcy velocity has increased slightly at 100 years compared to the results for 10 years. Comparing the statistics between Case 1 and Case 2 shows that there are some effects on performance measures from decreasing the borehole distance. The Darcy velocities are higher and the travel times are slightly shorter. It should be noted however that the number of particles reaching the top surface is quite sparse and therefore the statistics might be biased.

Figure 3-10. *Case 2 with a borehole distance of 52 m. Vertical section through the middle of the model showing Darcy velocity vectors. Flow paths are illustrating flow field at simulation time 100 years.*

Figure 3-11. *Case 2 with a borehole distance of 52 m. Vertical section (close-up view) showing Darcy velocity vectors. Flow paths are illustrating flow field at simulation time 100 years.*
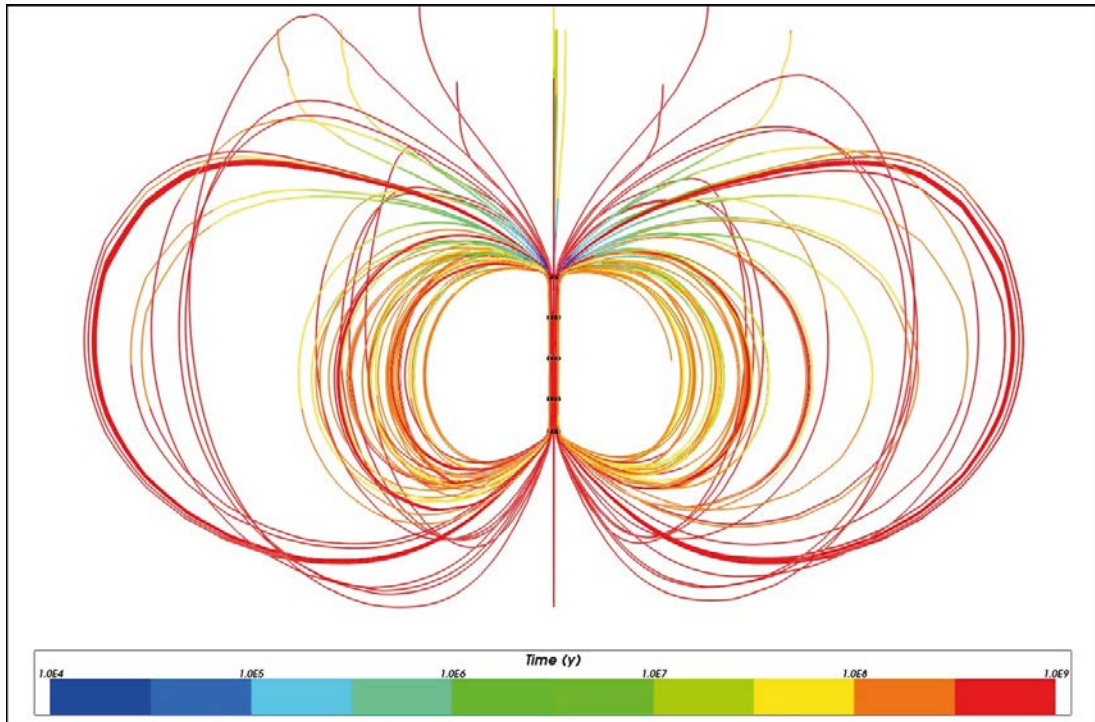
Figure 3-12. *Case 2 with a borehole distance of 52 m. Vertical section showing flow paths coloured by advective travel time along the paths. Flow paths are illustrating flow field at simulation time 100 years.*

3.3   Sensitivity to borehole properties

This section examines the effects of poor backfill properties in the boreholes. The upper part of the boreholes, i.e. down to 3,000 m depth, includes various materials such as concrete, asphalt and bentonite. The deeper section of the boreholes, between 3,000 and 5,000 m depth include the buffer material around the canisters and the damaged zone (DZ) around the drilled boreholes.

The hydraulic properties of the sealing and buffer materials were changed according to the scheme shown in Table 3-2. The initial purpose of conducting an extensive sensitivity analysis of the hydraulic properties was to investigate some numerical issues occurring when solving the models. That is the reason for making stepwise changes to the hydraulic properties one at a time. In the final variant, with the highest permeabilities[1], the following changes were made compared to Case 1 and Case 2:

- The SEALING permeability was changed from $5 \cdot 10^{-18}$ m^2 to $5 \cdot 10^{-14}$ m^2.

- The BUFFER permeability was changed from $1 \cdot 10^{-16}$ m^2 to $1 \cdot 10^{-14}$ m^2.

These variants, Case 3 and Case 4, are the only ones reported together with Case 1 and Case 2, for 100 m and 52 m borehole distance respectively.

---

[1] Hydraulic conductivity K (m/s) is often used instead of permeability k (m^2): K= k·(ρ·g/μ) where ρ is the density of the fluid, g is the acceleration of gravity and μ is the dynamic viscosity of the fluid.

Table 3-2. Summary of sensitivities. Reported cases (1–6) are coloured in green and marked in bold. The hydraulic properties that were changed compared to the Base Case are marked in red.

Case	Model	Sealing (m²)	Buffer (m²)	Borehole c/c (m)
1	DBH_heat_2_3	5E–18	1E–16	100
	DBH_heat_2_4	5E–18	5E–16	100
	DBH_heat_2_5	5E–18	1E–15	100
	DBH_heat_2_6	5E–18	5E–15	100
	DBH_heat_2_7	5E–18	1E–14	100
	DBH_heat_2_8	1E–17	1E–16	100
	DBH_heat_2_9	5E–17	1E–16	100
	DBH_heat_2_10	1E–16	1E–16	100
	DBH_heat_2_11	5E–16	1E–16	100
	DBH_heat_2_12	5E–17	1E–15	100
	DBH_heat_2_13	5E–17	1E–14	100
	DBH_heat_2_14	5E–16	1E–15	100
	DBH_heat_2_15	5E–16	1E–14	100
	DBH_heat_2_16	5E–15	1E–14	100
3	DBH_heat_2_17	5E–14	1E–14	100
2	DBH_heat_3_3	5E–18	1E–16	52
	DBH_heat_3_4	5E–18	5E–16	50
	DBH_heat_3_7	5E–18	1E–14	50
	DBH_heat_3_11	5E–16	1E–16	50
	DBH_heat_3_12	5E–17	1E–15	50
	DBH_heat_3_14	5E–16	1E–15	50
	DBH_heat_3_15	5E–16	1E–14	50
	DBH_heat_3_16	5E–15	1E–14	50
4	DBH_heat_3_17	5E–14	1E–14	52
5	DBH_heat_6_3	5E–18	1E–16	100
6	DBH_heat_6_17	5E–14	1E–14	100

3.3.1 Case 3: 100 m borehole distance

Case 3 is based on the Case 1 model but with the hydraulic properties of the sealing and the buffer changed as follows:

The SEALING permeability was changed from $5 \cdot 10^{-18}$ m² to $5 \cdot 10^{-14}$ m².

The BUFFER permeability was changed from $1 \cdot 10^{-16}$ m² to $1 \cdot 10^{-14}$ m².

The sealing and buffer materials in the boreholes are crucial for the function of the deep borehole repository. A highly permeable backfill provides fast pathways from the canisters up to the surface. This effect can be enhanced by the heating of the rock around the boreholes and the choice of borehole distance in the repository. The purpose of this variant is to analyse the effect of poor backfill properties in the boreholes, on the groundwater flow.

Figure 3-13 and 3-14 show Darcy velocity vectors on a vertical section through the middle of the model for Case 3 with a borehole distance of 100 m after 10 years of simulation. Flow paths for particles released at five different depths in the buffer material of the boreholes are shown in black. The groundwater flow pattern around the boreholes differs significantly compared to Case 1 even if the water velocities are very similar. All along the borehole, what was previously a very regular flow pattern is now disturbed and forming local circular convection cells along the full length of the boreholes.
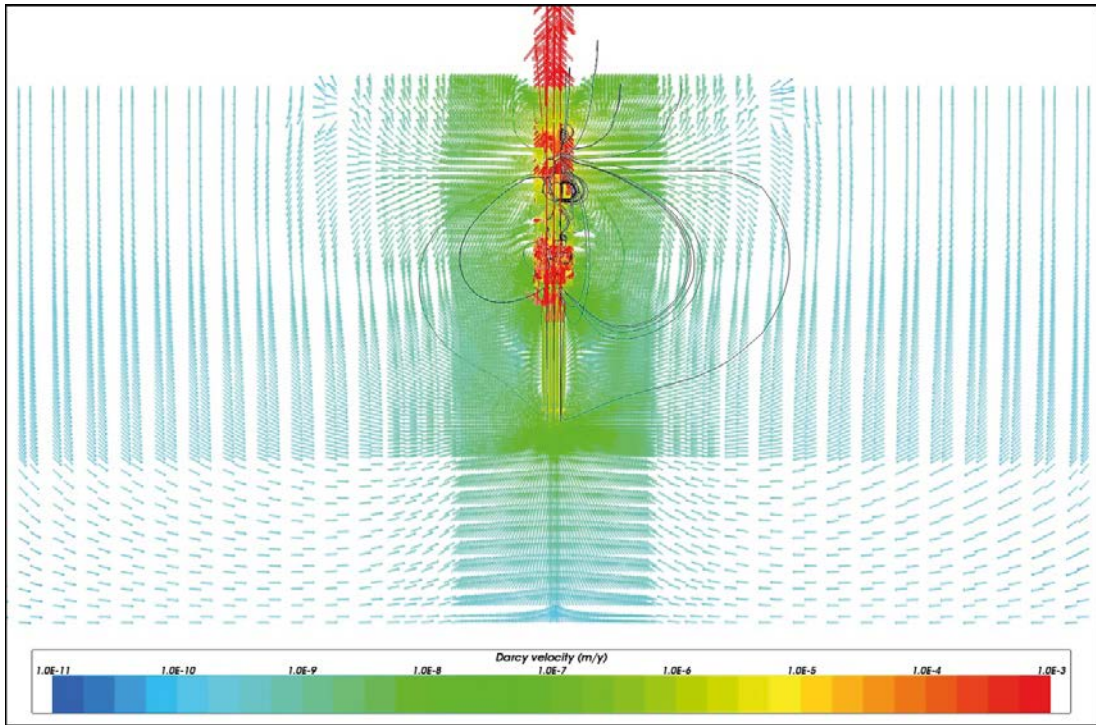
Figure 3-13. *Case 3 with a borehole distance of 100 m. Vertical section through the middle of the model showing Darcy velocity vectors. Flow paths are illustrating flow field at simulation time 10 years.*
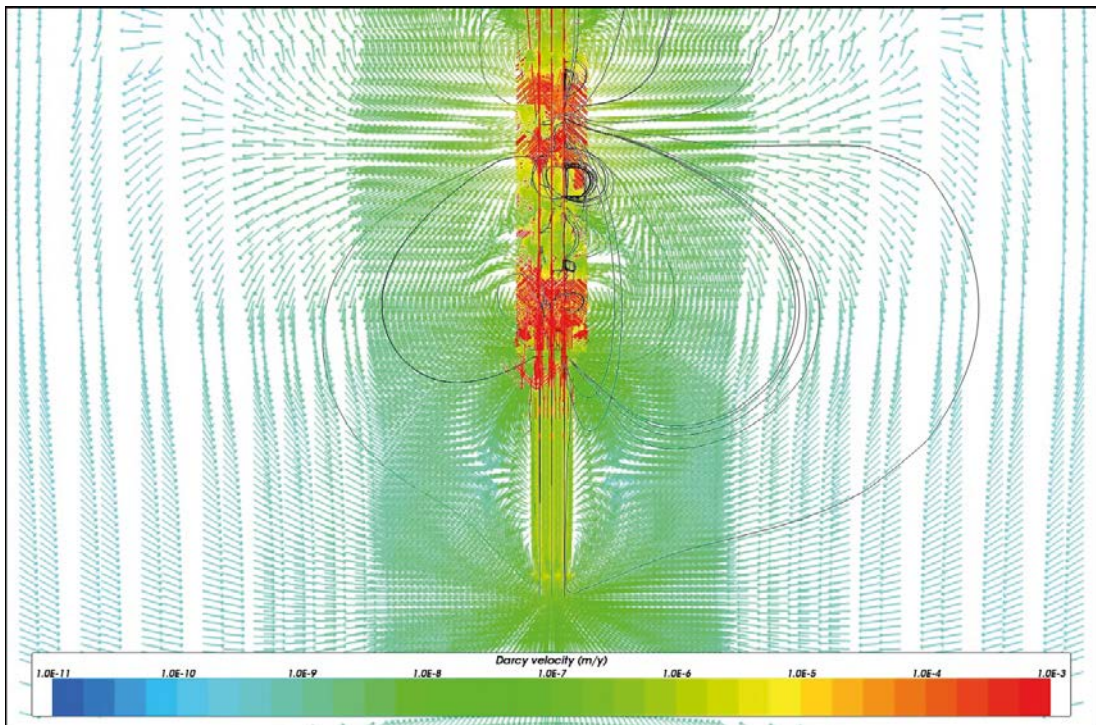
Figure 3-14. *Case 3 with a borehole distance of 100 m. Vertical section (close-up view) showing Darcy velocity vectors. Flow paths are illustrating flow field at simulation time 10 years.*

In Figure 3-15, the pathways of the released particles are coloured by travel time along the paths. The figure shows that the travel times have decreased about two orders of magnitude, to approximately 10^6 years, compared to Case 1 after 10 years of simulation.

In Figure 3-16 and 3-17, the brine distribution is shown on a vertical section through the middle of the model for Case 3 after 10 years of simulation. In the close-up view over the brine interface, it can be seen that the brine has started to move upwards along the permeable boreholes, while freshwater is moving downwards from the top. This change in the flow pattern compared to Case 1 is caused by the increased permeability of the buffer and the sealing in combination with the heat from the canisters. The generated heat from the canisters warms up the saline groundwater and the density decreases which forces the saline groundwater to move upwards in the boreholes. The created convection causes freshwater to move in the opposite direction downwards into the boreholes. The asymmetric behaviour of the salinity distribution indicates that there might be some numerically induced effects in the solution, possibly caused by the heavily distorted elements within the boreholes. It is however hard to estimate the magnitude of this problem.

The transport performance measures shown in Table 3-3 confirm what is seen in Figure 3-13 to Figure 3-15. The maximum initial Darcy velocity is $3 \cdot 10^{-3}$ m/year which is the same as for Case 1 and the minimum travel time is $1.8 \cdot 10^6$ years which is much shorter than for Case 1. As before, the shortest pathways come from particles released at the top of the canister sections of the boreholes.

Figure 3-18 to Figure 3-22 show results for a snapshot at 100 years of simulation time for Case 3. As before, the groundwater flow pattern is still disturbed by localised convection cells. The water velocities have increased both inside and outside of the boreholes due to the generated heat from the canisters.

After 100 years of simulation, the brine has mixed considerably with freshwater over the initial brine interface, see Figure 3-21 and 3-22. The up-coning of brine has almost reached the elevation of the down coming freshwater.
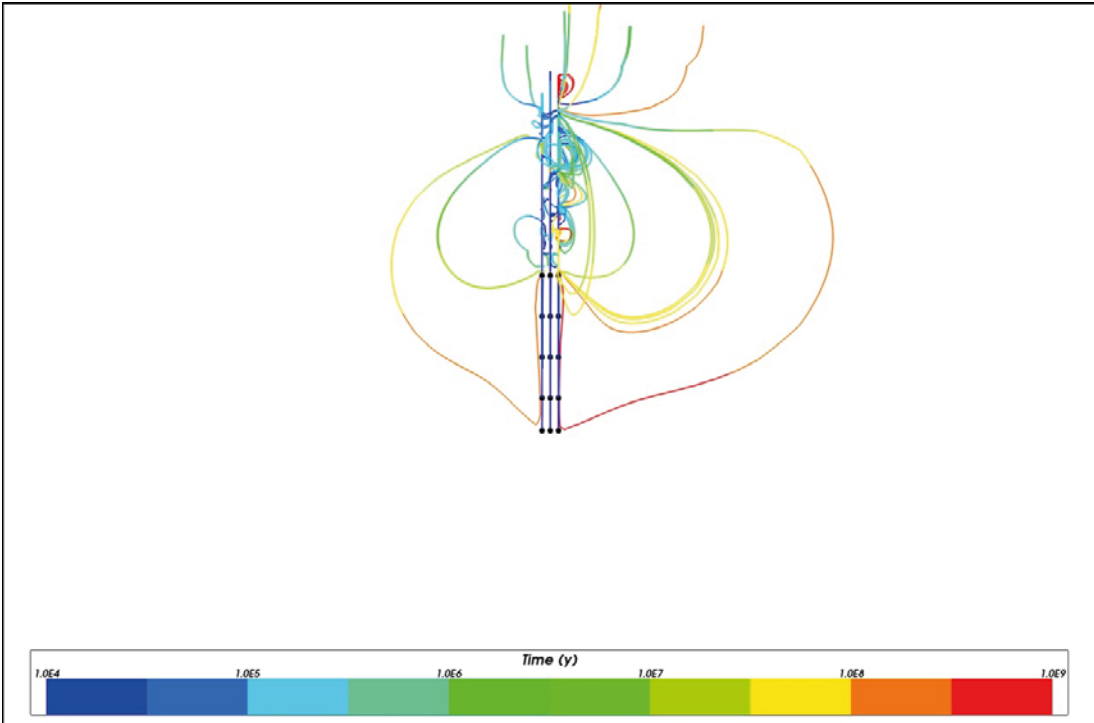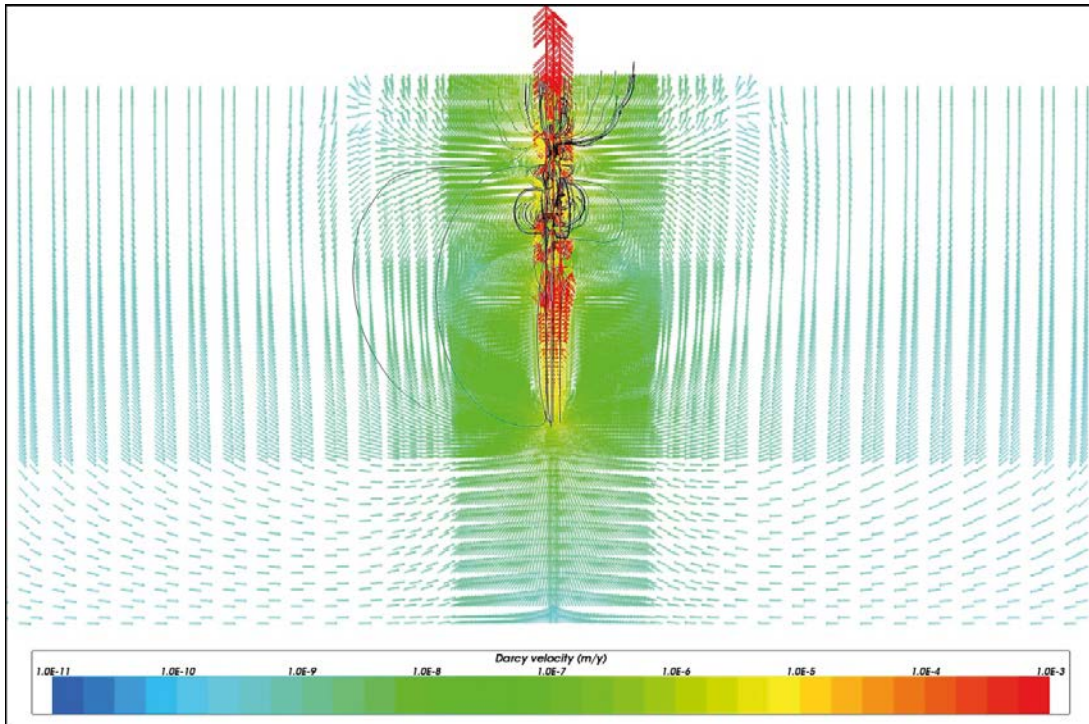

Figure 3-15. Case 3 with a borehole distance of 100 m. Vertical section showing flow paths coloured by advective travel time along the paths. Flow paths are illustrating flow field at simulation time 10 years.
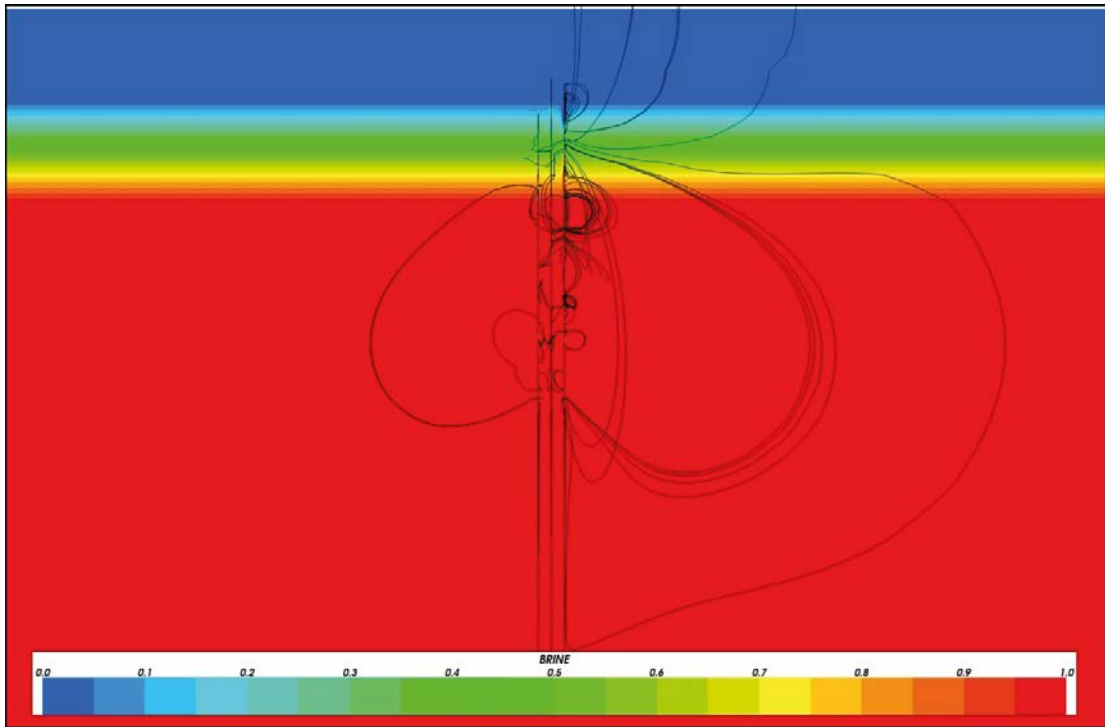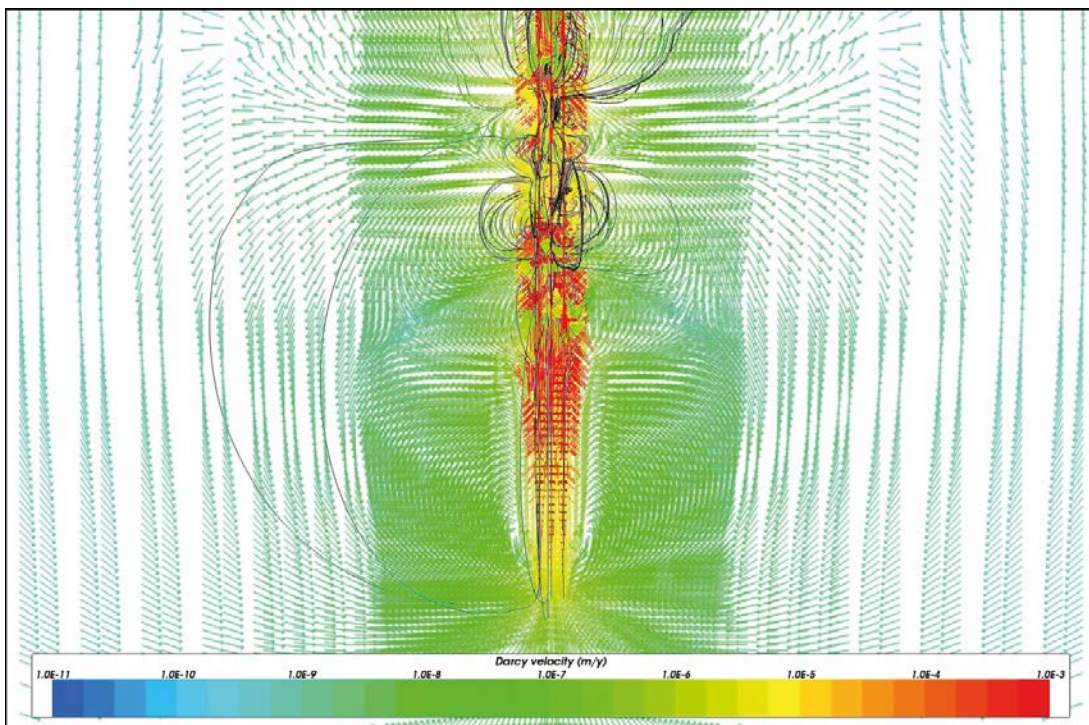
Figure 3-16. Case 3 with a borehole distance of 100 m. Vertical section through the middle of the model showing the brine distribution. Flow paths are illustrating flow field at simulation time 10 years.
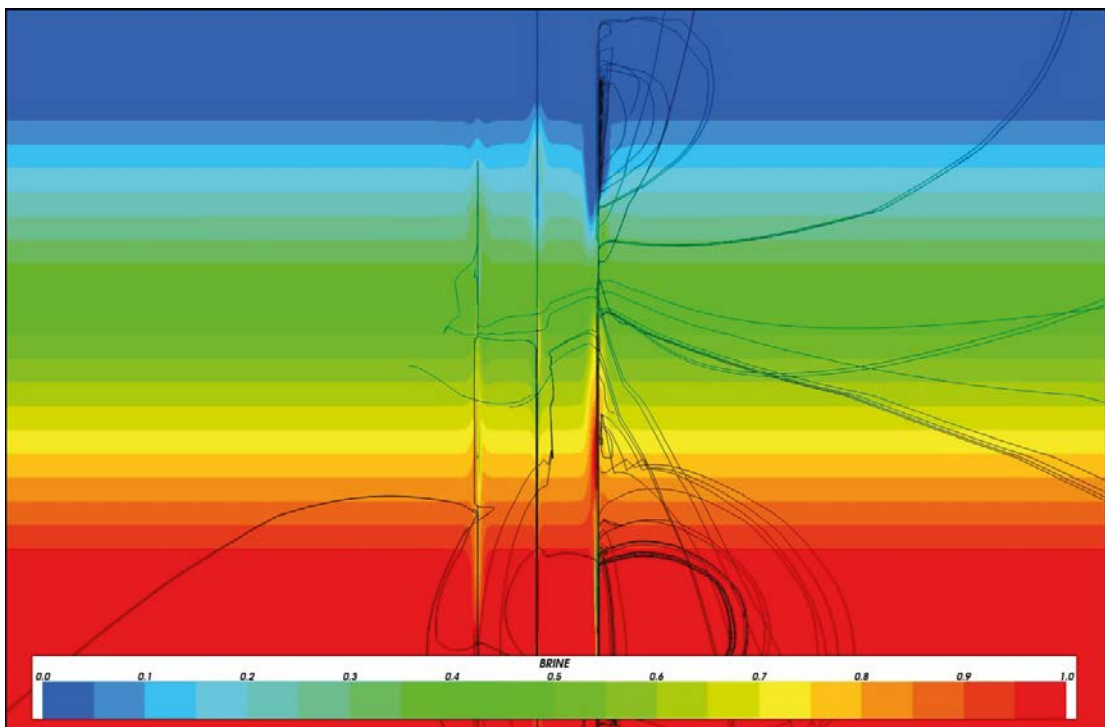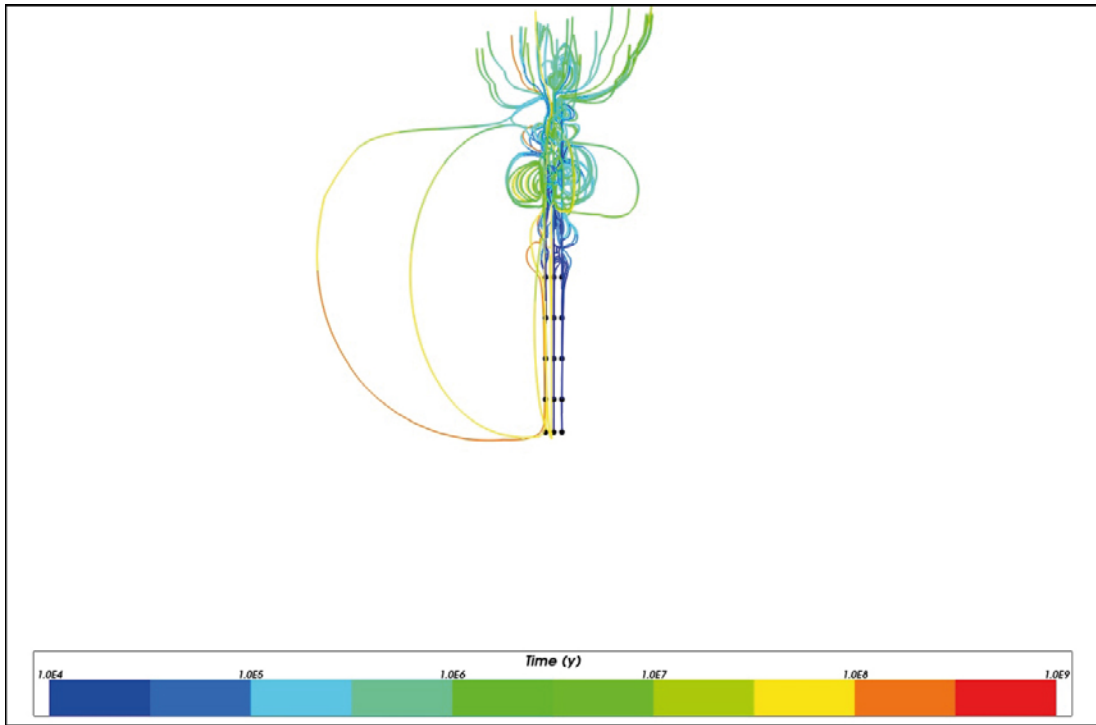

Figure 3-17. Case 3 with a borehole distance of 100 m. Vertical section (close-up view) showing the brine distribution. Flow paths are illustrating flow field at simulation time 10 years.
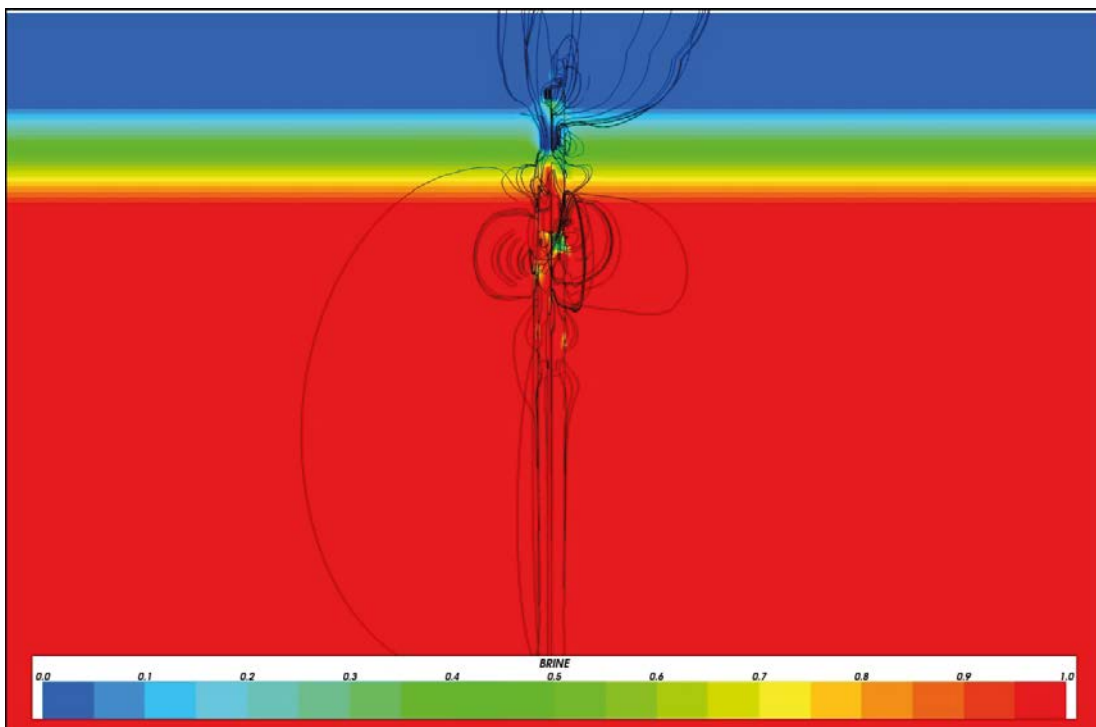
Figure 3-18. *Case 3 with a borehole distance of 100 m. Vertical section through the middle of the model showing Darcy velocity vectors. Flow paths are illustrating flow field at simulation time 100 years.*
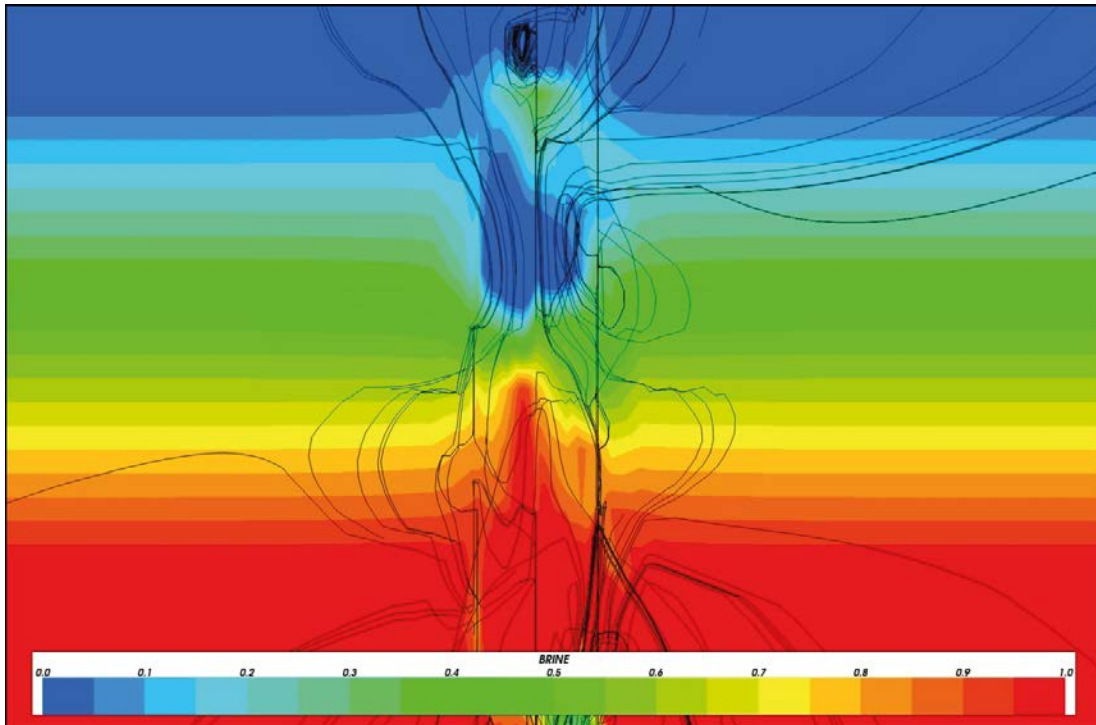

Figure 3-19. *Case 3 with a borehole distance of 100 m. Vertical section (close-up view) showing Darcy velocity vectors. Flow paths are illustrating flow field at simulation time 100 years.*

Figure 3-20. *Case 3 with a borehole distance of 100 m. Vertical section showing flow paths coloured by advective travel time along the paths. Flow paths are illustrating flow field at simulation time 100 years.*

Figure 3-21. *Case 3 with a borehole distance of 100 m. Vertical section through the middle of the model showing the brine distribution. Flow paths are illustrating flow field at simulation time 100 years.*

Figure 3-22. Case 3 with a borehole distance of 100 m. Vertical section (close-up view) showing the brine distribution. Flow paths are illustrating flow field at simulation time 100 years.

The statistics in Table 3-3 show that the minimum travel time has decreased by one order of magnitude, compared to the results for 10 years. The fastest paths are now at $3.6 \cdot 10^5$ years. The statistics suggest that the maximum initial Darcy velocity actually has decreased, but the velocity vectors in Figure 3-19 indicate the opposite. The explanation could be the small statistical population, which might not capture the whole situation along the boreholes. In addition, the particles are always released very close to the canister, which might skew the results compared to what is going on in the flow field further out radially in the borehole.

3.3.2 Case 4: 52 m borehole distance

In Case 4, the same material properties were used as in Case 3. The only difference is the reduced borehole distance, which is 52 m instead of 100 m.

Compared to the Case 1 model, the hydraulic properties of the sealing and the buffer were changed as follows:

- The SEALING permeability was changed from $5 \cdot 10^{-18}$ m^2 to $5 \cdot 10^{-14}$ m^2.
- The BUFFER permeability was changed from $1 \cdot 10^{-16}$ m^2 to $1 \cdot 10^{-14}$ m^2.

As for Case 3, the purpose of this variant is to analyse the effect of poor backfill properties in the boreholes, on the groundwater flow.

Figure 3-23 and 3-24 show Darcy velocity vectors on a vertical section through the middle of the model for Case 3 with a borehole distance of 52 m after 10 years of simulation. Flow paths for particles released at five different depths in the buffer material of the boreholes are shown in black. The groundwater flow pattern around the boreholes is similar to Case 3. All along the borehole, the flow pattern is disturbed and forming local circular convection cells along the full length of the boreholes.

In Figure 3-25, the pathways of the released particles are coloured by travel time along the paths. The figure shows that the travel times are of the same magnitude as in Case 3, i.e. approximately 10^6 years, after 10 years of simulation.
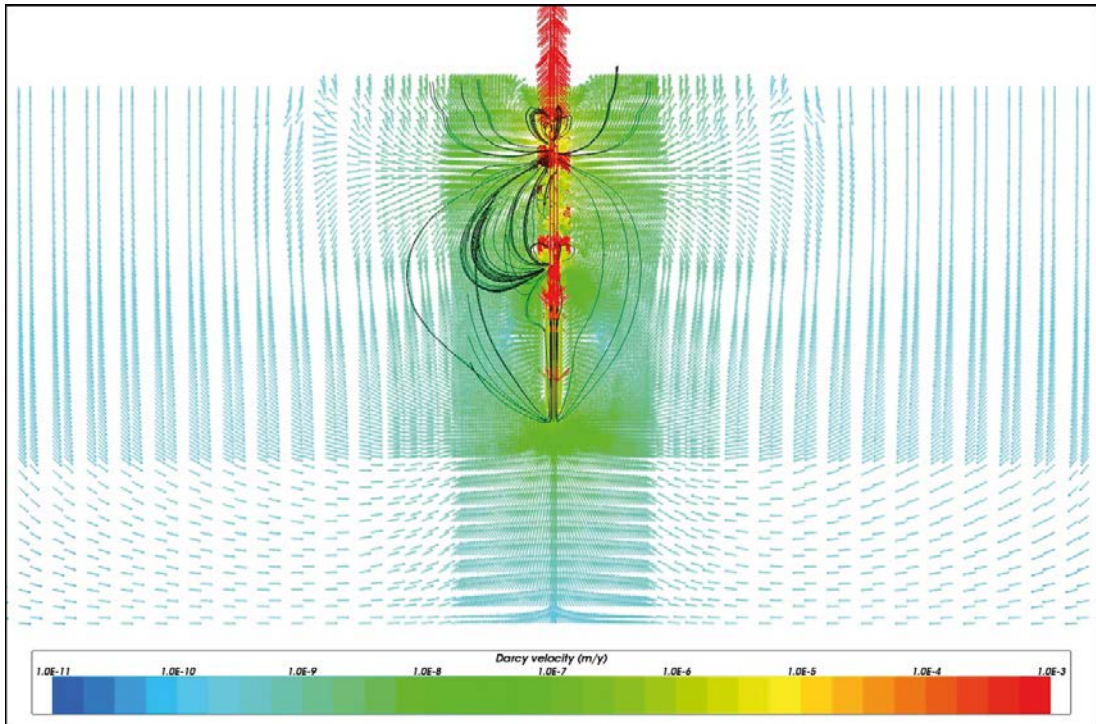
Figure 3-23. Case 4 with a borehole distance of 52 m. Vertical section through the middle of the model showing Darcy velocity vectors. Flow paths are illustrating flow field at simulation time 10 years.
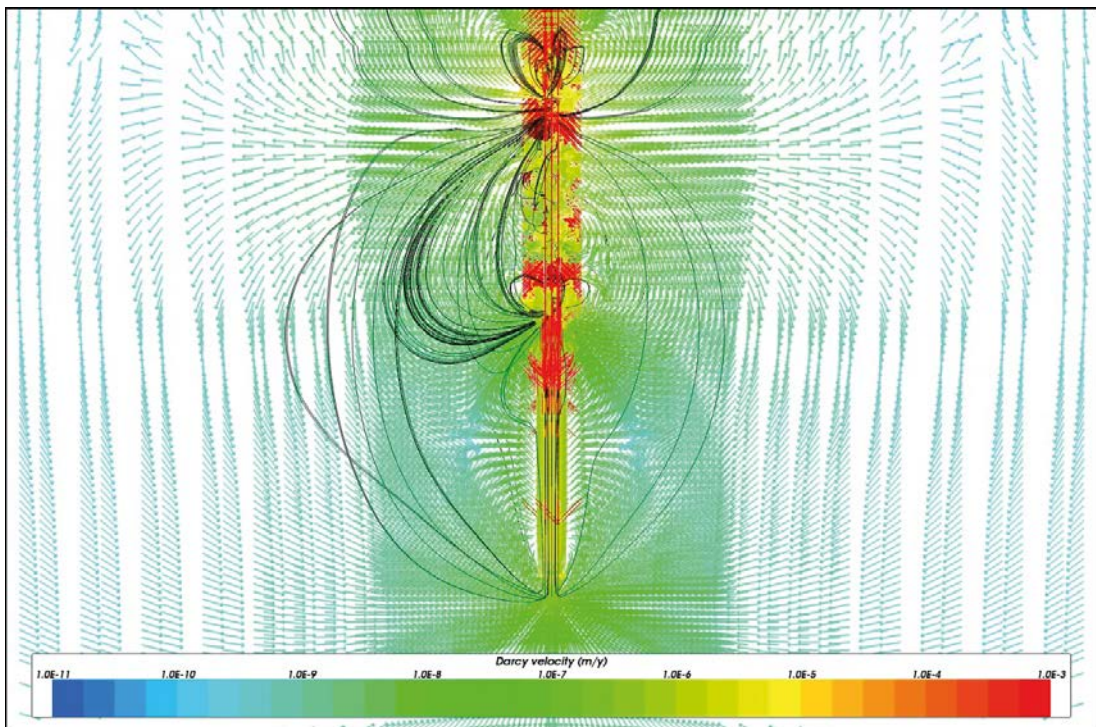
Figure 3-24. Case 4 with a borehole distance of 52 m. Vertical section (close-up view) showing Darcy velocity vectors. Flow paths are illustrating flow field at simulation time 10 years.
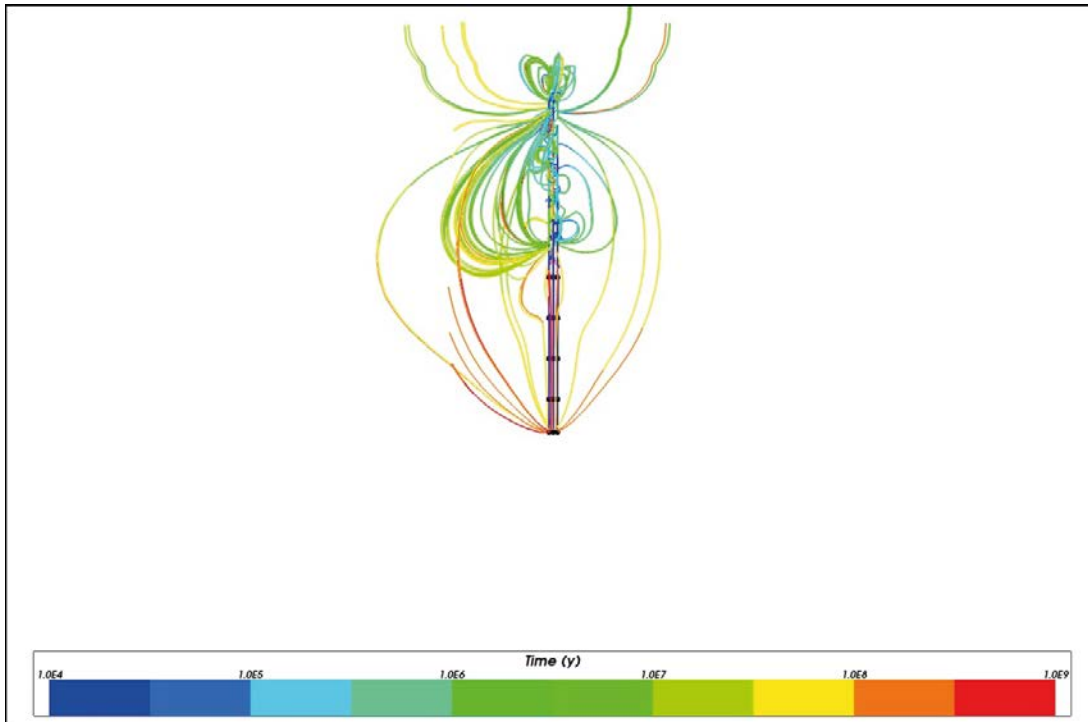
Figure 3-25. *Case 4 with a borehole distance of 52 m. Vertical section showing flow paths coloured by advective travel time along the paths. Flow paths are illustrating flow field at simulation time 10 years.*

In Figure 3-26 and 3-27, the brine distribution is shown on a vertical section through the middle of the model for Case 4 after 10 years of simulation. In the close-up view over the brine interface, it can be seen that the brine has started to move upwards along the permeable boreholes, while freshwater is moving downwards from the top. This situation is in line with the results seen for Case 3 and is caused by the increased permeability of the buffer and the sealing in combination with the heat from the canisters. The asymmetric behaviour of the salinity distribution indicates that there might be some numerically induced effects in the solution, possibly caused by heavily distorted elements within the boreholes. It is however hard to estimate the magnitude of this problem.

The transport performance measures are shown in Table 3-3. The maximum initial Darcy velocity is $3 \cdot 10^{-3}$ m/year which is the same as for Case 1 and Case 3 and the minimum travel time is $7.6 \cdot 10^{6}$ years which is much shorter than for Case 1 but slightly higher compared to Case 3 after 10 years of simulation. The latter fact is maybe slightly surprising since one would expect a shorter travel time with the decreased borehole distance but as stated earlier, with a small statistical population the results are not always as expected.

Figure 3-28 to Figure 3-32 show results for a snapshot at 100 years of simulation time for Case 4. As before, the groundwater flow pattern is disturbed by localised convection cells. Compared to the situation after 10 years of simulation, the water velocities have increased both inside and outside of the boreholes due to the generated heat from the canisters. The flow inside the boreholes are directed both upwards and downward.

After 100 years of simulation, the brine has mixed considerably with freshwater over the initial brine interface, see Figure 3-31 and 3-32. The mixing is even more extensive than for Case 3 and creates circular loops in the flow field, which can be seen from the flowpaths in the salinity transition area.

The statistics in Table 3-3 show that the minimum travel time has decreased by more than one order of magnitude, compared to the results for 10 years. The fastest paths are now at $1.7 \cdot 10^{5}$ years. The statistics also show that the maximum initial Darcy velocity actually has increased to $3.6 \cdot 10^{-3}$ m/year.
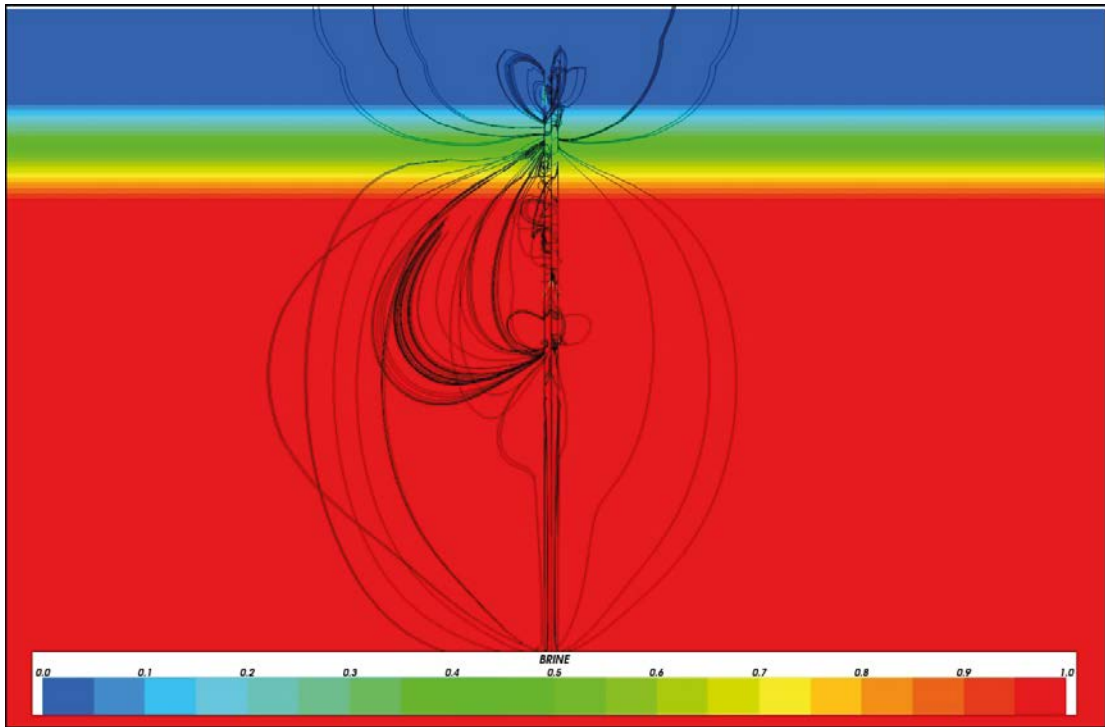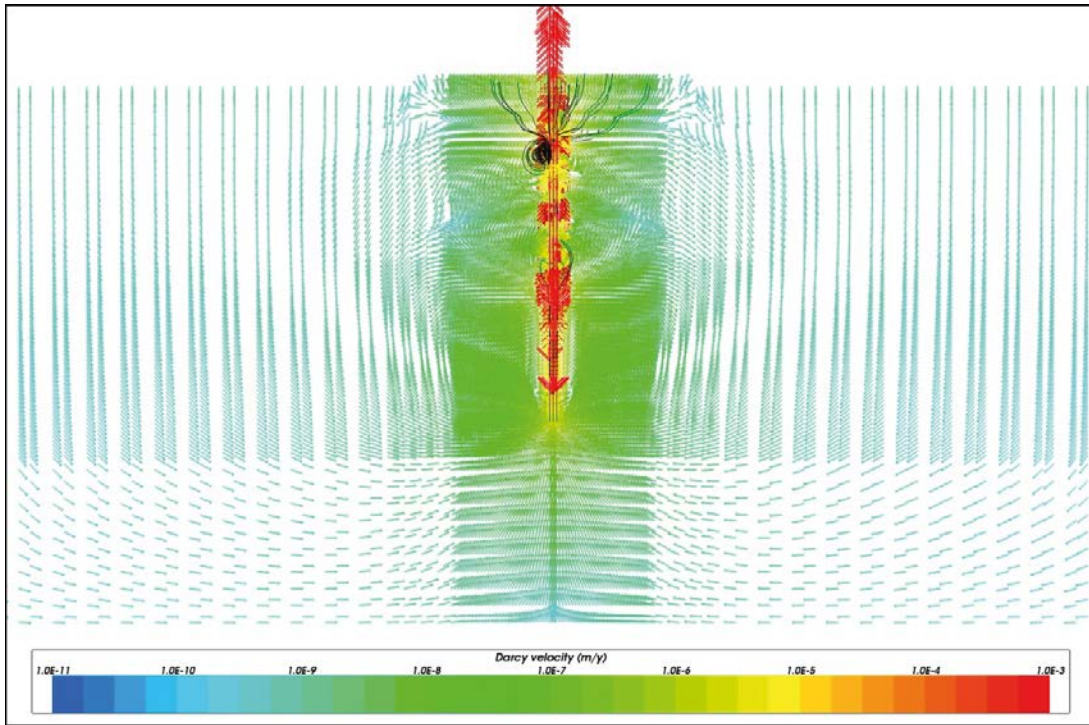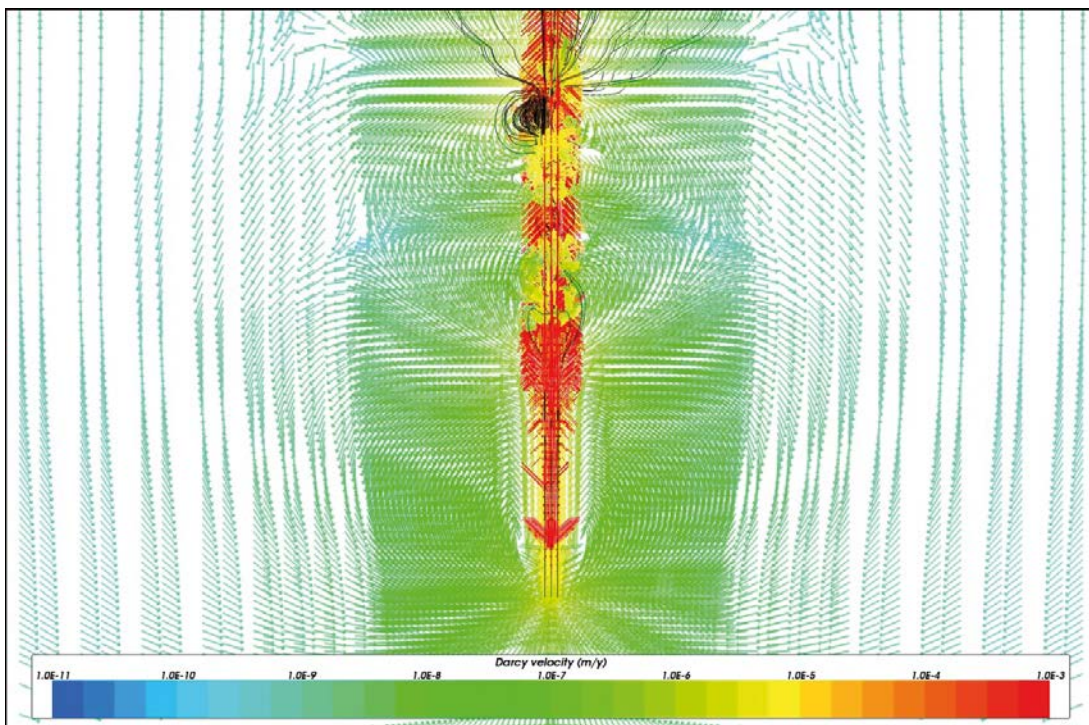
Figure 3-26. *Case 4 with a borehole distance of 52 m. Vertical section through the middle of the model showing the brine distribution. Flow paths are illustrating flow field at simulation time 10 years.*
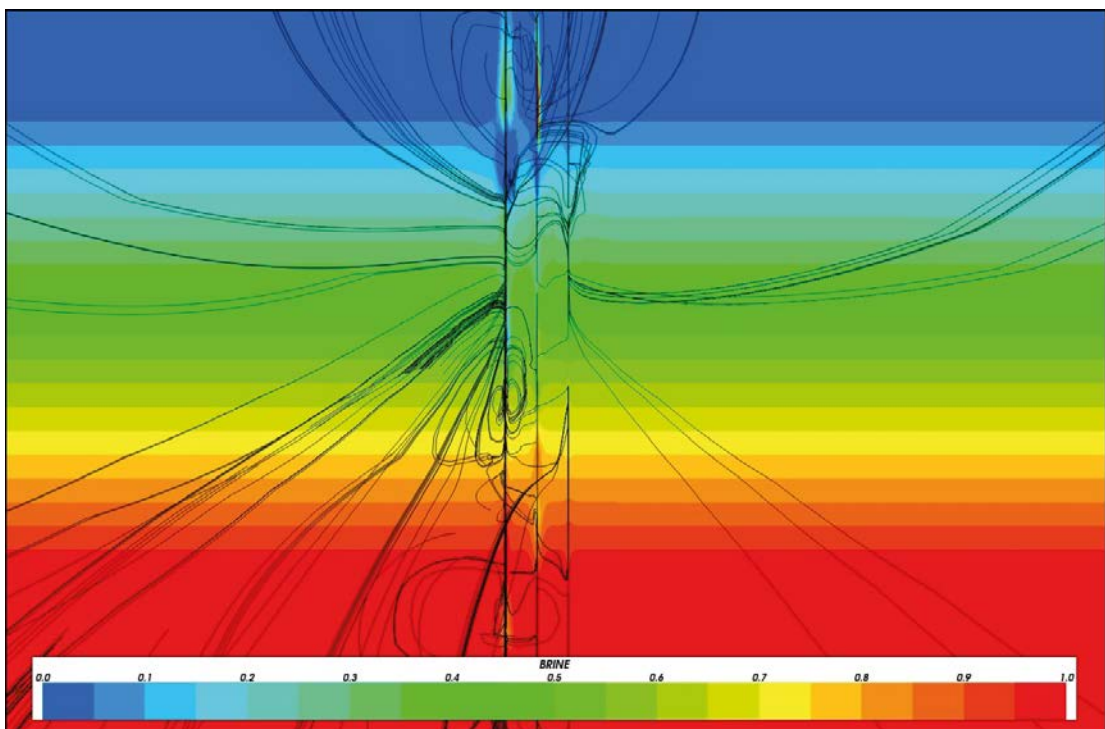
Figure 3-27. *Case 4 with a borehole distance of 52 m. Vertical section (close-up view) showing the brine distribution. Flow paths are illustrating flow field at simulation time 10 years.*

Figure 3-28. *Case 4 with a borehole distance of 52 m. Vertical section through the middle of the model showing Darcy velocity vectors. Flow paths are illustrating flow field at simulation time 100 years.*

Figure 3-29. *Case 4 with a borehole distance of 52 m. Vertical section (close-up view) showing Darcy velocity vectors. Flow paths are illustrating flow field at simulation time 100 years.*

Figure 3-30. Case 4 with a borehole distance of 52 m. Vertical section showing flow paths coloured by advective travel time along the paths. Flow paths are illustrating flow field at simulation time 100 years.

Figure 3-31. Case 4 with a borehole distance of 52 m. Vertical section through the middle of the model showing the brine distribution. Flow paths are illustrating flow field at simulation time 100 years.
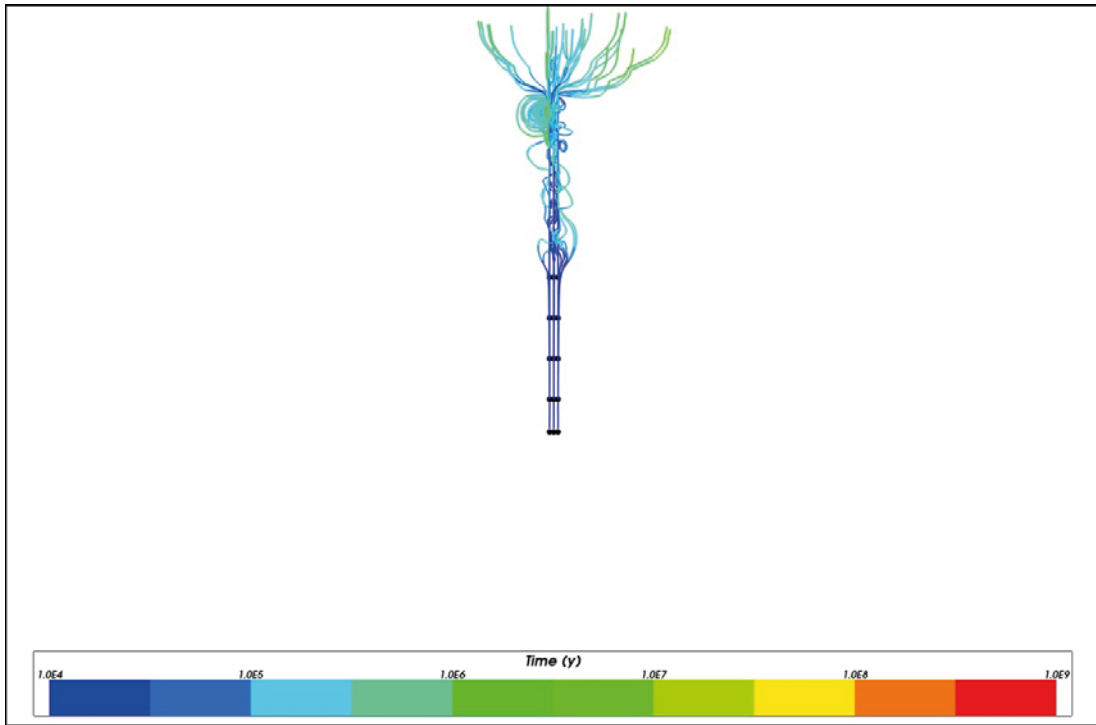
Figure 3-32. *Case 4 with a borehole distance of 52 m. Vertical section (close-up view) showing the brine distribution. Flow paths are illustrating flow field at simulation time 100 years.*
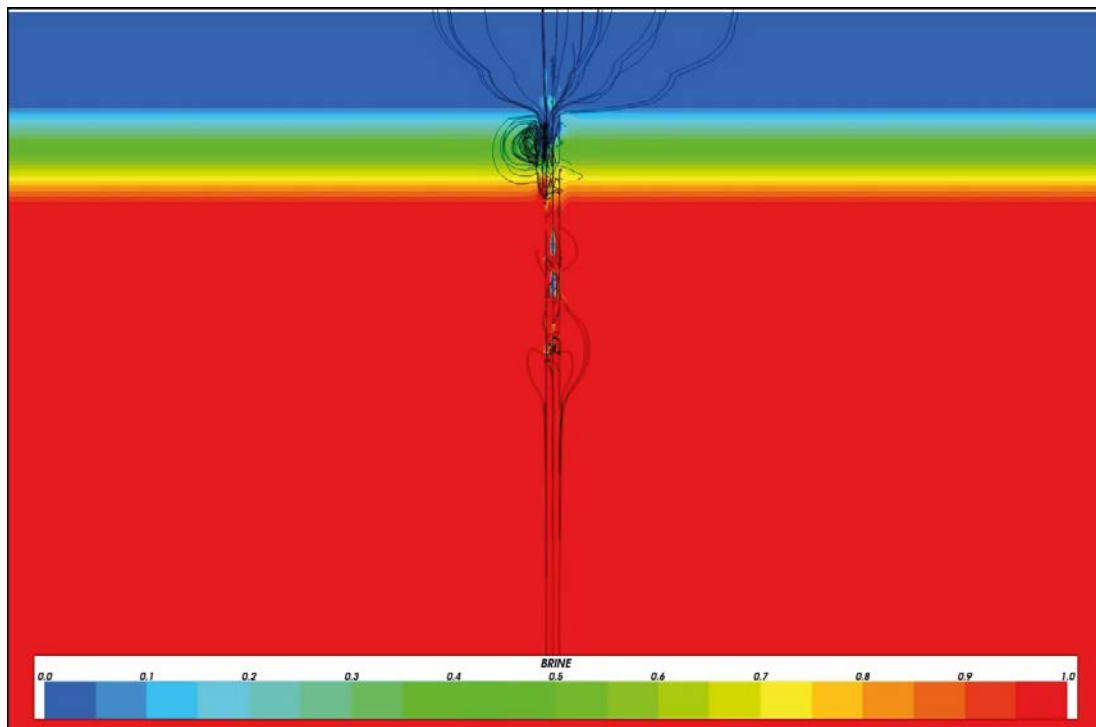
3.4 Sensitivity to position of the saline interface

This section examines the effects of changing the position and shape of the saline interface. The transition from freshwater to full brine occurs between –1,400 and –1,500 m depth, compared to –700 and –1,500 m for Case 1 to Case 4.

3.4.1 Case 5: Base Case properties

Case 5 uses the same properties as Case 1 (base case) but has a modified salinity distribution. The purpose of this variant is to analyse the effect of a sharper transition from freshwater to full brine.

Figure 3-33 shows Darcy velocity vectors on a vertical section through the middle of the model for Case 5 after 10 years of simulation. Flow paths for particles released at five different depths in the buffer material of the boreholes are shown in black. The groundwater flow pattern around the boreholes is very similar to Case 1. All along the borehole, the flow pattern is disturbed and forming local circular convection cells along the full length of the boreholes.

In Figure 3-34 and 3-35, the brine distribution is shown on a vertical section through the middle of the model for Case 5 after 10 years of simulation. It is clear that the brine interface has remained undisturbed, indicating that the groundwater flow across the saline interface is not high enough to mix the freshwater and the brine.

The transport performance measures for Case 5 are shown in Table 3-3. The maximum initial Darcy velocity and the minimum travel time are the same as for Case 1. This is not surprising given the properties of the model, apart from the saline interface, are left unchanged. Apparently the effect on deep groundwater flow from a sharper saline transition is negligible.

Figure 3-36 to Figure 3-38 show results for a snapshot at 100 years of simulation time for Case 5. Compared to the situation after 10 years of simulation, the water velocities are slightly higher. There is no mixing of freshwater and brine over the saline interface after 100 years of simulation.

The statistics in Table 3-3 show that the performance measures for 100 years of simulation have not changed compared to Case 1.

Figure 3-33. *Case 5 with a modified saline interface. Vertical section through the middle of the model showing Darcy velocity vectors. Flow paths are illustrating flow field at simulation time 10 years.*
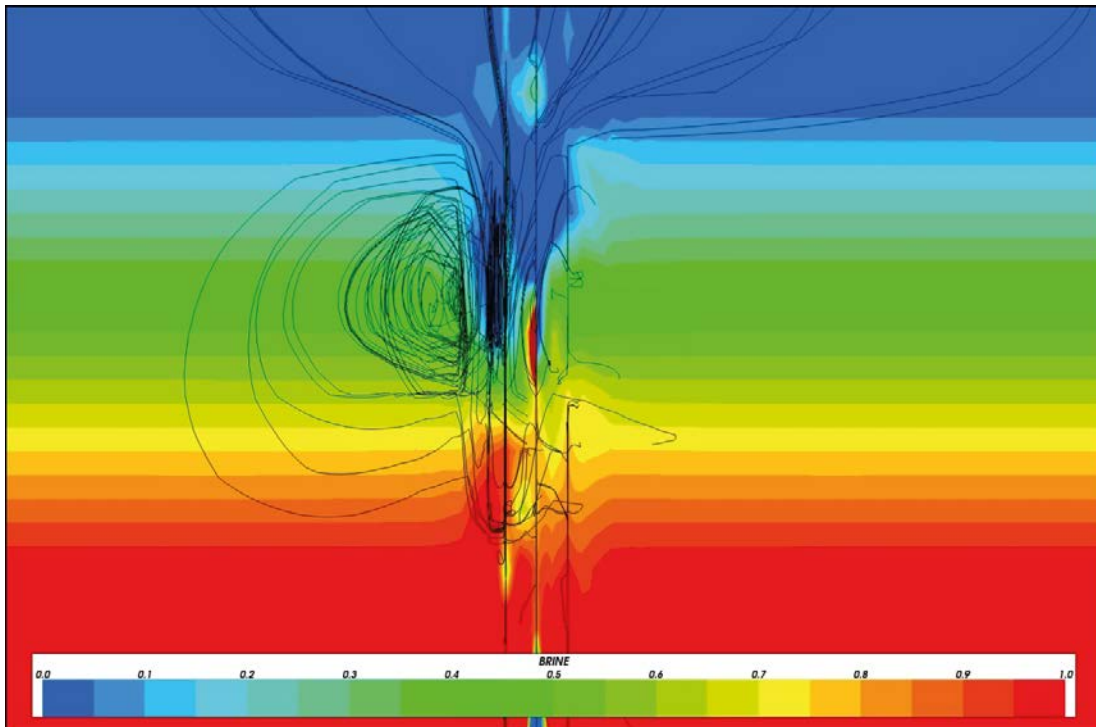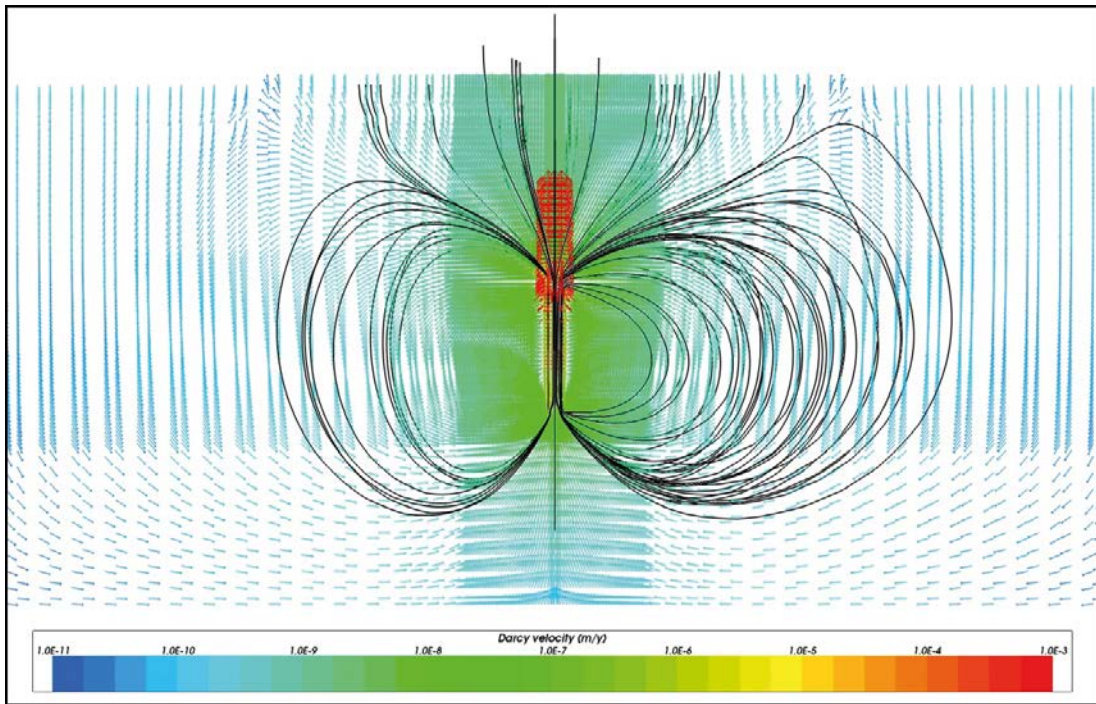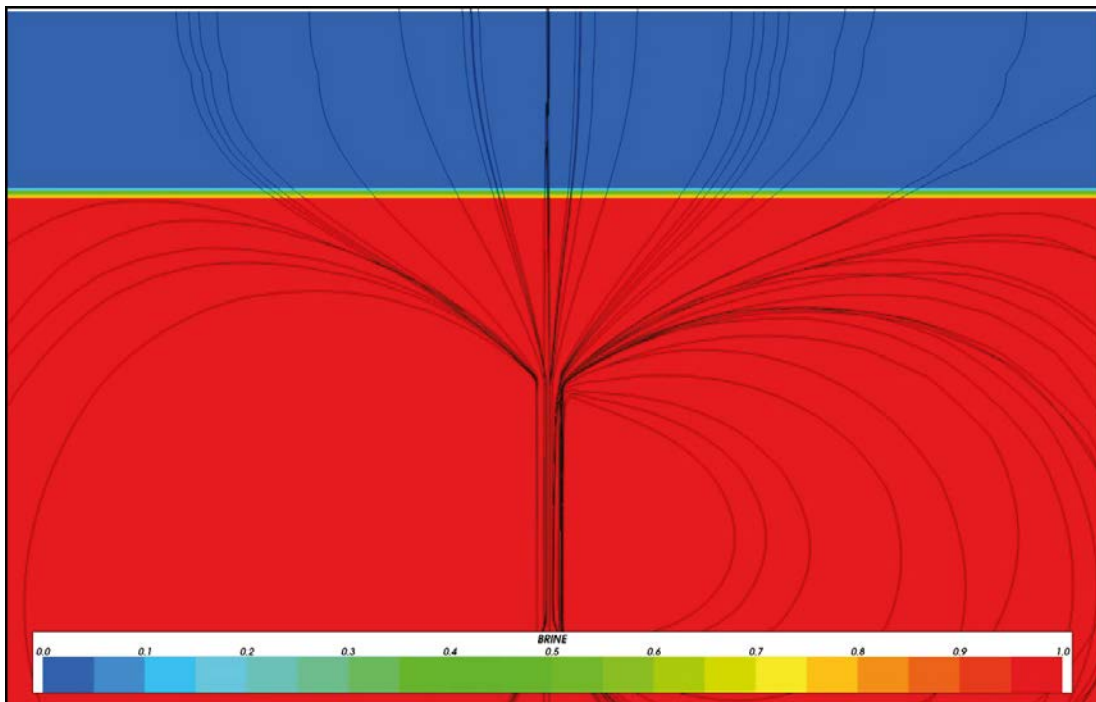

Figure 3-34. *Case 5 with a modified saline interface. Vertical section through the middle of the model showing the brine distribution. Flow paths are illustrating flow field at simulation time 10 years.*
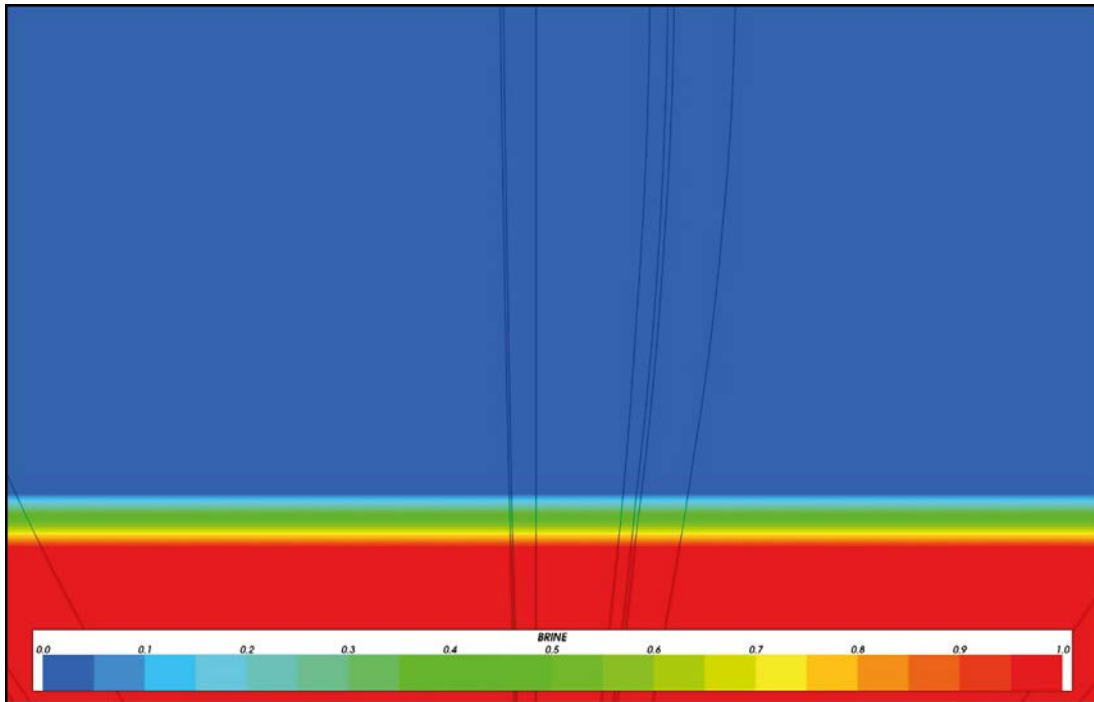
Figure 3-35. *Case 5 with a modified saline interface. Vertical section (close-up view) showing the brine distribution. Flow paths are illustrating flow field at simulation time 10 years.*

Figure 3-36. *Case 5 with a modified saline interface. Vertical section through the middle of the model showing Darcy velocity vectors. Flow paths are illustrating flow field at simulation time 100 years.*
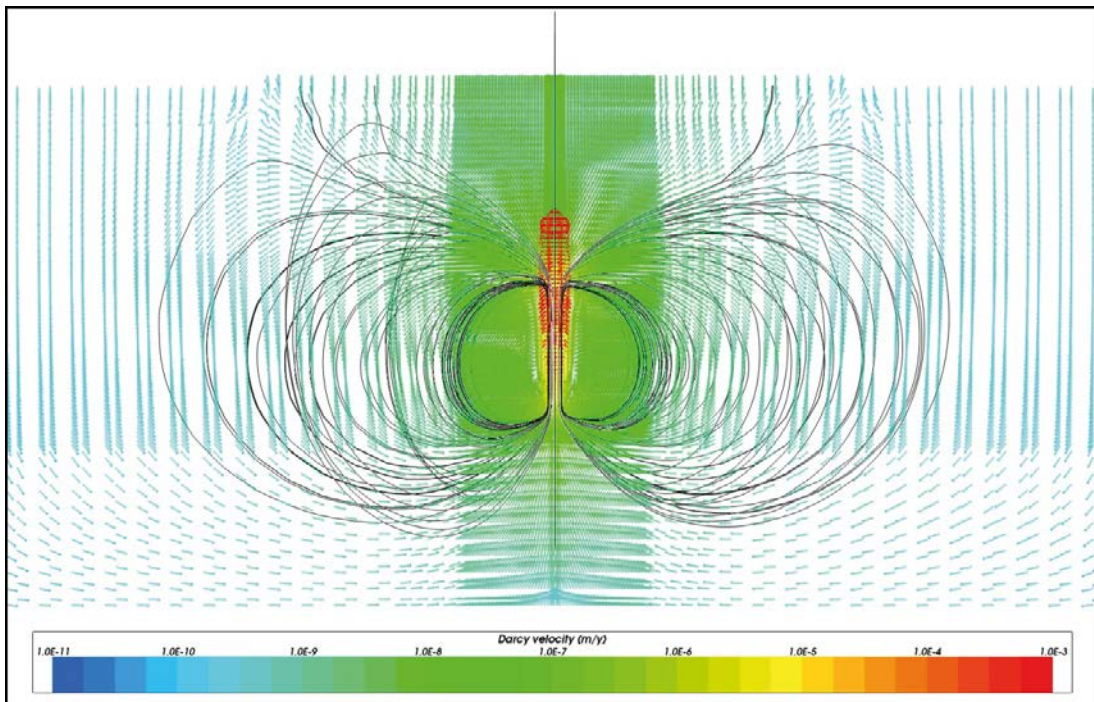
Figure 3-37. Case 5 with a modified saline interface. Vertical section through the middle of the model showing the brine distribution. Flow paths are illustrating flow field at simulation time 100 years.

Figure 3-38. Case 5 with a modified saline interface. Vertical section (close-up view) showing the brine distribution. Flow paths are illustrating flow field at simulation time 100 years.

3.4.2 Case 6: Increased permeability in boreholes

Case 6 uses the same properties as Case 3 with increased permeability in boreholes. In addition, a modified salinity distribution is applied. The purpose of this variant is to analyse the effect of a sharper transition from freshwater to full brine in combination with poor backfill properties in the boreholes.

Figure 3-39 shows Darcy velocity vectors on a vertical section through the middle of the model for Case 6 after 10 years of simulation. Flow paths for particles released at five different depths in the buffer material of the boreholes are shown in black. The groundwater flow pattern around the boreholes differs significantly compared to Case 5 even if the water velocities are similar. All along the borehole, the flow pattern is now disturbed and forming local circular convection cells along the full length of the boreholes.

In Figure 3-40 and 3-41, the brine distribution is shown on a vertical section through the middle of the model for Case 6 after 10 years of simulation. In the close-up view over the brine interface, it can be seen that the brine has started to slowly move upwards along the permeable boreholes, while freshwater is moving downwards from the top. This change in the flow pattern compared to Case 5 is caused by the increased permeability of the buffer and the sealing in combination with the heat from the canisters. This mechanism was described in greater detail in the Case 3 section.

The transport performance measures for Case 6 are shown in Table 3-3. As expected, the maximum initial Darcy velocity and the minimum travel time are similar to Case 3, again suggesting that the effect on deep groundwater flow from a sharper saline transition is negligible.

Figure 3-42 to Figure 3-44 show results for a snapshot at 100 years of simulation time for Case 6. As before, the groundwater flow pattern is still disturbed by localised convection cells. The water velocities have increased both inside and outside of the boreholes due to the generated heat from the canisters.

Figure 3-39. *Case 6 with a modified saline interface and increased permeability in boreholes. Vertical section through the middle of the model showing Darcy velocity vectors. Flow paths are illustrating flow field at simulation time 10 years.*
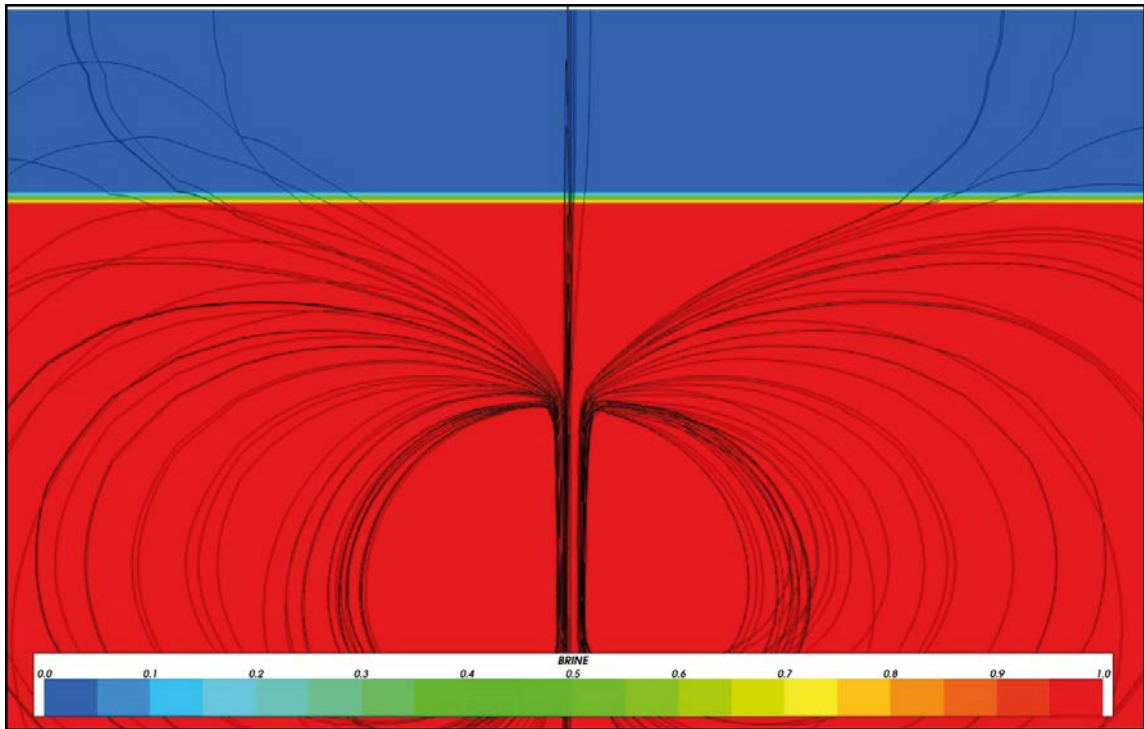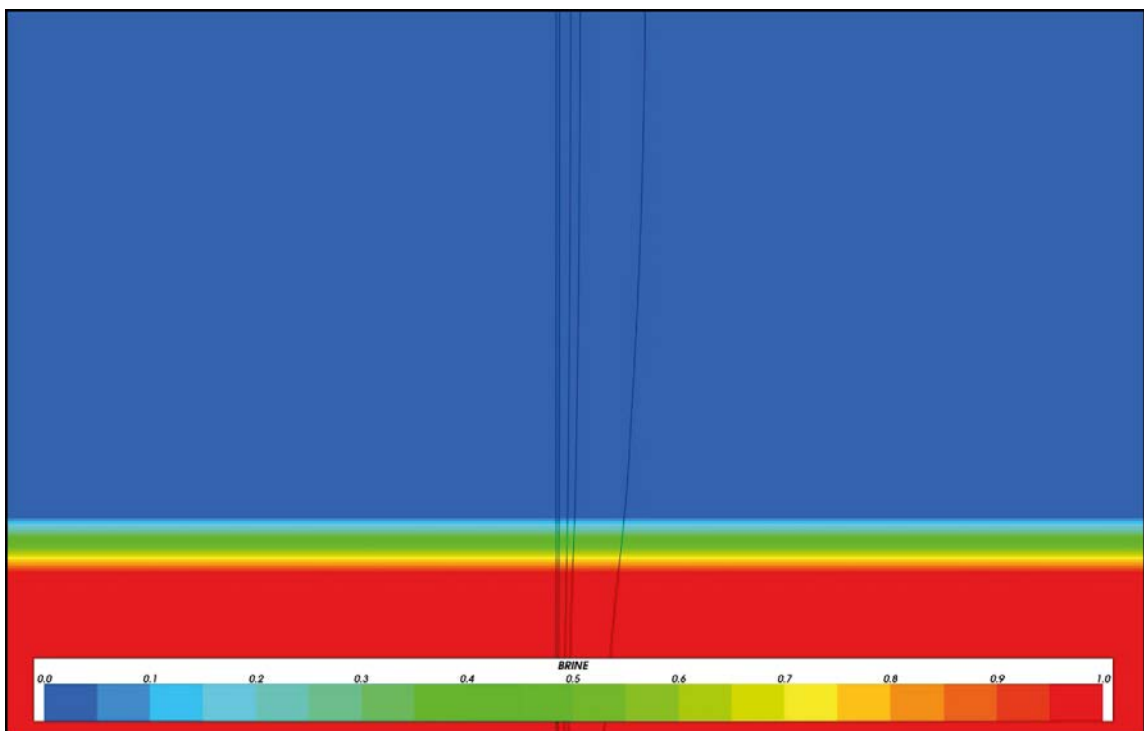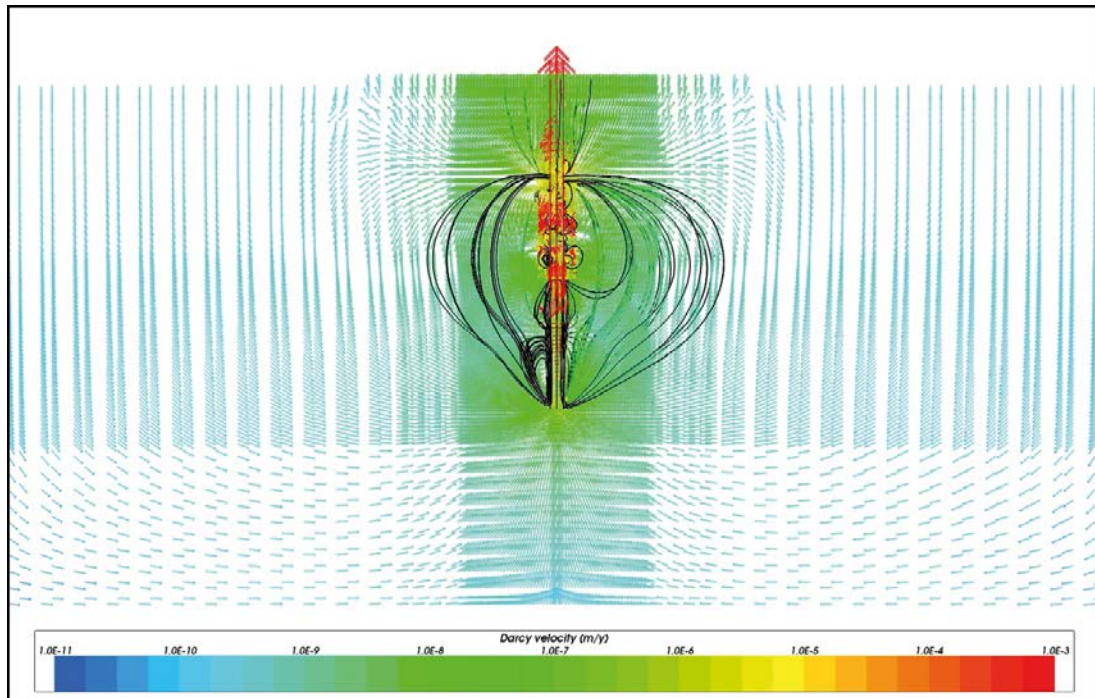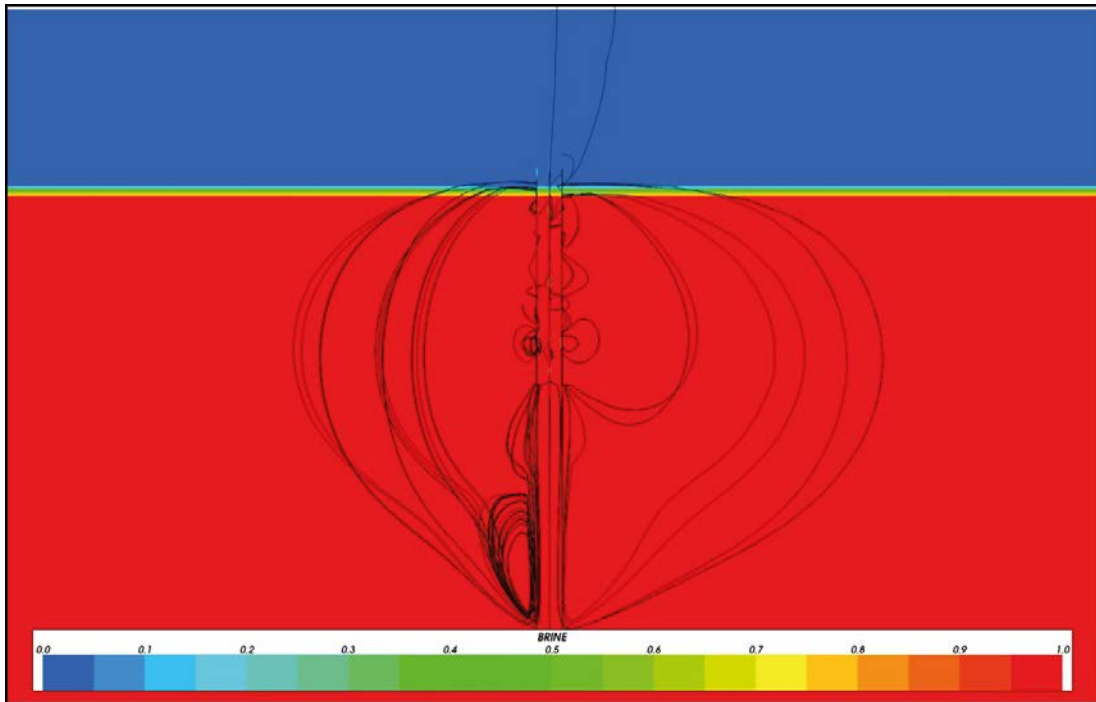
Figure 3-40. *Case 6 with a modified saline interface and increased permeability in boreholes. Vertical section through the middle of the model showing the brine distribution. Flow paths are illustrating flow field at simulation time 10 years.*

Figure 3-41. *Case 6 with a modified saline interface and increased permeability in boreholes. Vertical section (close-up view) showing the brine distribution. Flow paths are illustrating flow field at simulation time 10 years.*

Figure 3-42. *Case 6 with a modified saline interface and increased permeability in boreholes. Vertical section through the middle of the model showing Darcy velocity vectors. Flow paths are illustrating flow field at simulation time 100 years.*
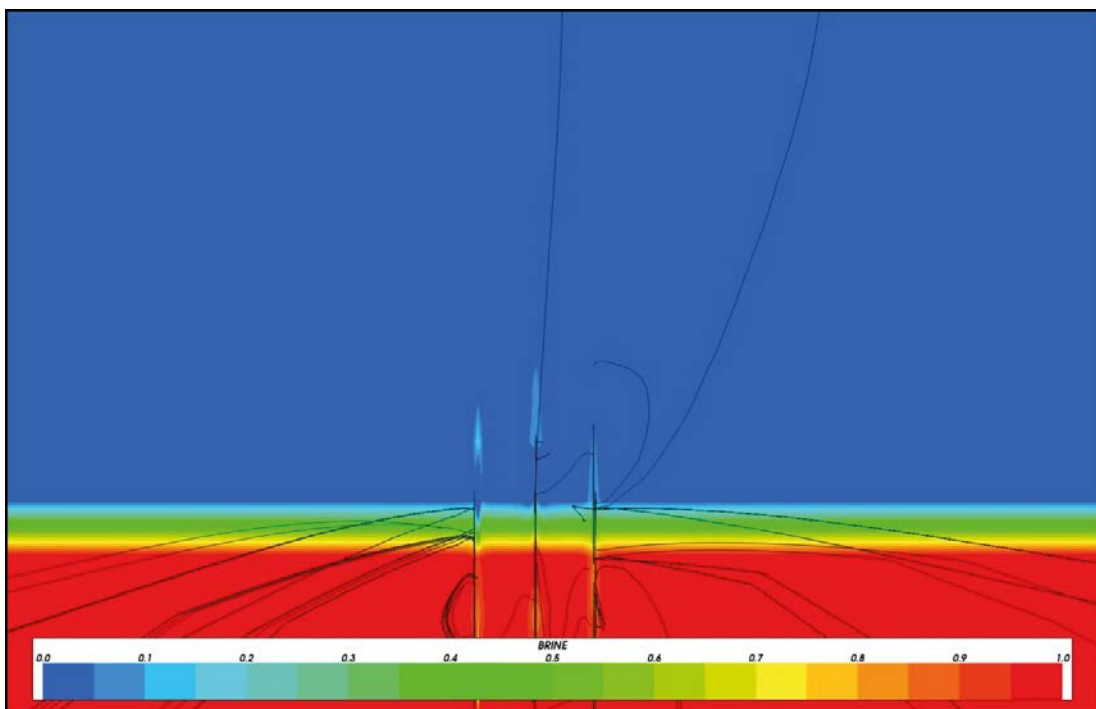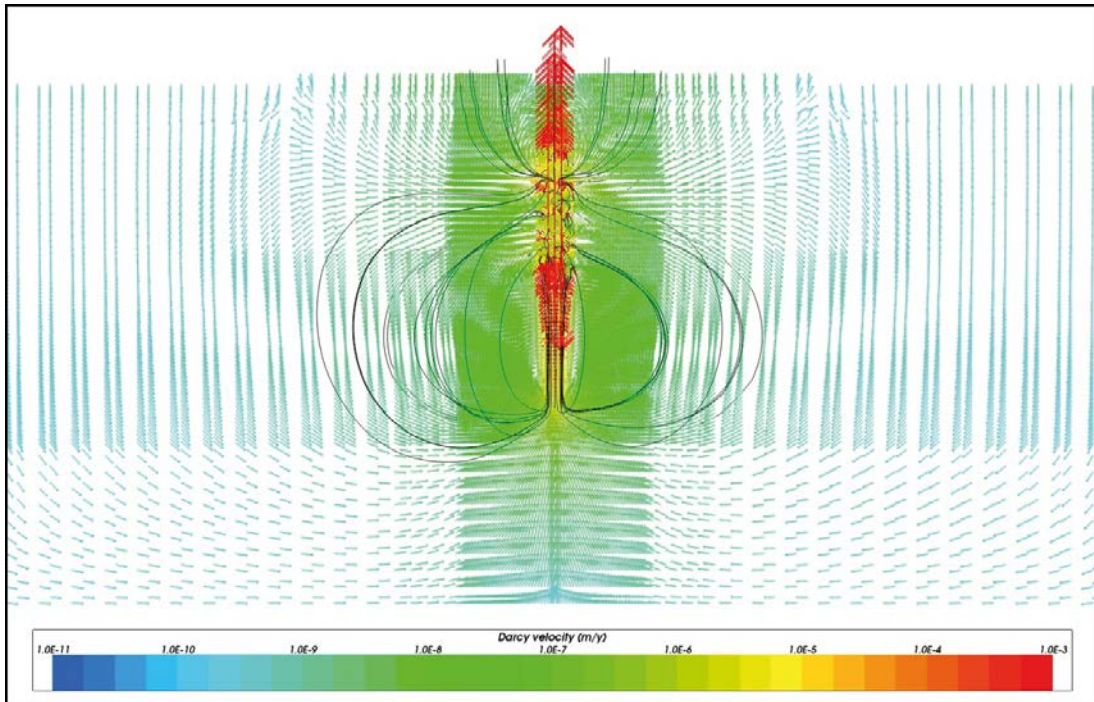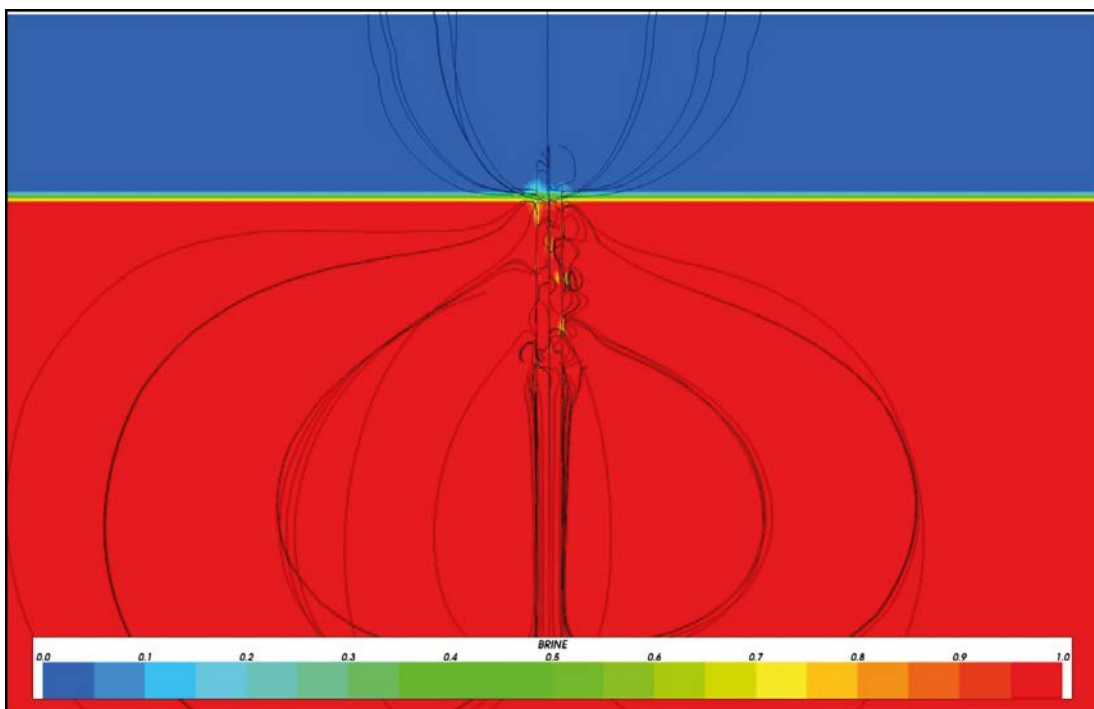

Figure 3-43. *Case 6 with a modified saline interface and increased permeability in boreholes. Vertical section through the middle of the model showing the brine distribution. Flow paths are illustrating flow field at simulation time 100 years.*
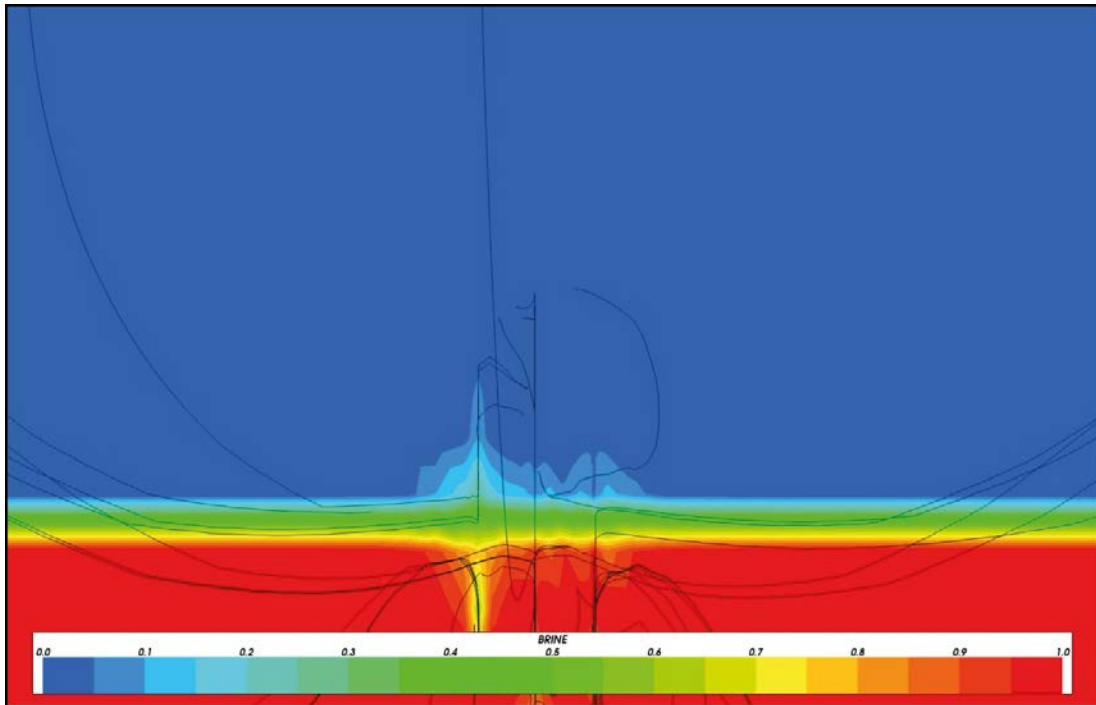
Figure 3-44. *Case 6 with a modified saline interface and increased permeability in boreholes. Vertical section (close-up view) showing the brine distribution. Flow paths are illustrating flow field at simulation time 100 years.*

After 100 years of simulation, the mixing of freshwater and brine has become more pronounced over the initial brine interface. However, compared to Case 3 the mixing is much less developed suggesting that a sharper saline interface has a reducing effect on the mixing of freshwater and brine.

The statistics in Table 3-3 show that the performance measures are roughly the same as for Case 3. There is however a significant difference in the minimum travel time for 100 years of simulation which has increased by one order of magnitude compared to Case 3. An explanation could be the more intact saline interface in Case 6 preventing upward flow to a larger extent compared to Case 3.

3.5   Transport performance measures

In Table 3-3, a statistical summary of the modelled cases is shown. The table shows the minimum and maximum values of the calculated transport performance measures; $U_{0,r}$ – initial Darcy velocity, t_r – travel time and L_r – path length, for particle release times 10 and 100 years. Only particles reaching the top surface of the model are analysed. In addition, particles that do not travel in a direct way to the surface but rather form an artificial loop formed pathway through the model, were also been removed from the statistics. In order to filter out such particles a path length criteria of 7,000 m was used, so that only particles with shorter pathways were kept. Since particles were released from depths of –3,000 m to –5,000 m, the shortest path to the surface is greater than 3,000 m. If a particle would form a loop through the model, the path would be significantly longer than 7,000 m.

As expected, the particles started at the highest elevations also generally give the shortest pathways and travel times. It should be noted though that even the shortest travel times are much longer compared to the time needed for the canister temperatures to drop to the background bedrock temperature. This means that particles released in static flow fields, as was done here, will not be representative for the groundwater flow situation in which the particles would actually travel, if the particle travel times are much longer than the time scale on which the generated heat decreases within the canisters. The conclusion is then that the travel times in reality would be even longer, provided that nothing else changes within the system, e.g. a puls of glacial melt water enters the rock or new deformation zones form etc.

Table 3-3. Statistical summary of modelled cases showing the minimum and maximum values of the transport performance measures; $U_{0,r}$ – initial Darcy velocity, t_r – travel time and L_r – path length, for particle release times 10 and 100 years.

Case	Properties	Borehole c/c (m)	Release time (yr)	Min($U_{0,r}$) (m/yr)	Max($U_{0,r}$) (m/yr)	Min(t_r) (yr)	Max(t_r) (yr)	Min(L_r) (m)	Max(L_r) (m)
1	Base Case (Marsic et al. 2006)	100	10	1.29E–03	2.76E–03	1.79E+08	2.06E+11	3.06E+03	6.66E+03
1	Base Case (Marsic et al. 2006)	100	100	7.09E–04	1.97E–03	2.19E+07	4.38E+10	3.05E+03	4.95E+03
2	Base Case (Marsic et al. 2006)	52	10	1.32E–03	3.00E–03	1.21E+08	2.02E+11	3.06E+03	6.28E+03
2	Base Case (Marsic et al. 2006)	52	100	1.09E–03	3.57E–03	2.04E+07	4.19E+10	3.05E+03	6.68E+03
3	Increased permeability in BUFFER and SEALING	100	10	1.54E–03	2.76E–03	1.83E+06	3.17E+06	3.61E+03	6.58E+03
3	Increased permeability in BUFFER and SEALING	100	100	8.92E–04	1.97E–03	3.60E+05	4.51E+06	3.81E+03	6.97E+03
4	Increased permeability in BUFFER and SEALING	52	10	1.56E–03	3.00E–03	7.59E+06	1.53E+07	5.06E+03	6.89E+03
4	Increased permeability in BUFFER and SEALING	52	100	1.42E–03	3.57E–03	1.69E+05	8.54E+06	4.03E+03	6.95E+03
5	Modified saline interface	100	10	1.29E–03	2.76E–03	1.77E+08	2.03E+11	3.06E+03	6.62E+03
5	Modified saline interface	100	100	7.09E–04	1.97E–03	2.20E+07	4.43E+10	3.05E+03	4.95E+03
6	Modified saline interface Increased permeability in BUFFER and SEALING	100	10	1.59E–03	2.76E–03	3.62E+06	7.40E+06	3.16E+03	5.40E+03
6	Modified saline interface Increased permeability in BUFFER and SEALING	100	100	9.52E–04	1.97E–03	4.94E+06	2.93E+08	3.88E+03	6.75E+03

4 Discussion

In this report calculations are presented of buoyancy driven groundwater flow caused by the emission of residual heat from spent nuclear fuel deposited in deep boreholes from the ground surface in combination with the natural geothermal gradient. This work has been conducted within SKB's programme for evaluation of alternative methods for final disposal of spent nuclear fuel. The main objective of the present study has been to investigate if the thermal output from spent nuclear fuel disposed in deep boreholes would create sufficient buoyancy to jeopardise the stability of the groundwater system created by the salinity at depth.

This study is a continuation of the work that was done in Marsic et al. (2006) where an extensive sensitivity analysis was carried out varying different parameters and model features. In the present study, the focus has been on the effects on groundwater flow from reducing the borehole distance from 500 m, which was used in Marsic et al. (2006), to 100 m and 52 m respectively. In addition, the effects of changing the properties of the borehole sealing (the buffer and the sealing) and the position and shape of the halocline forming the interface between the deep saline groundwater and the fresh groundwater above the halocline, were analysed.

Thermal buoyancy has in this study been the only driving force for groundwater flow. This means, for example, that also the fresh water above the halocline is regarded to be stagnant except for movements induced by the buoyancy forces. If other gradients, e.g. surface topography, were applied to the system, this could potentially shorten the transport times for groundwater from disposal depth to the surface compared to those presented in this report. However, the magnitude of this effect is hard to foresee without performing the calculations.

Effects of decreased borehole distance

Given the assumptions and repository layout used in the present model, the results from the calculated variants show that decreasing the borehole distance is not sufficient to destabilise the saline groundwater. The main effect from decreasing the borehole distance is that the rock temperature increases. For the 100 m variant, the maximum increase in temperature is about 5°C in the rock surrounding the boreholes. For the 52 m variant, the temperature effect is more pronounced. The maximum increase in temperature is about 10°C in the rock surrounding the boreholes and the increase remains for a several hundred years. Even so, the change in density due to the increase in temperature is not enough to cause any significant flows upwards around the boreholes. Even if convection cells are formed around the repository due to the generated heat, the Darcy velocities induced by the heat transport are very low. The convection created by the heating does not significantly change the stability of the virtually stagnant saline groundwater at depth and the salt interface stays virtually unchanged compared to the initial condition. A reason for this is that the power of the heat source is too low and that its duration is too short to create a significant effect. Already after 500 years the thermal output is reduced to 10% of its initial value. The potential effects on the groundwater flow are therefore expected within the first couple of hundred years.

The calculated performance values for the unchanged hydraulic properties of the sealing and the buffer, show that the minimum travel times are in the range 10^7–10^8 years, which is similar to the results for the Base Case in Marsic et al. (2006). The calculated hypothetical travel times for the groundwater are in general very long, orders of magnitude longer, compared to the duration of the decaying heat source. Therefore, the results in terms of performance measure should be treated more as an indication of a very slow and stabile system rather than being realistic values of the transport of released particles.

Effects of poor backfill properties

The effects of poor backfill properties in the boreholes were examined in two variants by varying the hydraulic properties of the sealing and the buffer material. The upper part of the boreholes, i.e. down to 3,000 m depth, includes various materials such as concrete, asphalt and bentonite. The deeper section of the boreholes, between 3,000 and 5,000 m depth include the buffer material.

Compared to the Base Case in Marsic et al. (2006), the permeability of the sealing was increased four orders of magnitude and the permeability of the buffer was increased two orders of magnitude. Although the permeability increase is large, the higher permeability could still be considered realistic as the deep borehole concept does not allow a controlled construction of the near field surrounding the emplaced canisters.

These changes proved to have a significant effect on the groundwater flow around the boreholes. The Darcy velocities increase both inside and outside the boreholes. Around the brine interface, between –700 and –1,500 m elevation, the saline water at depth mixes with fresh groundwater from above and the initially sharp brine interface becomes distorted. This is also reflected in the calculated transport performance measures where the minimum travel times decrease by two orders of magnitude compared to the Base Case with lower borehole permeabilities.

Effects of changing the position and shape of the saline interface

In the Base Case, the brine interface was placed between –700 and –1,500 m elevation. By changing the transition from freshwater to full brine from –1,400 to –1,500 m depth, the effects of a sharper saline interface on the groundwater flow pattern could be analysed.

As would be expected, applying a sharper saline interface to the base case model does not change the results. However, when a sharper saline interface is used in combination with poor backfill properties in the boreholes the mixing of freshwater and brine over the interface is reduced compared to the situation with a less sharp interface.

Conclusions

The present study shows that the calculated performance measures are not very sensitive to the simulated borehole distance, at least not within the range treated here, i.e. a borehole c/c of 500 m to 52 m, provided that the backfill of the boreholes is good enough. However, the model proves to be rather sensitive to the hydraulic properties of the boreholes and even more so in combination with a decreased borehole distance. This indicates that the choice of backfill materials in the boreholes and the execution of the sealing of boreholes will be an important factor for the performance of a deep borehole repository. It should be noted that the nature of the deep borehole disposal method makes it difficult to control relevant parameters of the backfill and sealing materials as they have to be handled remotely on the true sense of the word.

Results also indicate that the position and shape of the saline interface could be of importance for the safety of a deep repository. Geoscientific information indicates that the salinity of the groundwater can vary in an irregular fashion over depth (Marsic and Grundfelt 2013). This makes it probable that the salinity can increase from none to a saline brine over a zone of a certain extension. The calculations performed in this study indicate that the halocline in this situation is more sensitive to disturbance from thermal buoyancy than a sharper halocline.

There are many uncertainties with a very simplified model as the one used in the present study. It is difficult to foresee every effect of the simplifications implemented in the model before the modelling has been performed. In the present study, it was decided to include only nine of the about 80 boreholes because the thermal effect that the boreholes would have on each other was assumed to be limited. However, when decreasing the borehole distance to 52 m it turned out that the heating of the rock between the boreholes was so significant that it cannot be ruled out that the results would be different when adding more boreholes to the model.

The mixing of brine and freshwater at the interface can be affected by numerical phenomena. It was seen in Marsic et al. (2006), that the level of grid refinement is of great importance for the results, in particular when trying to represent small-scale structures. Ideally, one would like to use element sizes no larger than the size of the small-scale structures included in the model. In this study, we have thin layers of buffer and damaged zone around the canisters in the boreholes. These dimensions are on the decimetre scale. This should be compared to the vertical element size used for the elements in the boreholes which 50 m, resulting in a distorted aspect ratio that could cause numerical effects.

References

SKB's (Svensk Kärnbränslehantering AB) publications can be found at www.skb.se/publications.

Agrenius L, 2006. Clab – Resteffekt i förvaringsbassängerna. In Pettersson M, Grundfelt B. Förlängd lagring i Clab. SKB R-06-62, Svensk Kärnbränslehantering AB, Appendix 1. (In Swedish.)

AMEC, 2012. ConnectFlow Technical Summary. AMEC/ENV/CONNECTFLOW/15, AMEC, UK.

Arnold B W, Brady P V, Bauer S J, Herrick C, Pye S, Finger J, 2011. Reference design and operations for deep borehole disposal of high level radioactive waste. SAND2011-6749, Sandia National Laboratories, Albuquerque, NM.

Beswick J, 2008. Status of technology for deep borehole disposal. Report for NDA, Contract NP 01185, EPS International.

Birgersson L, Skagius K, Wiborgh M, Widén H, 1992. Project Alternative Systems Study – PASS. Analysis of performance and long-term safety of repository concepts. SKB TR 92-43, Svensk Kärnbränslehantering AB.

Brady P V, Arnold B W, Freeze G A, Swift P N, Bauer S J, Kanney J L, Rechard R P, Stein J S, 2009. Deep borehole disposal of high-level radioactive waste. SAND2009-4401, Sandia National Laboratories, Albuquerque, NM.

Grundfelt B, 2010. Jämförelse mellan KBS-3-metoden och deponering i djupa borrhål för slutligt omhändertagande av använt kärnbränsle. SKB R-10-13, Svensk Kärnbränslehantering AB. (In Swedish.)

Juhlin C, Sandstedt H, 1989. Storage of nuclear waste in deep boreholes: feasibility study and assessment of economic potential. SKB TR-89-39, Svensk Kärnbränslehantering AB.

Juhlin C, Wallroth T, Smelie J, Eliasson T, Ljunggren C, Leijon B, Beswick J, 1998. Very Deep Hole Concept – Geoscientific appraisal of conditions at great depth. SKB TR 98-05, Svensk Kärnbränslehantering AB.

Marsic N, Grundfelt B, 2013. Review of geoscientific data of relevance to disposal of spent nuclear fuel in deep boreholes in crystalline rock. SKB P-13-12, Svensk Kärnbränslehantering AB.

Marsic N, Grundfelt B, Wiborgh M, 2006. Very deep borehole concept. Thermal effects on groundwater flow. SKB-R-06-59, Svensk Kärnbränslehantering AB.

Odén A, 2013. Förutsättningar för borrning av och deponering i djupa borrhål. SKB P-13-08, Svensk Kärnbränslehantering AB. (In Swedish.)

SKB, 1992. Project on Alternative Systems Study (PASS). Final report. SKB TR 93-04, Svensk Kärnbränslehantering AB.

SKB, 2010. Plan 2010. Kostnader från och med år 2012 för kärnkraftens radioaktiva restprodukter. Underlag sör avgifter och säkerheter åren 2012–2014. Svensk Kärnbränslehantering AB.

Smellie J, 2004. Recent geoscientific information relating to deep crustal studies. SKB R-04-09, Svensk Kärnbränslehantering AB.